5-2015

Development and Demonstration of Critical Components of Aluminum Based Energy Storage Devices Using the Chloroaluminate Ionic Liquids

Mengqi Zhang
University of Tennessee - Knoxville, mzhang17@vols.utk.edu

Recommended Citation

Zhang, Mengqi, "Development and Demonstration of Critical Components of Aluminum Based Energy Storage Devices Using the Chloroaluminate Ionic Liquids. " PhD diss., University of Tennessee, 2015.
https://trace.tennessee.edu/utk_graddiss/3317

To the Graduate Council:

I am submitting herewith a dissertation written by Mengqi Zhang entitled "Development and Demonstration of Critical Components of Aluminum Based Energy Storage Devices Using the Chloroaluminate Ionic Liquids." I have examined the final electronic copy of this dissertation for form and content and recommend that it be accepted in partial fulfillment of the requirements for the degree of Doctor of Philosophy, with a major in Chemical Engineering.

Thomas A. Zawodzinski, Major Professor

We have read this dissertation and recommend its acceptance:

Robert M. Counce, Jack S. Watson, Matthew M. Mench

Accepted for the Council:
Dixie L. Thompson

Vice Provost and Dean of the Graduate School

(Original signatures are on file with official student records.)

Development and Demonstration of Critical Components of Aluminum Based Energy Storage Devices Using the Chloroaluminate Ionic Liquids

A Dissertation Presented for the
Doctor of Philosophy
Degree
The University of Tennessee, Knoxville

Mengqi Zhang
May 2015

DEDICATION

To my spiritual support, my special and beloved wife
Chen

ACKNOWLEDGEMENTS

I would like to thank my advisors, Dr. Robert (Pete) Counce and Dr. Thomas Zawodzinski, for all support and guidance throughout the entire study in the University of Tennessee, Knoxville. Also, I appreciate the help and suggestion from my committee members, Dr. Jack Watson and Dr. Mattew Mench. Thanks Dr. Paul Trulove for his instruction on my experimental work. I thank the funding support by NSF TN-SCORE (EPS 1004083).

I would also like to thank the support from other group members. The groups could not be full of friendliness, cooperation and innovation without them. Thanks Dr. Gabriel’s hard work on keeping all lab work in a good coordination. I also appreciate Dr. Papandrew’s support and follow on my research direction. Dr. Foister also generously provide me instructions on experimental work and his purified chemicals. Thanks Kat Frost to organize all office and business work in good order. Mark and Nick in Dr. Counce’s group help a lot to maintain the friendly lab atmosphere. Finally, I would like to thank all my Chinese group members, such as Tang, Ming, Bai, Congling and Eva for their support and kindness.

Finally, I want to express my gratitude to my family, my wife and my parents. Without the encouragement and care, irrespective of day or night, from my wife, I would not insist on my Ph.D life for five years and finish this dissertation in a good shape. I appreciate the all support and expectations from my parents to educate me to work hard on pursuing my Ph.D study aboard.

ABSTRACT

This dissertation considers the development of porous carbon materials as the substrates for Al deposition/dissolution in an Al based ionic liquid flow battery (ILFB) and demonstration of an Al based hybrid supercapacitor. The Aluminum chloride/ 1-ethyl-3-methylimidazolium chloride chloroaluminate ionic liquid is utilized as the electrolyte for these Al based energy storage devices. The ILFB has less capital cost than the all-vanadium redox flow battery because of the inexpensive $AlCl_3$. The feasibility to equip a tank of solid aluminum chloride in an ILFB system aiming to improve energy density is investigated. A critical range of temperature data (50-130 celsius degree) for aluminum chloride dissolution and precipitation from saturated chloroaluminate ionic liquids is measured by differential scanning calorimetry. The process of Al deposition on porous carbon materials is investigated in the static electrolyte and a flow-through cell aiming to improve the current density, the amount of Al deposits stored in substrates and limit the dendrite growth. Fourier transform infrared spectroscopy and scanning electron microscope are applied to characterize the Al deposits on the porous carbon materials. By the flow-through method providing enhanced diffusion to porous carbon materials, the current density of Al deposition on carbon paper is remarkably higher than that on Al disk. However, dendrites prefer to grow on the Al disk substrate. The electrolyte flow rate and the flow direction also play important roles in determining current densities and dendrite formation for Al deposition on porous carbon materials. We successfully demonstrate an Al based hybrid supercapacitor using high surface area carbon materials such as graphene and activated carbon. The activated carbon is preferred because of less catalytic ability to evolve chlorine. The mismatch between the small pore size of activated carbon and the large ion size of complex ions results in the high charge-transfer resistance measured by the electrochemical impedance measurements. The wettability of electrodes determined by different polymer binders, Polytetrafluoroethylene and the aqueous base modified styrene butadiene rubber, has a significant effect on specific capacitance of activated carbon. The hydrophilic property of SBR may promote the entrance of ions to the micropores of activated carbon.

TABLE OF CONTENTS

LIST OF TABLES

LIST OF FIGURES

CHAPTER 1

Introduction and Motivation

1.1 Background

1.1.1 The demands on electric energy storage (EES)

The development of the current society is usually accompanied with the large consumption of fossil energy, such as petroleum, coal and natural gas.[1,2] However, the usage of fossil energy is unsustainable and leads to emissions of carbon, sulfur, nitrogen related pollutants.[3,4] To attenuate the impact of fossil fuel consumption on the global environment, there has been various sustainable energy developments in wind, solar, hyro and other renewable resources.[5-7] But the integrations of the renewable energy are limited by the intermittent characteristic of wind and solar leading to instability of electric grid.[8-10] EES, however, may become a potential method to address these issues. Among different technologies on EES, the all-vanadium redox flow batteries (VRFB) has been widely developed and may become a potential candidate in EES applications based on the consideration of the power density and cyclic stability. However, there are still several disadvantages of VRFBs such as the high capital cost of electrolytes and low energy density.[11-16] In addition, electric vehicles (EVs) have been developed to decrease the dependence on the fossil fuels and reduce the automobile exhausts.[11,12,17] While the reliability and the charging/discharging rate of the Lithium-ion battery (LIB) has been improved, the sluggish kinetics and diffusion of Li ion on electrode materials still limits the emerging applications in EVs.[18-22] Therefore, it is of high priority to develop advanced energy storage devices which overcome the disadvantages in VRFB and LIB technologies.

1.1.2 Aluminum-based energy storage devices

Recently, we introduce several Aluminum (Al) based energy storage devices featuring the high specific energy and an abundant reserve of Al. They are an Al based ionic liquid flow battery (ILFB) and an Al based hybrid supercapacitor. These devices aims to improve energy/power density with lower capital cost. The ILFB focuses on the improvement of energy density over VRFBs while the Al based hybrid supercapacitor aims to perform higher power density than the LIB. Both of these Al based energy storage devices use acidic $AlCl_3$/EMIC (molar ratio >1) chloroaluminate shown in Figure 1.1. The ionic liquid is expected to be liquid in the temperature over -50℃ depending on the acidity.

1.1.2.1 Principles and structure of ILFB

Dissolved $AlCl_3$ is the only active material to be consumed and regenerated during charging and discharging. The schematic structure of ILFB is shown in Figure 1.2. Unlike other concepts using ILs, the melt component ($AlCl_3$) is used as an electrochemically active couple, leading to maximum concentration of active species. During charging, the IL composition of stoichiometric $2AlCl_3$:1EMIC is passed into the battery. Cl_2 is produced at the positive electrode and retained in the system or stored while Al is plated on the negative electrode.[23-26] The electrochemical reactions (charging process) are listed below.

Positive electrode: $4AlCl_4^- \leftrightarrow Cl_2 + 2Al_2Cl_7^- + 2e^-$ (1)

Negative electrode: $4Al_2Cl_7^- + 3e^- \leftrightarrow Al + 7AlCl_4^-$ (2)

The charging reaction results in the depletion of $AlCl_3$, lowering the acidity of the IL.

Circulating the electrolyte through a reservoir containing $AlCl_3$ re-acidifies the IL for the next pass through the cell. Configured as a flow battery using a solid-state reservoir, the theoretical energy density is estimated as high as 1435Wh/kg (based on the theoretical energy density of $AlCl_3$). Also, the nature of the reactions in the cell eliminates the need for membranes.

1.1.2.2 History and limitations

Fundamentally, the ILFB shares the similar electrochemical reactions with the developed Al/Cl_2 battery. The first Al/Cl_2 battery prototype operating at approximate 175 ℃ was proposed in 1972 by United States Air Force Academy.[27] Their cell was composed of Al anode, a cathode with Cl_2 stored in powered graphite and an $AlCl_3/NaCl$ electrolyte. The open circuit voltage (OCV) is 2.55V and current density can reach 800mA/cm^2 calculated based on Al anode surface area. The primary issues involving this Al/Cl_2 battery were the high operation temperature, relatively low conductivity of melts and low Cl_2 storage capacity in graphite. Since 1972 the invention of room temperature ionic liquids (RTIL) such as imidazolium chloroaluminate paved the way for Al/Cl_2 battery at room temperature; in 1985 Auborn and Barberio indicated the potential application of RTIL applied to Al deposition/dissolution for the battery design.[28] In 1988 Gifford and Palmisano first entered the research field of room temperature Al/Cl_2 batteries using substituted imidazolium chloroaluminate. They synthesized the 1,2-dimethyl-3-propylimidazolium chloride (DMPIC) as the electrolyte for Al/Cl_2 battery to avoid the chlorination of the proton on 2nd C in the EMI cation.[23] However, the low Cl_2 storage capacity of graphite is still a limiting factor. Though some researchers focusedon solving Cl_2 reduction issue for the cathode and proposed a model and mechanism for the Cl_2 injection electrode, the irreversibility of Cl_2 cathode is always the barrier hindering the development of Al/Cl_2 battery.[24,25] Hass and his colleagues in 1989 also proposed two kinds of cathode materials, porous graphite and Ti-Ti/Ru oxide for chlorine reduction.[29] Since the research progress during 1980s, the developments of the Al/Cl_2 battery are rarely reported largely due to lack of the cathode materials for Cl_2 storage and compatible electrolytes.

The ILFB addresses the problems confronted in previous Al/Cl_2 batteries. First, chlorine is no longer required to be stored in the positive electrode; it can be either evolved and stored in the gas tank or dissolved in the chloroaluminate. Secondly, the Al plating can be processed by maintaining the acidity of the chloroaluminate instead of the decreasing acidity of the chloroaluminate in the previous design. Thirdly, the efficiency of Al deposition/dissolution should be improved as the mass transfer of the flowing electrolyte can enhance the ionic diffusion to Al nuclei growth.

1.1.2.3 Aluminum negative electrode

Although Al is favored to grow on most conductive substrates, it is still important to find a suitable substrate to improve the efficiency of the Al electrode and limit the dendrite formation. A key issue for this electrode will be to deposit relatively large quantities of Al during each cycle so significant quantities of Al can be stored on the electrode. During repeated charge-discharge cycles, it will be necessary to maintain the same general shape of the electrode to insure that the same quantity of Al can be replated for the next cycle. The shape of electrodes that provide both sufficient storage capacity and electrode area is preferred. Compared to a planar substrate, the porous carbon materials have the natural advantages as the substrate for Al deposition/dissolution because the porous structure provides the space for deposition.[30] Furthermore, it is challenging to understand how the nuclei of Al form and grow on the porous carbon materials as the difference of morphology with the planar substrate. Especially, under the circumstance of the flowing electrolyte, it is still unknown how Al deposition is affected by ionic diffusion and electric field on the porous carbon materials. Therefore, in this dissertation, Al deposition/dissolution for the negative electrode in the ILFB is investigated on porous carbon materials such as carbon paper and reticulated vitreous carbon (RVC). In addition, as an advantage of porous electrode, a flow-through electrode for Al deposition is investigated with the improved mass transfer of ions to electrode surface which may allow greater Al plating/stripping current density on the porous carbon.

1.1.2.4 Potential materials for the positive electrode

To investigate the Cl_2 cathodes for the ILFB, at first the cation in the acidic chloroaluminate ionic liquids should be stable when Cl_2 is evolved from the ionic liquids. For example, if the imidazolium based ionic liquids are used, the H on the 2nd C of the imidazolium ring should be replaced by an electron donor. Otherwise, the chloride can substitute for the proton on the 2nd C of the imidazolium ring and this chloride substituted imidazolium cation is unstable in the conditions where Al plating/stripping occurs. Secondly, it is required to find an efficient catalysts to reduce the Cl_2. Platinum (Pt), a popular catalyst for oxygen reduction reaction (ORR), may become an appropriate candidate for Cl_2 reduction but the high cost and possible side reaction with Cl_2 may limit its application for the Cl_2 reduction reaction. However, the success of $(Ru_{0.09}Co_{0.91})_3O_4$ applied in a H_2/Cl_2 regenerative fuel cell[31] suggests that metal oxide such as RuO_2, CoO_2 or TiO_2 may also be the candidates to catalyze the Cl_2 reduction reaction in the acidic chloroaluminate ionic liquids.

As Al deposition/dissolution also occur in the bromoaluminate, eg. $AlBr_3$/1-ethyl-3-methylimidazolium bromide (EMIB) ionic liquids, the concept of ILFB could also be applied to Al/Br_2 flow battery. We anticipate many benefits of this approach, including improved ease of electrocatalysis of bromine reactions, ability to suppress Br_2 volatility and less reactivity. But this would come at the expense of lower energy density for a battery. In addition, because of its plethora of oxidation states, sulfur positive electrodes are now of intense interest. In acidic $NaCl/AlCl_3$ molten salts, sulfide in the form of AlSCl can be quasi-reversibly oxidized to sulfur and even to SCl_3^+ on a glassy carbon electrode. However, electrochemical reactions of sulfur in room temperature ionic liquids are quite different than those in the $NaCl/AlCl_3$ molten salts.[32-34] It is reported that sulfur can be oxidized to S^+, S_2^+ and SCl_3^+ (when the potential over is 2.2V vs Al/Al(III)) in the acidic $AlCl_3$/N-butylpyridinium chloride (BPC) ionic liquid but these oxidized products have only short lifetime in the ionic liquid. Though reduction peaks are observed in our preliminary data in Figure 1.3, the data indicate kinetically controlled behavior. Side reactions between S_2Cl_2 and imidazolium ring under the catalysis of $Al_2Cl_7^-$ may occur. In addition, the decomposition of SCl_3^+ may occur. The possible chemical reaction is shown below.

$$2SCl_3^+ + 4AlCl_4^- \rightleftharpoons S_2Cl_2 + 3Cl_2 + 2Al_2Cl_7^- \tag{3}$$

Therefore, a composite of metal oxides may also improve the kinetic behavior on sulfur related electrochemical reactions. Compared to $AlCl_3$, $AlBr_3$ used to prepare ionic liquids is a weaker Lewis acid and will have less capability to catalyze side chemical reactions. It is valuable to investigate how sulfur oxidation reactions occur in bromoaluminates. In the ILFB concept, the limited solubility of sulfur species can be overcome by using a highly soluble mediator to interconvert sulfur species.

1.1.2.5 Al based hybrid supercpacitor

The Al based hybrid supercapacitor has the Al negative electrode and high surface area carbon positive electrode. The electrochemical reactions are shown below.

Positive side (EDLC): $AlCl_4^- + nC \leftrightarrow AlCl_4^- \cdot C_n^+ + e^-$ (4)

Negative side (Battery): $4Al_2Cl_7^- + 3e^- \leftrightarrow 7AlCl_4^- + Al$ (5)

The high surface area carbon materials usually have specific surface area over 500m^2/g and in different forms: activated carbon, carbon black, carbon nanotubes, carbon nanofibers and graphene nanoplaletes. The advantage of the high specific surface area of these carbon materials has stimulated the development of symmetric electric double-layer capacitors (EDLC).[35-37] However, the energy density of symmetric EDLC is limited by the capacity of electrochemical adsorption/desorption. The energy produced by ion-adsorbed/desorbed during electrochemical double layer formation cannot be comparable with that in Faradaic reaction process. So it is better idea to mix the properties of electrochemical double-layer capacitor (non-Faradaic process) with a Faradaic process.[38-46] But concern should be taken to merge the slower Faradaic process with faster non-Faradaic process. For example researchers are currently interested in applying lithium intercalation anode or magnesium (Mg) anode to these hybrid (asymmetric) EDLC. But slow kinetics on Mg anode in the phenyl-magnesium-chloride might just collect the both disadvantages from battery and EDLC. Low power density has to be applied during battery charging to plate Mg efficiently. However, as the fast kinetics of Al deposition in the chloroaluminate ionic liquids, it may be technically possible for the hybrid EDLC to reach energy densities of more than 70Wh/kg at 1A/g.

1.2 Motivation and goal of the dissertation

Research in this dissertation primarily focuses on the development of negative electrodes in ILFB and demonstrates the Al based hybrid supercapacitor. However, in order to investigate the components affecting the capital cost of VRFB, the initial part (Chapter 3) of the dissertation performs a detailed capital cost analysis of VRFB. It also will be beneficial to understand parts of VRFB take the relative contributions of the total capital cost. It also leads to design of a better energy storage device with lower capital costs. For example, the potential high cost from the electrolyte in VRFB stimulates the idea of ILFB with a tank of the solid $AlCl_3$ which could decrease the capital costs of ILFB.

Al deposition/dissolution occurs on the negative electrode during ILFB charging and discharging. The fundamental study of Al electrodeposition indicates that Al growth is controlled by both kinetic and mass transfer. The lack of effective mass transfer under high current density electrodeposition can lead to dendrite formation which short-circuits the cell. As the high current density is commonly required by such an energy storage device, the possibility to use porous materials as substrates for Al plating/stripping attracts our research interests. Thus, the experiments of Al deposition/dissolution are studied on porous carbon materials such as carbon paper (Chapter 4). As the high surface area of porous carbon materials, we initially expect to observe higher current density of Al deposition on carbon paper than those on planar substrates. The investigation of dendrite formation and growth on the porous carbon materials is required, as the ILFB requires the storage of large amount of Al deposits on the substrate to ensure the high energy density. In addition, the melting/freezing points of the over-saturated $AlCl_3$/EMIC ionic liquids (Chapter 5) are investigated in the dissertation in order to provide the thermodynamic information on $AlCl_3$ dissolution/precipitation from the saturated $AlCl_3$/EMIC ionic liquids. The critical temperature for $AlCl_3$ dissolution/precipitation from the saturated $AlCl_3$/EMIC ionic liquids should be observed on the phase diagram of $AlCl_3$ in the $AlCl_3$/EMIC ionic liquid.

In the design of ILFB, as the Al deposition should be operated on the porous carbon materials with the flowing electrolyte, we designed and built a three electrode flow-through cell for Al deposition on carbon paper (Chapter 6). This cell can be used to simulate the environment where Al deposition occurs under the effect of flowing electrolyte. It has been widely understood that the growth of Al nuclei is controlled by the ionic diffusion process to the electrode surface. However, little is known about Al deposition on the porous materials by a flow-through method. We expect that Al nuclei could grow more on the inner part of carbon paper in order to improve the ability of Al storage on the porous carbon materials. The current density of Al deposition may also be affected by the flowing electrolyte. The dendrite formation and growth may be alleviated by the flow-through method if the diffusion flux of ions is sufficiently fast.

In addition to the above studies of Al deposition on porous carbon materials, the Al based hybrid supercapacitor is demonstrated (Chapter 7) in the dissertation. Activated carbon and graphene nano-platelets are studied as the high surface area carbon materials for EDLC electrodes. The electrochemical characterizations of the Al based hybrid supercapacitor is performed to measure specific capacitance and discuss the charging/discharging profiles. Different polymer binders may have an effect on the wettability of the EDLC electrode with the chloroaluminate ionic liquid and thus impact the performance of the Al based hybrid supercapacitor.

In this dissertation, both capital cost analysis and experiments are utilized to demonstrate the feasibility of ILFB and Al based hybrid supercapacitor. To improve the current density of Al deposition/dissolution and limit the dendrite formation/growth, porous carbon materials are utilized as substrates for Al deposition/dissolution. The flow-through method is adopted to investigate the effect of enhanced flowing electrolyte on the current density and dendrite growth of Al deposition. To acquire the thermodynamic information to precipitate/ dissolve $AlCl_3$ in the saturated $AlCl_3$/EMIC ionic liquid, melting/freezing points of the over-saturated $AlCl_3$/EMIC ionic liquids are measured. Finally, we demonstrates the feasibility of Al based hybrid supercapacitor using an activated carbon electrode. The effect of polymer binders is discussed as it relates to the change of wettability property of EDLC electrode.

Reference

[1] Boden, T. A., Marland, G., & Andres, R. J. (2009). Global, regional, and national fossil-fuel CO2 emissions. *Carbon Dioxide Information Analysis Center, Oak Ridge National Laboratory, US Department of Energy, Oak Ridge, Tenn., USA doi*, *10*.

[2] Burnham, A., Han, J., Clark, C. E., Wang, M., Dunn, J. B., & Palou-Rivera, I. (2011). Life-cycle greenhouse gas emissions of shale gas, natural gas, coal, and petroleum. *Environmental science & technology*, *46*(2), 619-627.

[3] Gustavsson, L., Börjesson, P., Johansson, B., & Svenningsson, P. (1995). Reducing CO_2 emissions by substituting biomass for fossil fuels. *Energy*,*20*(11), 1097-1113.

[4] Streets, D. G., & Waldhoff, S. T. (2000). Present and future emissions of air pollutants in China: SO_2, NO_x, and CO. *Atmospheric Environment*, *34*(3), 363-374.

[5] Painuly, J. P. (2001). Barriers to renewable energy penetration; a framework for analysis. *Renewable energy*, *24*(1), 73-89.

[6] Johansson, T. B., & Burnham, L. (Eds.). (1993). *Renewable energy: sources for fuels and electricity*. Island press.

[7] Lund, H. (2007). Renewable energy strategies for sustainable development.*Energy*, *32*(6), 912-919.

[8] Barton, J. P., & Infield, D. G. (2004). Energy storage and its use with intermittent renewable energy. *Ieee Transactions on Energy Conversion*, *19*(2), 441–448. doi:Doi 10.1109/Tec.2003.822305

[9] Divya, K. C., & Ostergaard, J. (2009). Battery energy storage technology for power systems-An overview. *Electric Power Systems Research*, *79*(4), 511–520. doi:DOI 10.1016/j.epsr.2008.09.017

[10] Nema, P., Nema, R. K., & Rangnekar, S. (2009). A current and future state of art development of hybrid energy system using wind and PV-solar: A review. *Renewable & Sustainable Energy Reviews*, *13*(8), 2096–2103. doi:10.1016/j.rser.2008.10.006

[11] Yang, Z. G., Zhang, J. L., Kintner-Meyer, M. C. W., Lu, X. C., Choi, D. W., Lemmon, J. P., & Liu, J. (2011). Electrochemical Energy Storage for Green Grid. *Chemical Reviews*, *111*(5), 3577–3613. doi:Doi 10.1021/Cr100290v

[12] Larcher, D., & Tarascon, J. (2014). Towards greener and more sustainable batteries for electrical energy storage. *Nature Publishing Group, 7*(January). doi:10.1038/nchem.2085

[13] Li, L., Kim, S., Wang, W., Vijayakumar, M., Nie, Z., Chen, B, Yang, Z. (2011). A stable vanadium redox-flow battery with high energy density for large-scale energy storage. *Advanced Energy Materials*, *1*(3), 394–400. doi:10.1002/aenm.201100008

[14] Skyllas-Kazacos, M. (1986). New All-Vanadium Redox Flow Cell. *Journal of The Electrochemical Society*. doi:10.1149/1.2108706

[15] Rychcik, M., & Skyllas-Kazacos, M. (1988). Characteristics of A New All-Vanadium Redox Flow Battery. *Journal of Power Sources*, *22*(1), 59–67.

[16] Zhang, M., Moore, M., Watson, J. S., Zawodzinski, T. a., & Counce, R. M. (2012). Capital Cost Sensitivity Analysis of an All-Vanadium Redox-Flow Battery. *Journal of the Electrochemical Society*, *159*(8), A1183–A1188. doi:10.1149/2.041208jes

[17] Chan, C. C. (1993). An overview of electric vehicle technology. *Proceedings of the IEEE (Institute of Electrical and Electronics Engineers);(United States)*, *81*(9).

[18] Green, R. C., Wang, L., & Alam, M. (2011). The impact of plug-in hybrid electric vehicles on distribution networks: A review and outlook. *Renewable and Sustainable Energy Reviews*, *15*(1), 544-553.

[19] Grosjean, C., Miranda, P. H., Perrin, M., & Poggi, P. (2012). Assessment of world lithium resources and consequences of their geographic distribution on the expected development of the electric vehicle industry. *Renewable and Sustainable Energy Reviews*, *16*(3), 1735-1744.

[20] Wang, H., Cui, L., Yang, Y., & Casalongue, H. S. (2010). Mn_3O_4-Graphene Hybrid as a High-Capacity Anode Material for Lithium Ion, 13978–13980.

[21] Zhang, S. S. (2006). A review on electrolyte additives for lithium-ion batteries. *Journal of Power Sources*, *162*(July), 1379–1394. doi:10.1016/j.jpowsour.2006.07.074

[22] Lu, L., Han, X., Li, J., Hua, J., & Ouyang, M. (2013). A review on the key issues for lithium-ion battery management in electric vehicles. *Journal of Power Sources*, *226*, 272–288. doi:10.1016/j.jpowsour.2012.10.060

[23] Gifford, P., & Palmisano, J. (1988). An aluminum/chlorine rechargeable cell employing a room temperature molten salt electrolyte. *Journal of the Electrochemical Society*, *135*(13), 650–654.

[24] Lantelme, F., Alexopoulos, H., Devilliers, D., Chemla, M., Electrochimie, L., Pierre, U., & Cedex, F. P. (1991). A Gas Electrode : Behavior of the Chlorine Injection Electrode in Fused Alkali Chlorides. *Journal of Electrochemical Society*, *138*(6), 1665–1671.

[25] Lantelme, F., & Alexopoulos, H. (1989). Role of gas bubbles adsorbed on a carbon electrode: electroreduction of chlorine gas in fused salts. *Journal of Applied Electrochemistry, 19*, 649–656.

[26] Li, Q., & Bjerrum, N. J. (2002). Aluminum as anode for energy storage and conversion : a review, *110*(October 2001), 1–10.

[27] Brabson, G., Fannin, A., King, L., & Seegmiller, D. (1972). Aluminum-Chlorine Battery. *United States AIR FORCE*, (May).

[28] Auborn, J., & Barberio, Y. (1985). An ambient temperature secondary aluminum electrode: its cycling rates and its cycling efficiencies. *Journal of the Electrochemical Society*, *132*(March), 598. Retrieved from http://link.aip.org/link/?JESOAN/132/598/1

[29] Equey, J. F., & Haas, O. (1989). Al/Cl_2 battery with slightly acidic NaCl electrolyte. II. Ti-Ti[Ru oxide chlorine cathodes. *Journal of Applied Electrochemistry, 19*, 147–151.

[30] Zhang, M., Watson, J. S., Counce, R. M., Trulove, P. C., & Zawodzinski, T. A. (2014). Electrochemistry and Morphology Studies of Aluminum Plating/Stripping in a Chloroaluminate Ionic Liquid on Porous Carbon Materials. *Journal of the Electrochemical Society*, *161*(4), D163–D167. doi:10.1149/2.048404jes

[31] Huskinson, B., Rugolo, J., Mondal, S. K., & Aziz, M. J. (2012). A high power density, high efficiency hydrogen–chlorine regenerative fuel cell with a low precious metal content catalyst. *Energy & Environmental Science*, *5*(9), 8690. doi:10.1039/c2ee22274d

[32] Marassi, R., Laher, T. M., Trimble, D. S., & Mamantov, G. (1985). Electrochemical and Spectroscopic Studies of Sulfur in Aluminum Chloride-N-(n-Butyl) Pyridinium Chloride. *Journal of The Electrochemical Society*. doi:10.1149/1.2114180

[33] Marassi, R., Mamantov, G., Matsunaga, M., Springer, S. E., & Wiaux, J. P. (1979). Electrooxidation of Sulfur in Molten $AlCl_3NaCl$(63–37 Mole Percent). *Journal of The Electrochemical Society*, *126*(2), 231. doi:10.1149/1.2129010

[34] Norvell, V. E., Tanemoto, K., Mamantov, G., & Klatt, L. N. (1981). U.V.-Visible and Electron Spin Resonance Spectroelectrochemical Studies of Sulfur Oxidation in

AlCl[sub 3]-NaCl (63/37 m/o) Melt. *Journal of The Electrochemical Society*. doi:10.1149/1.2127603

[35] Wang, G., Zhang, L., & Zhang, J. (2012). A review of electrode materials for electrochemical supercapacitors. *Chemical Society Reviews*, *41*, 797. doi:10.1039/c1cs15060j

[36] Frackowiak, E. (2007). Carbon materials for supercapacitor application. *Physical Chemistry Chemical Physics : PCCP*, *9*(15), 1774–85. doi:10.1039/b618139m

[37] Zhu, Y., Murali, S., Stoller, M. D., Ganesh, K. J., Cai, W., Ferreira, P. J., Ruoff, R. S. (2011). Carbon-based supercapacitors produced by activation of graphene. *Science (New York, N.Y.)*, *332*(6037), 1537–41. doi:10.1126/science.1200770

[38] Karthikeyan, K., Aravindan, V., Lee, S. B., Jang, I. C., Lim, H. H., Park, G. J.,Lee, Y. S. (2010). A novel asymmetric hybrid supercapacitor based on Li2FeSiO 4 and activated carbon electrodes. *Journal of Alloys and Compounds*, *504*(1), 224–227. doi:10.1016/j.jallcom.2010.05.097

[39] Wang, R., Lang, J., Zhang, P., Lin, Z., & Yan, X. (2015). Fast and Large Lithium Storage in 3D Porous VN Nanowires-Graphene Composite as a Superior Anode Toward High-Performance Hybrid Supercapacitors. *Advanced Functional Materials*, n/a–n/a. doi:10.1002/adfm.201404472

[40] Vlad, A., Singh, N., Rolland, J., Melinte, S., Ajayan, P. M., & Gohy, J.F. (2014). Hybrid supercapacitor-battery materials for fast electrochemical charge storage. *Scientific Reports*, *4*, 4315. doi:10.1038/srep04315

[41] Kim, H., Park, K. Y., Cho, M. Y., Kim, M. H., Hong, J., Jung, S. K. & Kang, K. (2014). High-Performance Hybrid Supercapacitor Based on Graphene-Wrapped $Li_4Ti_5O_{12}$ and Activated Carbon. *ChemElectroChem*,*1*(1), 125-130.

[42] Vasanthi, R., Kalpana, D., & Renganathan, N. G. (2008). Olivine-type nanoparticle for hybrid supercapacitors. *Journal of Solid State Electrochemistry*, *12*, 961–969. doi:10.1007/s10008-007-0438-6

[43] Naoi, K., Ishimoto, S., Isobe, Y., & Aoyagi, S. (2010). High-rate nano-crystalline Li4Ti5O12 attached on carbon nano-fibers for hybrid supercapacitors. *Journal of Power Sources*, *195*(18), 6250–6254. doi:10.1016/j.jpowsour.2009.12.104

[44] Yoo, H. D., Shterenberg, I., Gofer, Y., Doe, R. E., Fischer, C. C., Ceder, G., & Aurbach, D. (2014). A Magnesium-Activated Carbon Hybrid Capacitor. *Journal of the Electrochemical Society*, *161*(3), A410–A415. doi:10.1149/2.082403jes

[45] Hudak, N. S. (2014). Chloroaluminate-doped conducting polymers as positive electrodes in rechargeable aluminum batteries. *Journal of Physical Chemistry C*, *118*, 5203–5215. doi:10.1021/jp500593d

[46] Tsuda, T., Kokubo, I., Kawabata, M., Yamagata, M., Ishikawa, M., Kusumoto, S.,Kuwabata, S. (2014). Electrochemical Energy Storage Device with a Lewis Acidic AlBr3-1-Ethyl-3-methylimidazolioum Bromide Room-Temperature Ionic Liquid. *Journal of the Electrochemical Society*, *161*(6), A908–A914. doi:10.1149/2.029406jes

Appendix

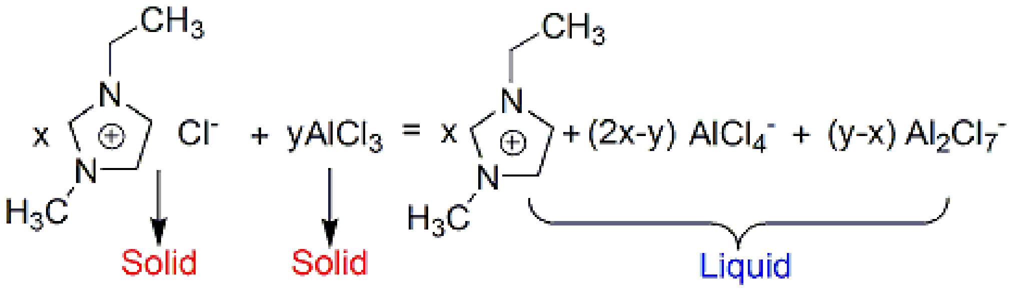

Figure 1. 1 The reaction producing the acidic $AlCl_3$/EMIC chloroaluminate ionic liquid

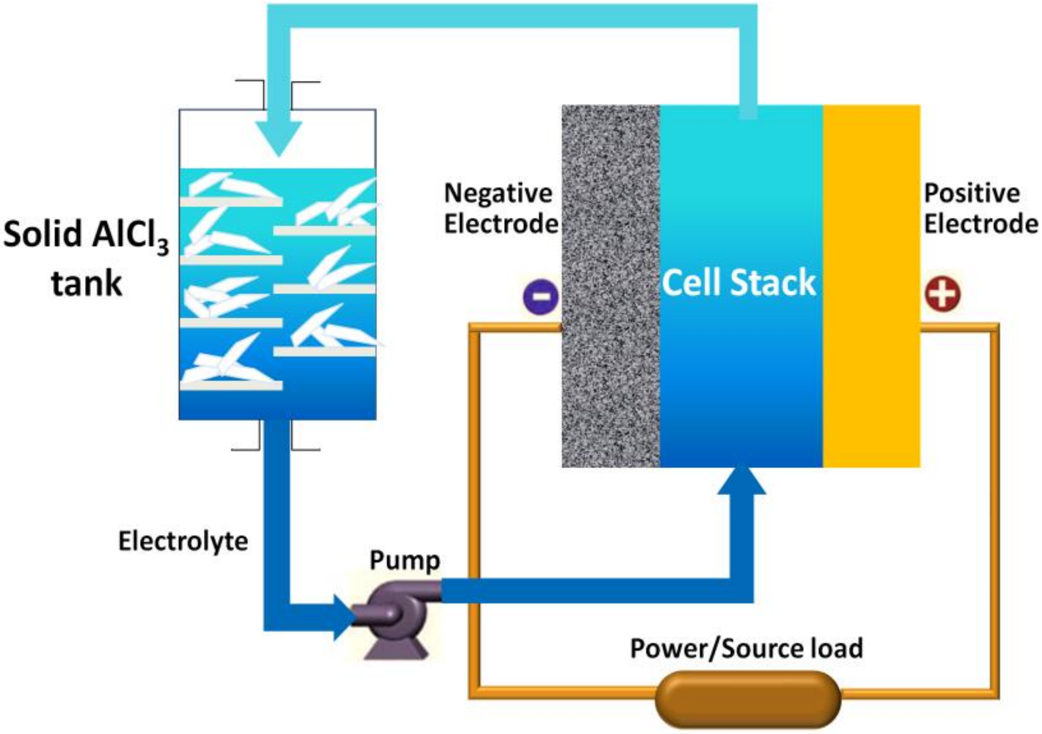

Figure 1. 2 Schematic illustration of ILFB concept

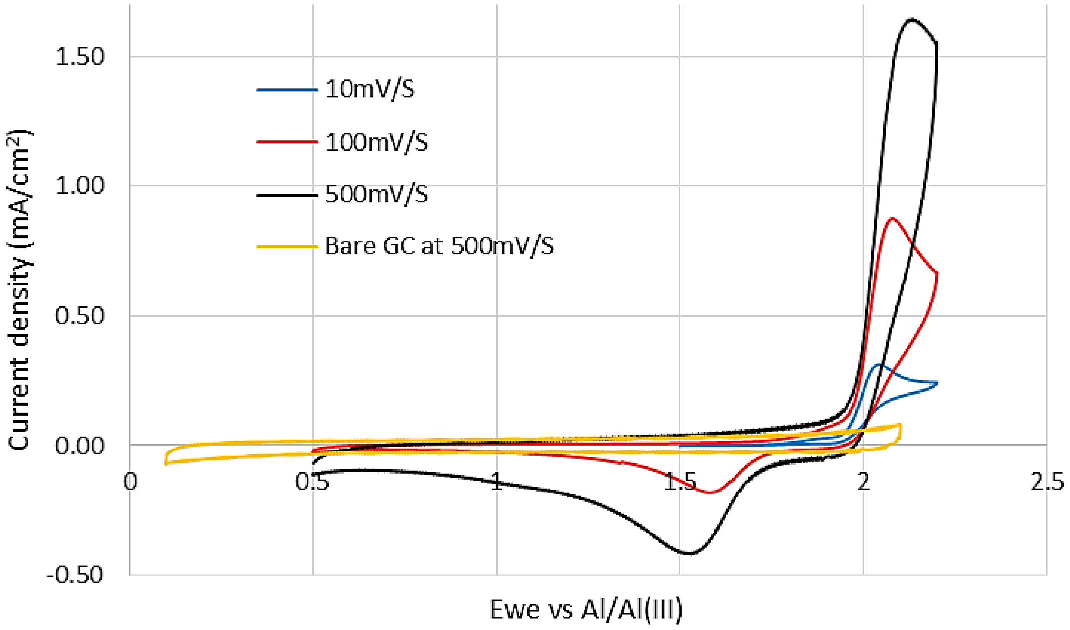

Figure 1. 3 Cyclic voltammograms of sulfur dissolved in 1.5AlCl$_3$: EMIC ionic liquid on glassy carbon electrode

CHAPTER 2

Literature Reviews

2.1 Al based ionic liquid flow battery

2.1.1 General information on ionic liquids

Widely concerned, ionic liquids consisting solely cations and anions are molten salts melting at or below 100 ℃[1-3]. The so-called “red oil” occurring in Friedel-Crafrs reaction is the first documented ionic liquid observed in mid 19th century. It results from the sigma complex, a stable intermediate cation in Friedel-Crafts reaction, and $Al_2Cl_7^-$ anions. (see the structure formula in Figure 2.1). In the history of ionic liquid researches and developments, such room temperature molten salts can be classified into three groups:

(a) $AlCl_3$ and organic salts based ionic liquids, its representatives of organic cations are 1-butylpyridinium (BP^+), 1-ethyl-3methylimidazolium (EMI^+) and their derivatives

(b) the same as organic cations as (a) but with anions, eg. BF_4^-, PF_6^- and SbF_6^-

(c) the same as organic cations as (a) but with organic anions, eg. $CF_3SO_3^-$, $(CF_3SO_2)_2N^-$

The latest groups of ionic liquids are considered with less sensitivity to moisture under ambient condition and called air and water stable ionic liquid[3]. Ionic liquids have attracted great research interests since 1970s when Osteryoung[4] and Wilkes[5] found organic cations for electrochemical stable $AlCl_3$ based ionic liquids, i.e. chloroaluminate.

The advantages of ionic liquids are wide electrochemical windows (>4V)[1], extremely low vapor pressure and good conductivity (10^{-3}-10^{-2} S/cm)[6]. These properties bring ionic liquids to excellent supporting electrolytes for electrodeposition of metal and alloy and battery applications. Nowadays, a series of metals, Al, Ti, Ta, Nb, Mo, W, that are impossible to electrodeposit in aqueous electrolyte, can be electrolyzed under low temperature by using ionic liquid as the electrolytes. Even alloy, semiconductors and nanostructured metals can be electrodeposited in ionic liquid and these propel the development of several industries[7]. The other application area of ionic liquid focuses on the energy management. The safety concerns for applications of lithium battery into electrical vehicles bring the attention to the ionic liquids because of its negligible vapor pressure and non-flammability.

2.1.2 Chloroaluminates

In the late 1970s and early 1980s, room temperature ionic liquids composed of aluminum chloride and either N-1-butylpyridinium chloride (BPC)[8] or 1-methyl-3-ethylimidazolium chloride (EMIC)[9] have been found by Osteryoung group and Wilkes group. They are generally called as chloroaluminate. Reactions between the organic chloride (RCl) and $AlCl_3$ are written as the followings.[10]

$$\begin{gathered} x\mathrm{RCl} + y\mathrm{AlCl_3} \rightarrow y\mathrm{RAlCl_4} + (x - y)\mathrm{RCl} \\ \mathrm{MC} = y/x < 1 \end{gathered} \qquad (1)$$

and

$$\begin{gathered} x\mathrm{RCl} + y\mathrm{AlCl_3} \rightarrow (2x - y)\mathrm{RAlCl_4} + (y - x)\mathrm{RAl_2Cl_7} \\ 1 < \mathrm{MC} < 2 \end{gathered} \qquad (2)$$

Reactions (1) and (2) correspond to the formation of basic and acidic chloroaluminate melt respectively. When the molar ratio between RCl and $AlCl_3$ is exactly 1, the neutral chloroaluminate will formed as pure salt R^+ $AlCl_4^-$. These melts involve the anion equilibrium reaction, showed in reaction (3), with the equilibrium constant around 10^{-17}

[11]. The aluminum can only be electrodeposited in the acidic melt and butylpyridinium can be reduced by aluminum.[12]

$$2AlCl_4^- \rightleftarrows Cl^- + Al_2Cl_7^- \qquad (3)$$

As the good electrochemical stability of imidazolium cation, this series of cations has been successfully applied into the Al electrodeposition research at room temperature.

2.1.3 Synthesis and preparation methods

Wilkes and his colleagues are the first to report the synthesis and electrochemical research on dialkylimidazolium chloroaluminate melts[9] (see Figure. 2.2). Before the synthesis performed these reagents must be purified. 500g of 1-methylimidazole (99%, Aldrich) added with CaH_2 must be refluxing (~90 ℃) for 2 hours while distillation purification under vacuum. Ethyl chloride can be used and purchased directly from Aldrich (chloroethene >99.7%). The pressure bottle (withstand >6atm) is the place for reaction between 1-methylimidazole and ethyl chloride. The purified 1-methylimidazole should be put into the pressure bottle with following pouring chloroethene. The reation takes from 10 days to two weeks at room temperature. Approximately 500ml acentonitrile (Aldrich, >99.9%) should be added into the pressure bottle after the upper layer of liquid is poured off. Ethyl acetate will be used to precipitate EMIC in glovebox filled with Argon. When the acentonitrile/EMIC hits the ethyl acetate, EMIC will precipitate out. The precipitated EMIC will be dried under vacuum for at least one week before starting the preparation of chloroaluminate.[8-9]

The purification of $AlCl_3$ should be performed in a heavy wall glass tube by $AlCl_3$ sublimation process at above 200 ℃. $AlCl_3$ (Fluka, >99%) and 1g NaCl will added into the heavy wall glass tube in the glovebox. Cutted Al wires will also be placed in the tube. The tube should be placed into a furnace at 80 ℃ for 4 hours under vacuum. Then seal the glass tube by torch and the temperature will be increased to 200 ℃ for $AlCl_3$ sublimation. By slowly pulling the glass tube out of the furnace, the sublimed $AlCl_3$ will be cooled and form crystal at the top of the glass tube.[8-9] The chloroaluminate can be prepared by slowly adding imidazolium chloride on $AlCl_3$ crystal. After the formation of chloroaluminate melt, stirring the melt for good mixing.

2.1.4 Physical properties

The imidazolium chloroaluminates show their excellent physical properties, such viscosity, conductivity, melting temperature, for potential electrolytes in the battery applications. Wilkes and his colleagues investigated the physical properties of a series of imidazolium chloroaluminate in aspects of phase transitions, densities, electrical conductivities and densities in 1983[6]. The phase diagram for $AlCl_3$/EMIC is showed as the followings. The melting/freezing point for the chloroaluminate is highest at the neutral melts. For all range of $AlCl_3$/EMIC melt, the freezing points are below 10 ℃ and the glass transition points are especially lower than -50 ℃ (see Figure 2.3). When the molar fraction of $AlCl_3$ is over 66.7%, the melting points incline significantly. The details of phase transition for other imidazolium chloroaluminate are also reported by Wilkes's paper.

The densities do not vary much based on the molar fraction of $AlCl_3$. The reported density of $AlCl_3$/EMIC melts are in the range of 1.15-1.40g/cm^3 at 60 ℃. The higher molar fraction of $AlCl_3$, the higher density of chloroalumiante. At lower temperature, the density will increase. The specific conductivity is an important index indicating the excellent electrolyte for battery applications. Similarly to the rule in phase transition, the conductivity of $AlCl_3$/EMIC melt is highest at neutral chloroaluminate. The larger cation size seems to result in the lower specific conductivity. For the acidic $AlCl_3$/EMIC melt, the specific conductivity is in the range of 0.05-0.075 S/cm at 100 ℃ (see Figure 2.4). The viscosity of $AlCl_3$/EMIC melt decreases with the increase of $AlCl_3$ mole fraction. For the acidic chloroaluminate melts, the viscosity is less than 25cp at room temperature and become even lower when increasing the temperature (see Figure 2.5). The viscosity seems less sensitive to the melt cation structure.

The enthalpies of solution of $AlCl_3$ or EMIC in $AlCl_3$/EMIC melt are measured in Figure 2.6.[13] Dissolution of $AlCl_3$ into the acidic $AlCl_3$/EMIC melt is favored by temperature because of the endothermic reaction. The enthalpies of solution of $AlCl_3$ (ca. 10kJ/mol) do not vary on acidity of $AlCl_3$/EMIC melts. However, the large enthalpies of solution of EMIC in the acidic $AlCl_3$/EMIC melt indicate a strong exothermic reactions (65-78 kJ/mol). As the charging process of ILFB is equivalent to a process of consumption of $AlCl_3$ in the acidic $AlCl_3$/EMIC melt, the ILFB system may experience an exothermic process. While during the discharging process, the ILFB may seem an endothermic process.

2.1.5 Aluminum deposition/dissolution in ionic liquids

The primary research interests on Al electrodeposition in ionic liquids derive from the need for reduction of energy consumption during Al electrolysis. Until now the electrolysis of Aluminum in industry is still employing the Hall-Heroult Process. The electrolyte consisting of the Al_2O_3 and Na_3AlF_6 molten melts at 1000 ℃ is used in this process. Aluminum ions are reduced to aluminum metal at carbon cathode and the oxygen is produced at anode. Though Hall-Heroult Process have focused on reducing the melting point of Al_2O_3, the energy consumption is still as high as 13kWh/kg Al. However, by using imidazolium chloroaluminate for the electrolysis of Al, the energy consumption can be reduced by half compared with that in current industrial electrowinning.[14] For the aluminum electrodeposition in chloroaluminate, Carlin in 1992 is the first one to study its nucleation and morphology by fundamental electrochemical methods.[15] The half reaction for Al deposition in chloroaluminate melts is showed here.

$$4Al_2Cl_7^- + 3e^- \leftrightarrow Al + 7AlCl_4^-$$

Chronoamperometry is applied to investigate the process of nucleation formation. Scharifker and Hills's theoretical nucleation model is proposed to compare with experimental data for verification of nucleation process.[16] This method to verify the nucleation process has been wildly employed later. [17-21]

Instantaneous nucleation $(i/i_m)^2 = 1.9542(t/t_m)^{-1}\{1 - \exp[-1.2564(t/t_m)]\}^2$

Progressive nucleation $(i/i_m)^2 = 1.2254(t/t_m)^{-1}\{1 - \exp[-2.3367(t/t_m)^2]\}^2$

t_m indicates the when the current peak appears while i_m represents the peak current density in the current transient. It has been well accepted that the nucleation process of Al in chloroaluminate melts is a three-dimensional nucleation growth with diffusion control process. The nucleation growth of Al on Tungsten and glassy carbon is progressive nucleation and instantaneous nucleation, respectively. The underpotential deposition (UPD) of Al on Pt and W has been observed. The UPD is a process involving the formation of mono-molecular layer of Al on the substrate at less negative potential than that on Al. The plating/striping efficiency approaches to 100% indicating the production of stable and adherent Al on W substrate.

2.1.6 The development of Cl_2 cathode

The limitation of Al/Cl_2 rechargeable battery has always been considered as the irreversible reaction of Cl_2 reduction. Some researchers have proposed to utilize the mechanism of Cl_2 intercalation/ deintercalation in the graphite electrode.[22,23] However, the graphite has the limited storage capacity for Cl_2 intercalation ($C_{80}Cl$) at room temperature leading to low specific energy ca. 64Wh/kg.[24] Additionally, the use of Cl_2 intercalation/deintercalation mechanism may potentially bring down the battery performance related to current density. So the chlorine diffusion electrode should be a feasible design for the cathode. Lantelme and Alexopoulos investigate the role of Cl_2 bubbles for the Cl_2 reduction on vitreous carbon electrode in LiCl-KCl eutectic mixture.[25-26] They found that two regimes of Cl_2 reduction have been detected: for small overpotentials the electrode response obeys the classical laws of linear diffusion, for larger overpotentials the electrode behavior involves the gas coming from the bubbles. They proposed a model for Cl_2 redcution by diffusion control: dissolution of chlorine around a gas bubble, diffusion in the electrolyte, charge transfer and chloride ion migration. It is indicated that the largest part of the reaction occurs near the triple contact interface. For these alkyl molten salts system chlorine reduction do not need the help of catalysts. However, in the room temperature chloroaluminate melt, the chlorine reduction is required for the catalyst. Anderson and Taylor discussed some catalysts performance for the H_2/Cl_2 fuel cell. High surface area carbon black, carbon supported platinum (0.5mg Pt/cm^2) and Pb-Ru mixed metal oxide have been investigated to catalyze the Cl_2 reduction.[27] The polarization behavior for carbon supported platinum electrode is low (70mV at 1A/cm^2) compared with that of oxygen (see Figure 2.7). This indicates the feasibility of Cl_2 diffusion electrode used in Al/ Cl_2 rechargeable battery. By bubbling Cl_2 out of system and collecting them in a tank, the energy density and power density can both be significantly improved. Recently Compton and his colleagues reported the electrochemical reduction of Cl_2 several room temperature ionic liquid. The adsorption of Cl_2 on platinum electrode surface is contributed to an unusual observation of voltammetry where current decreases with increasing voltage scan rates.[28]

2.1.7 Chlorination of electrolyte

Although the design of storing Cl_2 into a tank and Cl_2 diffusion electrode is promising to improve the battery performance, Cl_2 can actually easily substitute the H group on the 2nd carbon of 1-ethyl-3-methylimidazolium cation. The half life of chlorine in $AlCl_3$/EMIC melts is only ca. 1 minute.[29] Though in pyridinium chloroaluminate system Cl_2 is relatively stable with the cation (half life of chlorine over 30mins), the pyridinium chloroaluminate can react with Al. The outcome of chlorination of imidazolium cation is the introduction of proton leading to hydrogen evolution and changes in physical properties of chloroaluminate melts. Additionally, the H^+ in acidic chloroalumite can result in the Bransted superacidity.[30-31] Therefore, to build an Al/Cl_2 rechargeable battery with Cl_2 diffusion electrode, new cations for chloroaluminate should be synthesized. Gifford and Palmisano used 1,2-dimethyl-3-propylimidazolium chloride (DMPMC) instead of EMIC for the electrolyte but bigger size of cation can sacrifice the physical properties of chloroaluminate, such as specific conductivity, viscosity and diffusivity leading to larger ohmic loss and lower current density. In 1993 Bjerrum group proposed the molten triazolium chloride system with specific conductivity between $4.02x10^{-5}$ and $7.78x10^{-2}$ S/cm in the range from -31 to 123 ℃ respectively.[32-33] This triazolium cation can be a promising candidate because of less reactivity with Cl_2.

2.2 Hybrid supercapacitor

Electric double-layer capacitor (EDLC), also known as supercapacitor or ultracapacitor, is an electric energy storage device that reversibly adsorb/desorbs ions by the electrostatic force on the electrode/electrolyte interface. The mechanism of EDLC result in the high power density, high energy efficiency and the excellent cycle ability. The EDLC usually has a symmetric structure with high surface area carbon materials on both electrodes. The capacitance of electrode materials which is proportional to the surface area and the electrochemical window of electrolytes determine the maximum energy density, while the low equivalent inner resistance leads to the power density of EDLC one order magnitude higher than that of LIB. However, for example, the EDLC using aqueous electrolyte usually has energy density less than 5Wh/kg. Thus, more and more researches focus on the ionic liquid electrolytes whose electrochemical windows can be over 5V.

Therefore, the emerging development and expansion of EVs requires a new energy storage device that merges advantages from both LIB and EDLC. The hybrid battery/ EDLC gradually attracts more scientific attention than ever. Generally, the hybrid battery/ EDLC has an asymmetric structure with a battery electrode where the Faradaic reaction occurs and an EDLC electrode which provides the interface to form electric double-layer. Typically, the lithium rich compound, such as $Li_4Ti_5O_{12}$, $LiMn_2O_4$, Li_2FeSiO_4 and $LiCoPO_4$, are chosen as the battery electrode materials. However, the slow kinetics and low columbic efficiency of Li de/intercalation do not match the fast reversible de/adsorption of ions on the electrode/electrolyte interface. Among these battery electrode candidates, only nano-size $Li_4Ti_5O_{12}$ growing on the carbon nanofiber shows its compatibility with the EDLC electrode and can be charged/discharged at high rate with the excellent cycle life. However, we may underestimate the potential application of metal electrodeposition/dissolution in the field of the hybrid battery/EDLC. The reversibly electrodeposition/dissolution of multivalent metals, such as Magnesium (Mg) and Aluminum (Al) at room temperature has become feasible in special prepared non-aqueous electrolytes. The electrolyte contains phenyl-magnesium-chloride

(PhMgCl)/THF has been applied for Mg deposition at room temperature without dendrite formation.

2.3 Characterization techniques

2.3.1 Electrochemistry

Cyclic voltammetry is the basic electrochemical method for qualifying the electrochemical reactions and description of reaction mechanisms. The voltammetry cell generally include three electrodes: working electrode, reference electrode and counter electrode. For the electrochemical experiments in chloroaluminate melt the reference electrode is usually a fritted tube with Al wire immersed into molar ratio 1.5:1 $AlCl_3$/EMIC melts. In convenience of measuring the overpotential of electrochemical reaction the reference electrode can be the Al wire immersed directly into the chloroaluminate electrolyte. The counter electrode is usually used as spiral Al wires immersed directly into the electrolyte. Through CV testing we can acquire information related to formal potential and reversibility of redox couples.

Rotating disk electrode technology can control the thickness of diffusion layer by rotating rate of the electrode and thus the steady-current is controlled by solution flow instead of the diffusion. It has been widely applied into the investigation of reaction mechanism related to redox chemistry and transport coefficient such as the ion diffusivity.

Chronoamperometry is a powerful electrochemical method for investigating the nucleation process of metal on the substrate. By controlling the potential on the working electrode versus the reference electrode, metals can be electrodeposited on the substrate at difference potential. The current transient can illustrated the process of nucleation and how the diffusion zones of nuclei change.

2.3.2 Materials science

A scanning electron microscopy (SEM) is a characterization technology for investigating the morphology and composition of the sample. By scanning a sample with a beam of electron, the signals from interaction of electron beam with atoms is recorded and used to map the surface morphology of the sample. The resolution of SEM can be at nano scale. SEM equipped with energy dispersive x-ray spectrometer (EDS) can analyze the composition of the sample. X-ray diffraction is a common characterization technology for revealing the crystal structure, chemical composition and physical properties. Fourier transform infrared spectroscopy (FTIR) is a characterization technique to obtain an infrared spectrum of absorption, emission, photoconductivity or Raman scattering of a solid, liquid or gas.

Reference

[1]. Endres, F. Ionic liquids: Solvents for the electrodeposition of metals and semiconductors. *ChemPhysChem* **3**, 144-145 (2002).

[2]. Wilkes, J.S. A short history of ionic liquids—from molten salts to neoteric solvents. *Green Chemistry* **4**, 73-80 (2002).

[3]. Endres, F. & El Abedin, S.Z. Air and water stable ionic liquids in physical chemistry. *Physical Chemistry Chemical Physics* **8**, 2101-2116 (2006).

[4]. Robinson, J. & Osteryoung, R.A. Electrochemical and Spectroscopic Study of Some Aromatic-Hydrocarbons in the Room-Temperature Molten-Salt System Aluminum Chloride-N-Butylpyridinium Chloride. *Journal of the American Chemical Society* **101**, 323-327 (1979).

[5]. Wilkes, J.S., Levisky, J.A., Wilson, R.A. & Hussey, C.L. Dialkylimidazolium Chloroaluminate Melts - a New Class of Room-Temperature Ionic Liquids for Electrochemistry, Spectroscopy, and Synthesis. *Inorganic Chemistry* **21**, 1263-1264 (1982).

[6]. Fannin, A.A., Wilkes, J.S., Floreani, D.A. *et al.* Properties of 1,3-Dialkylimidazolium Chloride-Aluminum Chloride Ionic Liquids. 2. Phase Transitions , Densities , Electrical Conductivities , and Viscosities. *Journal of physica Chemistry* **88**, 2614-2621 (1984).

[7]. Endres, F., MacFarlane, D., & Abbott, A. (Eds.). (2008). *Electrodeposition from ionic liquids*. John Wiley & Sons.

[8]. Robinson, J. & Osteryoung, R.A. Electrochemical and Spectroscopic Study of Some Aromatic-Hydrocarbons in the Room-Temperature Molten-Salt System Aluminum Chloride-N-Butylpyridinium Chloride. *Journal of the American Chemical Society* **101**, 323-327 (1979).

[9]. Wilkes, J.S., Levisky, J.A., Wilson, R.A. & Hussey, C.L. Dialkylimidazolium Chloroaluminate Melts - a New Class of Room-Temperature Ionic Liquids for Electrochemistry, Spectroscopy, and Synthesis. *Inorganic Chemistry* **21**, 1263-1264 (1982).

[10]. Lipsztajn, M. & Osteryoung, R.A. Electrochemistry in Neutral Ambient-Temperature Ionic Liquids .1. Studies of Iron(Iii), Neodymium(Iii), and Lithium(I). *Inorganic Chemistry* **24**, 716-719 (1985)

[11]. Karpinski, Z.J. & Osteryoung, R.A. Potentiometric Studies of the Chlorine Electrode in Ambient-Temperature Chloroaluminate Ionic Liquids - Determination of Equilibrium-Constants for Tetrachloroaluminate Ion Dissociation. *Inorganic Chemistry* **24**, 2259-2264 (1985).

[12]. Gale, R.J. & Osteryoung, R.A. Potentiometric Investigation of Dialuminum Heptachloride Foramtion in $AlCl_3$-1-Butylpyridinium Chloride Mixtures. *Inorganic Chemistry* **18**, 1603-1605 (1979).

[13]. Keil, P., & König, A. Enthalpies of solution of 1-ethyl-3-methyl-imidazolium chloride and aluminum chloride in molten chloroaluminate ionic liquids. *Thermochimica Acta*, ***524***(1-2), 202–204. (2011)

[14]. Zhang, M.M., Kamavaram, V. & Reddy, R.G. New electrolytes for aluminum production: Ionic liquids. *Journal of the Minerals Metals & Materials Society* **55**, A54-A57 (2003).

[15]. Carlin, R.T., Crawford, W. & Bersch, M. Nucleation and Morphology Studies of Aluminum Deposited from an Ambient-Temperature Chloroaluminate Molten Salt. *Journal of Electrochemical Society* **139**, 2720-2727 (1992).

[16]. Scharifker, B. & Hills, G. THEORETICAL AND EXPERIMENTAL MULTIPLE NUCLEATION STUDIES OF. *Electrochimica Acta* **28**, 879-889 (1982).

[17]. Jiang, T., Brym, M.J.C., Dube, G., Lasia, A. & Brisard, G.M. Electrodeposition of aluminium from ionic liquids: Part II - studies on the electrodeposition of aluminum from aluminum chloride (AICl(3)) - trimethylphenylammonium chloride (TMPAC) ionic liquids. *Surface & Coatings Technology* **201**, 10-18 (2006).

[18]. Lee, J., Miller, B., Shi, X. & Kalish, R. Aluminum deposition and nucleation on nitrogen-incorporated tetrahedral amorphous carbon electrodes in ambient temperature chloroaluminate melts. *Journal of Electrochemical Society* **147**, 3370-3376 (2000).

[19]. Kan, H.M., Wang, Z.W., Wang, X.Y. & Zhang, N. Electrochemical deposition of aluminum on W electrode from AlCl3-NaCl melts. *Transactions of Nonferrous Metals Society of China* **20**, 158-164 (2010).

[20]. Sun, I.W. & Lin, Y.F. Electrodeposition of zinc from a Lewis acidic zinc chloride-1-ethyl-3-methylimidazolium chloride molten salt. *Electrochimica Acta* **44**, 2771-2777 (1999).

[21]. Jiang, T., Chollier Brym, M.J., Dubé, G. et al. Electrodeposition of aluminium from ionic liquids: Part I—electrodeposition and surface morphology of aluminium from aluminium chloride (AlCl3)–1-ethyl-3-methylimidazolium chloride ([EMIm]Cl) ionic liquids. *Surface and Coatings Technology* **201**, 1-9 (2006).

[22]. Gifford, P. An aluminum/chlorine rechargeable cell employing a room temperature molten salt electrolyte. *Journal of the Electrochemical Society* **135**, 650-654 (1988).

[23]. Compton, R.G., Lowe, E.R. & Banks, C.E. Gas sensing using edge-plane

pyrolytic-graphite electrodes: electrochemical reduction of chlorine. *Analytical and Bioanalytical Chemistry* **382**, 1169-1174 (2005).

[24]. S. Maximovitch, G. Bronoel, N. T. Nghia, and J. Sarra- din, in "*Power Sources 6*," D.H. Collins, Editor, p. 751, Academic Press, London (1977).

[25]. Lantelme, F. & Alexopoulos, H. Role of gas bubbles adsorbed on a carbon electrode: electroreduction of chlorine gas in fused salts*. *Journal of Applied Electrochemistry* **19**, 649-656 (1989).

[26]. Lantelme, F., Alexopoulos, H., Devilliers, D. & Chemla, M. A gas electrode: behavior of the chlorine injection electrode in fused alkali chlorides. *Journal of the Electrochemical Society* **138**, 1665-1670 (1991).

[27]. Anderson, B., Taylor, E.J. & Gerald Wilemski A high performance hydrogen / chlorine space power applications fuel cell for. *Journal of Power Sources* **47**, 321-328 (1994).

[28]. Huang, X.-J. *et al.* Electroreduction of Chlorine Gas at Platinum Electrodes in Several Room Temperature Ionic Liquids: Evidence of Strong Adsorption on the Electrode Surface Revealed by Unusual Voltammetry in Which Currents Decrease with Increasing Voltage Scan Rates. *The Journal of Physical Chemistry C* **112**, 19477-19483 (2008).

[29]. Karpinski, Z.J. & Osteryoung, R.A. Potentiometric Studies of the Chlorine Electrode in Ambient-Temperature Chloroaluminate Ionic Liquids Determination of Equilibrium-Constants for Tetrachloroaluminate Ion Dissociation. *Inorganic Chemistry* **24**, 2259-2264 (1985).

[30]. Smith, G.P., Dworkin, A.S., Pagni, R.M. & Zingg, S.P. Bransted Superacidity of HC1 in a Liquid Chloroaluminate . A1C13- 1 -Ethyl-3-methyl- 1H-imidazolium Chloride. *Journal of American Chemitry Society* 525-530 (1989).

[31]. Noel, M. a. M., Trulove, P.C. & Osteryoung, R. a. Removal of protons from ambient-temperature chloroaluminate ionic liquids. *Analytical Chemistry* **63**, 2892-2896 (1991).

[32]. Vestergaard, B. Molten Triazolium Chloride Systems as New Aluminum Battery Electrolytes. *Journal of The Electrochemical Society* **140**, 3108 (1993).

[33]. Li, Q. & Bjerrum, N.J. Aluminum as anode for energy storage and conversion : a review. *Journal of power sources* **110**, 1-10 (2002).

Appendix

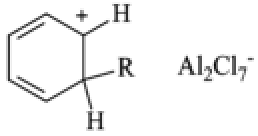

Figure 2. 1 The heptachlorodialuminate salt for $AlCl_3$-catalyzed reactions

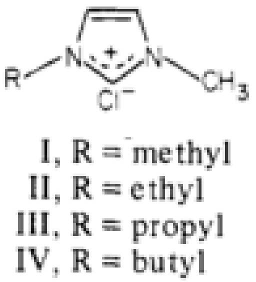

Figure 2. 2 Dialkylimidazolium cation for chloroaluminate

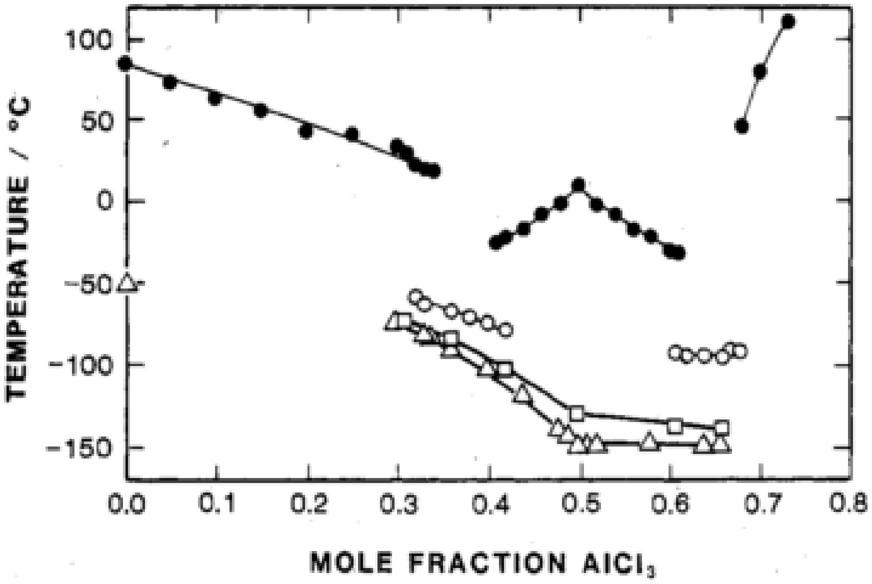

Figure 2. 3 Phase diagram for $AlCl_3$/EMIC: (●) melting point and freezing point; (○) experimental glass transition points[6]

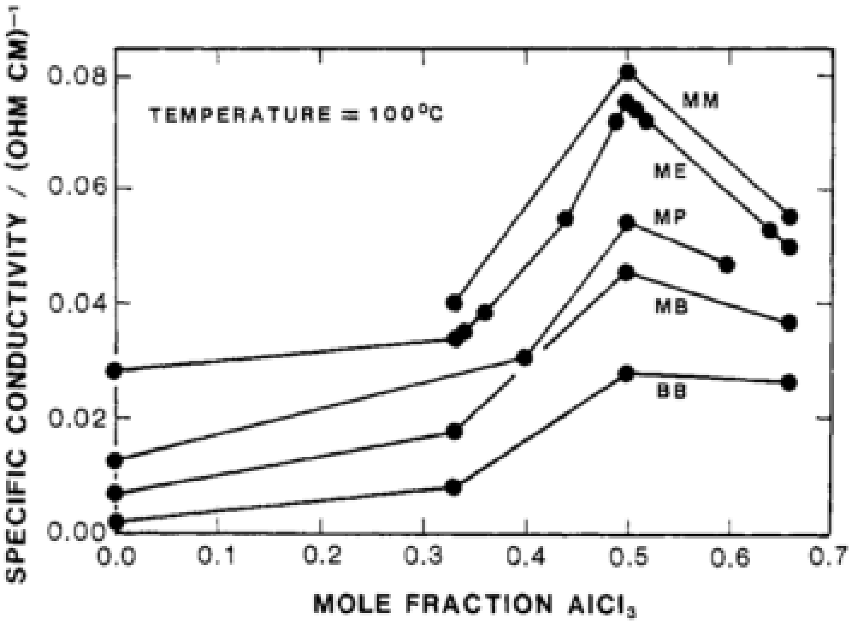

Figure 2. 4 Dependence of specific conductivity on $AlCl_3$/EMIC melt composition at 100 ℃[6]

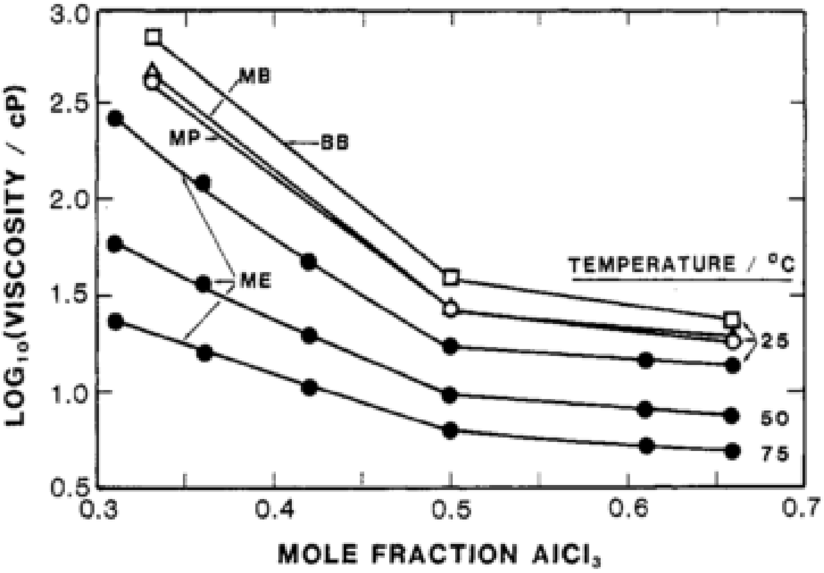

Figure 2. 5 Dependence of absolute viscosity on $R_1R_3ICl-AlCl_3$ melt composition and temperature.[6]

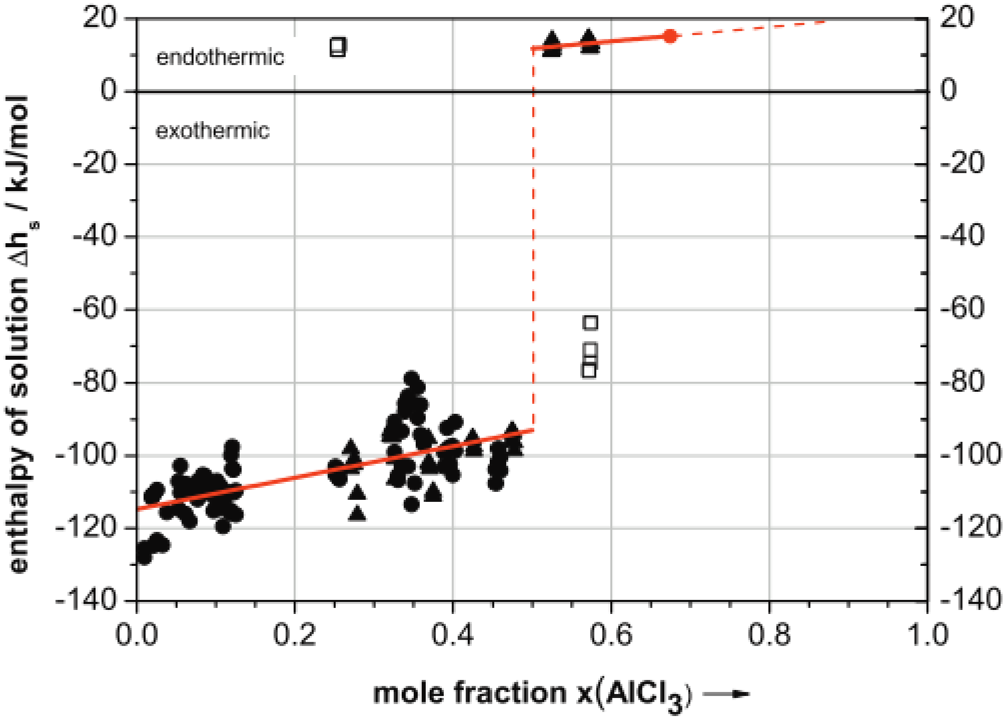

Figure 2. 6 Enthalpies of solution of EMIC at T = 323 K (square) and enthalpies of solution of $AlCl_3$ at T = 323 K (triangle) and 363 K (circle) in chloroaluminate melts with different mole fractions x($AlCl_3$); linear regression of enthalpies of solution of $AlCl_3$.[13]

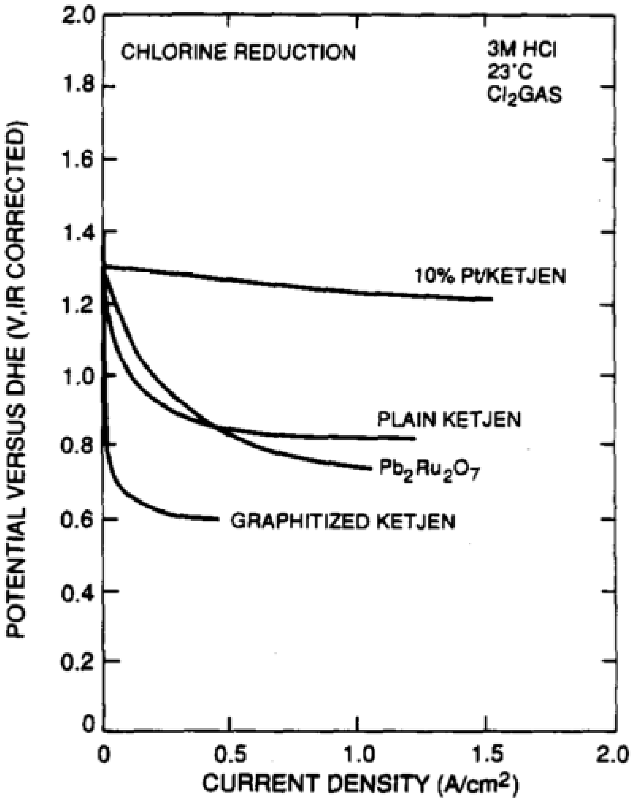

Figure 2. 7 Chlorine-reduction polarization curve in 3 M HCl at 23 ℃ with (a) 10% platinum/Ketjen; (b) plain Ketjen (c) graphitized Ketjen, and (d) lead-ruthenium oxide.[27]

CHAPTER 3

Capital Cost Sensitivity Analysis of an All-Vanadium Redox-Flow Battery

3.1 Introduction

Redox flow batteries (RFBs) are being developed for use in large-scale electrical grid storage. There are a number of potential benefits that could be provided by large-scale electrical grid storage RFBs. RFBs could be used to store energy during periods of low demand and supply power during periods of peak demand, forgoing the need for additional expensive investments in generating capacity to meet peak demand. Also, electrical energy generated from renewable resources such as wind or solar could be stored in a RFB for use when supplies of renewable power are limited. RFBs could help stabilize transmission lines, act as an uninterruptable power supply for sensitive equipment, and improve service reliability for customers [1]. In spite of research and development over the past few decades, however, practical implementation is hampered by various cost and performance issues typical of an immature state of development of the technology.

One critical factor for competitiveness of this technology is its installed (capital) cost. ARPA-e targets capital costs of \$100/kWh installed, an aggressive target for lowering the capital costs. Analysis is needed to consider if it is even feasible to meet this kind of target with current technology and to evaluate the changes that are most likely to result in large reductions in capital cost. Thus, economic analyses can provide focus to research activities. For example, the trade-off in cost between factors primarily associated with energy density (redox couples, achievable concentrations of electrolyte solutions) and electrical power density (electrochemical converter performance) will provide insight into appropriate priorities for different deployment scenarios.

In this work, we present an analysis of the cost factors associated with vanadium redox flow batteries (VRBs), which are widely viewed as a possible target technology. We previously analyzed VRB systems using chemical process engineering design strategies [2,3]. The major variables affecting the capital costs are identified.

3.2 Background

A VRB is a system utilizing a redox reaction to both charge and discharge the battery by means of a flow of the reactants through the electrochemical cells, see Figure 3.1. Each cell is divided into half-cells by means of a membrane permeable to protons, while the cell itself contains electrodes that collect or provide electrons for the redox reaction. The cells are arranged in stacks and connected in series to increase the electrical potential of the VRB, while stacks are connected in parallel to increase the current capability of the VRB. The redox reaction for the VRB is provided by two solutions of vanadium ions pumped through the cell stacks from storage tanks external to the stack. The tanks store the solutions and, thus, the energy supply for the stack. The solution pumped through the negative half-cells contains V^{2+} and $^{V3+}$ ions and the solution pumped through the positive half-cell contains V^{4+} and V^{5+} ions. Vanadium is dissolved in sulfuric acid to a typical concentration of one molar. The redox reactions occurring in the half cells while the battery is being charged are:

Negative Half-Cell: $V^{3+} + e^{-} \leftrightarrow V^{2+}$ (1)

Positive Half-Cell: $VO^{2+} + H^{2}O \leftrightarrow VO_2^{+} + 2H^{+} + e^{-}$ (2)

During discharge, the reactions are simply the reverse of these reactions.

The approach presented here for evaluating the sensitivity of the overall costs of a VRB to the selected design variables is taken, in part, from a paper by Moore, et al. in which a hierarchical method is used in the design process [4]. The core of this method is the categorization of the capital costs into identifiable areas that are examined in a step-by-step procedure, with each step building upon the previous step. The categories presented for analysis of the capital costs are:

Costs that scale in proportion to the power capacity;

Costs that scale in proportion to the energy capacity;

Costs that do not scale with size.

The first two categories constitute the greater portion of the capital costs of the battery and will be the areas in which the cost sensitivity analysis will focus.

The electrical power capacity is determined by the design of the cell stacks. The amount of electric current produced by a cell is dependent on the current density of the cell and the active electrode area. The cells in a stack are assumed to be identical, however, and the cost model presented here does not allow for any change in current through a stack. The desired voltage is achieved by selecting the appropriate number of cells in a stack. The electrical potential of a stack is increased when the cells in a stack are connected in series. Each cell adds to the electrical potential of the stack by the value of the added cells electrical potential. The desired total current is achieved by changing the area of the cells in a stack or by connecting additional cell stacks in parallel.

The electrical power of the VRB is dependent on the overall number of cells in the battery. The current capacity of a cell, thus the current capacity of a stack, is calculated by multiplying the current density of the electrode by the active electrode area. The current capacity of the VRB is calculated by multiplying the current capacity of a cell by the number of stacks, and the electrical potential of the battery is calculated by multiplying the electrical potential of one cell by the number of cells in a stack. The electrical power is then the product of the current capacity and the electrical potential.

The energy capacity of the VRB is determined by the concentration of vanadium and the volume of the process solutions. For a fixed concentration of vanadium, the greater the volume of the solutions, the more energy can be stored by the battery. Larger volumes will be required for battery designs that require a higher electrical energy capacity or a longer cycle time at a given power. An important consideration associated with the energy capacity of the VRB is the state of charge (SOC). The SOC defines the concentrations of the reactants and the products at any given point in time and represents the amount of energy the VRB is storing relative to its full capacity[6]. The SOC of the VRB is considered because the electrical potential of the battery is dependent on the SOC. This is illustrated by Figure 2, which shows the relationship of the electrical potential to the SOC [7]. While the graph of the cell potential in Figure 3.2 approaches the boundaries asymptotically the middle of the graph is approximately linear. It is therefore advantageous to set the limits of the SOC for the VRB within this middle region, where the dramatic drop-off or increase in electrical potential can be avoided. In addition, narrowing the limits of the SOC provides a smaller range of fluctuation in the power of the VRB. Any change in the SOC during a pass of solution through the cell stack will result in reduced efficiencies since the conducting electrodes will produce only the lower voltage from the exit conditions. To minimize the inefficiencies, the solution flow rates were maintained sufficiently high so that only incremental changes in the SOC occurred during a single pass through the stack. Thus, the SOC corresponds to a gradual change in the composition in the solution tanks with time as the vanadium ions are oxidized or reduced.

3.3 Method

The sensitivity analysis begins by defining a base case VRB. In this paper, the base case is based upon the following conditions:

Reaction Related Information

Stoichiometry (See Equations 1 and 2 above)

Temperature: Near room temperature (25 °C)

Concentration of vanadium: 1 M

Concentration of H_2SO_4: 5 M

Electrical power capacity: 1,000 kW

Energy capacity: 12,000 kW-hr

Cycle time (for charge or discharge): 12 hrs

State of charge considerations: Minimum = 0.20, Maximum = 0.80

Average Potential of cell: 1.26 Volts [9]

DC to DC efficiency: 0.91

Design Details

Size (cross-sectional area) of cell: 1 m^2

Cell stack size: 100 cells

Design current density of cell: 40 mA/cm^2

Materials of construction for tanks and heat exchangers: PVC and high Ni steel

Temperature adjustment in flow from cell stack: 15℃

Cost Information

Industrial Grade Vanadium cost: $21.13/kg of V [6]

Cell Construction Materials [11]

Ion-exchange membrane: \$500/m^2

Electrodes: \$51/m^2

Carbon felt: \$20/m^2

Costs are in 2011 U.S. dollars

The capital cost of this base case is about \$4.5 million, or about \$380 per kWh. The costs of the components as a percentage of total capital costs can be seen in Figure 3.3. From the above base case variables, a mathematical model was derived using the costs of different components of a VRB. The components are categorized according to their relationship to the electrical power capacity and energy capacity of the VRB. The variables chosen that are associated with the electrical power capacity of the VRB are the membrane cost and the current density. The variables chosen that are associated with the energy capacity of the VRB are the cycle time, the cost of the vanadium electrolyte, and the limits for the state of charge. The mathematical model derived is represented as a function of the components that affect the overall capital costs, taken as variables, in equation 3:

$$
\begin{aligned}
&\mathit{Overall\ capital\ costs} = 3016.9 \times \frac{\tau_c\ (hr) \times P\ (W) \times C_v(\$/g)}{(0.8 - S_{CL}) \times \eta_{OA}} + \ 0.794 \\
&\times \frac{P\,(W)\ \times (5151 + 202 \times\ C_M(\$/m^2) + 100 \times C_M\ (\$/m^2))}{I_D\ (mA/cm^2) \times \eta_{OA}^2} \\
&+ 355707.36 \times (\frac{\tau_c\ (hr)}{12})^{0.6} \\
&+ 830.72 \times \frac{P\,(W)}{\eta_{OA}} + 22509 \\
&+ 1227.6 \times (\frac{P\ (W)}{\eta_{OA}})^{0.6} + \ 15268.4 \times (\frac{P\ (W)}{\eta_{OA}})^{0.22}
\end{aligned} \tag{3}
$$

See Table 3. 1 for variable definitions. With this function the relative sensitivity index can be defined by equation 4:

$$Relative\ sensitivity\ index = abs\left(\frac{df}{dx}_{|BCP} \times \frac{x_0}{f_0}\right) \tag{4}$$

where BCP is the base case point, x is the cost component variable, f is the overall capital cost function, x_0 is the component variable at the base case, and f_0 is the overall capital cost at the base case. The relative sensitivity index is then a measure of the rate of change of the capital costs for a particular component variable at the base case values. Since the absolute value of the equation is taken, the higher the result, the greater the variable's influence on overall capital costs.

Other than the relative sensitivity analysis, we start with the base case values to understand the effects of changing variable values of a certain range; the variables are selected individually and given a range of values. The capital costs of the VRB are then calculated for each of these values and divided by the energy capacity of the VRB to attain the value for capital cost per kilowatt hour for comparison to the ARPA-e goal of \$100/kwh. The costs for the tanks, pumps, and heat exchangers were taken from a textbook by Ulrich [9].

The cost for the permeable membranes represents the majority of the costs for the cell stacks of a VRB. In the base case scenario, it alone represents about one-fourth of the total capital costs for the VRB. To test the sensitivity of the system cost to the membrane cost, the total capital costs for the VRB were calculated for membrane costs ranging from \$100/m^2 to the base case cost of \$500/m^2.

The current density of the electrodes has a significant effect on the number of stacks required. When the size of the cell is constant, the added current capacity increases the current through the stack, requiring fewer stacks in order to meet the electrical power requirement. The total capital costs were calculated for a range of current densi (5) mA/cm^2 to 100 mA/cm^2. The increase in current density of the electrodes increases the overpotential during charging and lowers the potential during discharge, and thus lowers the efficiency of the VRB. To calculate the efficiencies for different current densities, data was taken from two graphs from a paper by You [10]. The graphs from the paper can be seen in Figure 3.4. These graphs show that the cell voltage while charging and discharging is dependent on the SOC of the VRB. Graph (a) represents a current density of 40 mA/cm^2 while graph (b) represents a current density of 80 mA/cm2. The area beneath the charging curves represents the amount of energy used to charge the VRB, and the area beneath the discharging curves represents the amount of energy discharged from the VRB. The ratio of the discharged energy to the charging energy can then be used as the efficiency for that current density. An assumption was made that the relationship between current density and efficiency was linear. The linear dependence of efficiencies with current density was determined from the data at 40 mA/cm^2 and at 80 mA/cm^2 and an assumed efficiency of 1 at 0 mA/cm^2. This equation was calculated to be:

$$\eta_{OA} = 1 - 0.0021565 \times x$$

where x represents the current density in mA/cm^2.

The cycle time determines the amount of energy the VRB must store; the longer the cycle time, the greater the mass of vanadium electrolyte required to store the energy. The sensitivity of the overall capital costs to the cycle time is examined by holding the electrical power of the VRB at the base case value and changing the charge and discharge time for values between from 4 hours to 12 hours (total cycle time from 8 hours to 24 hours).

The major cost associated with the energy storage capacity of the VRB is the cost of the vanadium electrolyte, which at the base case value represents about 40% of the capital costs of the entire battery [13]. The base case, however, assumes industrial grade vanadium while most research into VRB has been done in the laboratory with a higher grade of vanadium. The higher grade of vanadium is significantly more expensive. If deployment of VRBs increases the demand for higher grade vanadium, the cost for higher grade vanadium could fall, possibly to prices somewhere between the current cost for low grade and current costs for higher grade vanadium. To examine the effects of this on the capital costs of a VRB, the costs of the vanadium were varied from the industrial base case value of $0.021 per gram to the laboratory grade value of $2.10 per gram.

As the SOC range becomes narrower, there is a need for a greater capacity of the vanadium electrolyte since less vanadium is utilized during each cycle. To examine the effect of this on the total capital costs of the VRB, the upper SOC limit is held at 0.8 while the lower SOC limit ranges from 0.2 to 0.7. For this study, the electric current density was a parameter of interest, so in all cases, the battery was charged and discharged at a constant current density.

The energy capacity of a VRB is a product of the power capacity and the cycle time. It is the amount of power (in kW) applied over a certain period of time (hours), and is measured in kilowatt-hours. If the energy capacity of a VRB is held constant, an increase in the power will provide for a decrease in the cycle time for the battery, while an increase in the cycle time will provide for a decrease in the power. The increase in power capacity requires the addition of stacks of cells, increasing the capital costs associated with the power capacity. The cycle time influences the amount of vanadium electrolyte required as well as the size of the tanks, which affects the capitals costs as well. To see the effects on the capital costs when power capacity increases and the cycle time decreases, the energy capacity is held constant while the power ranges from 1000 kW to 3000 kW and the charge/discharge time ranges from 12 hours to 4 hours (a total cycle time of 24 to 8 hours).

3.4 Results

The values of the relative sensitivity index are given in Table 3.2. When the power capacity is fixed, the cycle time has by far, the largest effect on capital cost with the price of vanadium having the next greatest effect. The cost of increasing the cycle time is a function of the cost of the vanadium; the longer the cycle time, the more vanadium electrolyte is necessary. This emphasizes the effect that the price of the vanadium electrolytes have on the capital costs. When the energy capacity is fixed, the power capacity and the cycle time have large and equal effects on the capital costs. The sensitivity of the capital cost per kWh to various variables is presented below with accompanying graphs. In each case, the remaining variables are held constant so that the effects of the intended variables on the overall capital costs is illustrated more clearly.

The sensitivity of the capital cost per kilowatt-hour to the costs of the membrane can be seen in Figure 3.5. The sensitivity of the capital costs to the membrane costs does not change as the membrane costs increase, but the capital costs do rise. With the present day costs (used as the base case cost) the capital cost per kilowatt-hour is about $391, which trends down to $284 per kilowatt when the membrane price is $40 per square meter, a DOE target for fuel cells.

The sensitivity of the capital costs per kilowatt-hour to the current density can be seen in Figure 3.6 for a family of curves representing different membrane costs. At lower current densities and higher membrane costs, the capital costs are quite sensitive to the current density. As the membrane cost is lowered, however, current density has less of an effect on the capital costs. For all the membrane costs, the capital costs become less sensitive to the current density as the current density is increased. This result can be explained by the cost of the materials related to the energy capacity of the VRB, which is $185 per kWh and does not change. As the costs related to the power capacity decrease, their contribution to the capital costs per kilowatt-hour becomes less and less significant, until the majority of the overall cost is related to the costs for the components associated with the energy capacity.

The sensitivity of capital costs to current density for different electrode prices can be seen in Figure 3. 7 for a family of curves representing different electrode prices. The increase in current density once again shows diminishing returns when approaching 100 mA/cm2. The electrode price does not affect the sensitivity of the capital costs to the current density, as the lines show the same level of curvature for each electrode price.

The sensitivity of the capital costs per kWh to the cycle time can be seen in Figure 3. 8. When the power capacity is constant at 1 MW, increasing the cycle time lowers the capital costs per kWh. The total capital costs will increase because of the larger tanks required and greater volume of vanadium electrolyte; however, the increase in the energy capacity of the VRB more than offsets this expense and lowers the capital costs per kWh. The sensitivity of the capital cost per kWh to the cost of vanadium can be seen in the semi-log graph in Figure 3. 9. The capital cost per kWh showed the greatest range when increasing the cost of the vanadium from the cost of industrial grade vanadium at $0.021 per gram to laboratory grade vanadium at $2.10 a gram. There is a 100 fold increase in the cost of the vanadium electrolytes, increasing the capital costs per kilowatt-hour from around $300 to around $12,000. The differences in the prices can be explained by the purity of the vanadium, with the laboratory grade vanadium being of much higher purity. It is then important for a VRB to be able to use the lowest purity of vanadium as possible, so that the price of the vanadium can be kept at a minimum.

The increase in the capital costs per kilowatt-hour as the SOC limits are narrowed can be seen in Figure 3. 10. As the SOC limits are narrowed by raising the lower limit toward a static upper limit of 0.80, the capital costs per kilowatt-hour increases. This increase becomes more dramatic the narrower the SOC range, in this case the higher value for the lower limit. This increase is due to the fact that as the lower limit of the SOC approaches the upper limit of 0.80, the difference in the volume of vanadium solution needed to store the energy at those limits becomes greater. For example, when the lower SOC limit is raised from 0.2 to 0.225, the volume of vanadium electrolyte solution needed increases by 4.3%; however, when the SOC limit is raised from 0.3 to 0.325, the volume of vanadium electrolyte solution needed increases by 5.2%.

Figure 3.11 shows the capital costs per kilowatt-hour of a VRB when the energy capacity is held constant at 12 MWh, the power capacity is raised, and the cycle time is decreased. The higher power capacity translates into greater capital costs for the VRB. From the perspective of the VRB system design, the extending cycle time with the reduction of power capacity can potentially cut down the total capital cost when the power capacity is not the first consideration.

(Replace this paragraph) The graphs Figure 3.10 shows the capital costs per kilowatt-hour of a VRB when the energy capacity is held constant at 12 MWh, and the power capacity is raised while the cycle time is decreased. The higher power capacity translates into greater capital costs for the VRB.

3.5 Conclusion

The relative sensitivity index for a fixed power capacity shows the importance of the costs of the vanadium to the overall capital costs. In addition, the capital costs per kilowatt-hour showed the greatest range when the vanadium costs were varied from the cost of industrial grade vanadium to the costs of laboratory grade vanadium. Note that a relatively large change in vanadium costs was considered in this analysis. Of course, the large change makes the cost of vanadium appear to be an especially important parameter. The large change in vanadium cost was used because it was apparent that the use of high purity vanadium at current prices (approximately $2,100 per kg) would be prohibitively expensive. It is clear that using vanadium costs near that of the lowest grade vanadium will be necessary to keep the capital costs of the VRB down. Vanadium costs like those for the laboratory grade vanadium would be almost 120 times greater than the ARPA-e goal. Better definition of vanadium purity requirements, less expensive sources of vanadium, and lower costs for reaching the required purity appear to be important needs for the VRB to meet or approach the ARPA-e goal.

When the energy capacity is held constant and the power capacity and cycle time are manipulated, the increased costs of the components related to the power capacity far outweigh the savings in the cost for the vanadium electrolyte and the tanks due to the lowered cycle time. This shows that there is a greater economic feasibility for VRB designs with a lower power capacity and longer cycle time for a set energy capacity.

The capital costs per kilowatt-hour are sensitive to the SOC limits, and the trade-off between the greater fluctuation in the power of the discharge and narrower SOC limits must be carefully weighed against this when designing a VRB. If it is necessary to have a narrower range of power while discharging, the rise in the capital costs of the VRB will be steep; however, VRB uses where the power discharge is allowed a greater range will make the VRB far more affordable.

The increase in current density showed diminishing returns due to the costs of the components associated with the energy capacity. While the increase in the current density had a significant effect on the costs of the components associated with the power capacity, increasing the current density will have to be coupled with ways to decrease the costs of the components associated with the energy capacity to have a greater effect.

Since varying only one variable at a time was inadequate to reach the ARPA-e goal of $100 per kWh for any of the variables, a more holistic approach must be taken in which multiple variables will be needed to reach the goal. Since some of the parameters reflect the different needs of individual electrical utility companies, it may be easier to meet or approach the cost goals for some applications than for others.

References

[1] *EPRI_DOE Handbook of Energy Storage for Transmission and Distribution Applications*, EPRI, Palo Alto, CA, and the U.S. Department of Energy, Washington, DC: 2003. 1001834.

[2] Douglas, J.M. *AIChE J.*, **31**, 353 (1985).

[3] *Vanadium Redox Flow Batteries: An In-Depth Analysis.* EPRI, Palo Alto, CA: 2007. 1014836

[4] Cellstrom Home Page. http://www.cellstrom.at/index.php?id=40&L=1 (accessed September 2011).

[5] Moore M., Counce R., Watson J., Zawodzinksi T., and Kamath H. A Step by Step Methodology for a Base Case Vanadium Redox-Flow Battery, *Chemical Engineering Education* (2011).

[6] You, D; Zhang, H.; Chen, J. *Electrochem. Acta*, **54**, 6827 (2009).

[7] U.S. Geological Survey. Mineral Industry Surveys. http://minerals.usgs.gov/minerals (accessed March, 2011).

[8] *Vanadium Redox Flow Batteries: An In-Depth Analysis.* EPRI, Palo Alto, CA: 2007. 1014836

[9] Ulrich, G.; Vasudevan, P. *Chemical Engineering Process Design and Economics: A Practical Guide*, pp 383-397, Process Publishing, Durham, (2004).

Appendix

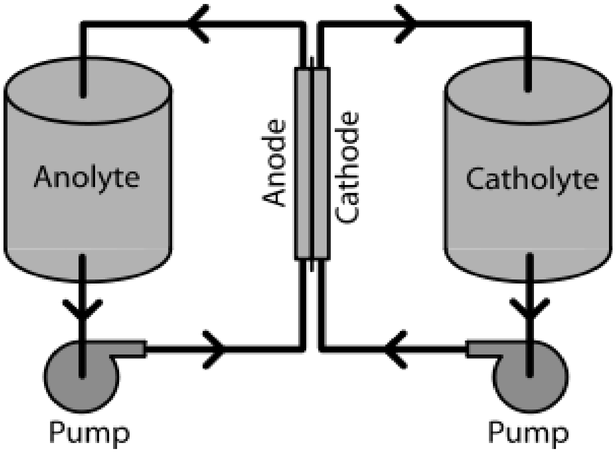

Figure 3. 1 Schematic representation of a vanadium redox –flow battery [4].

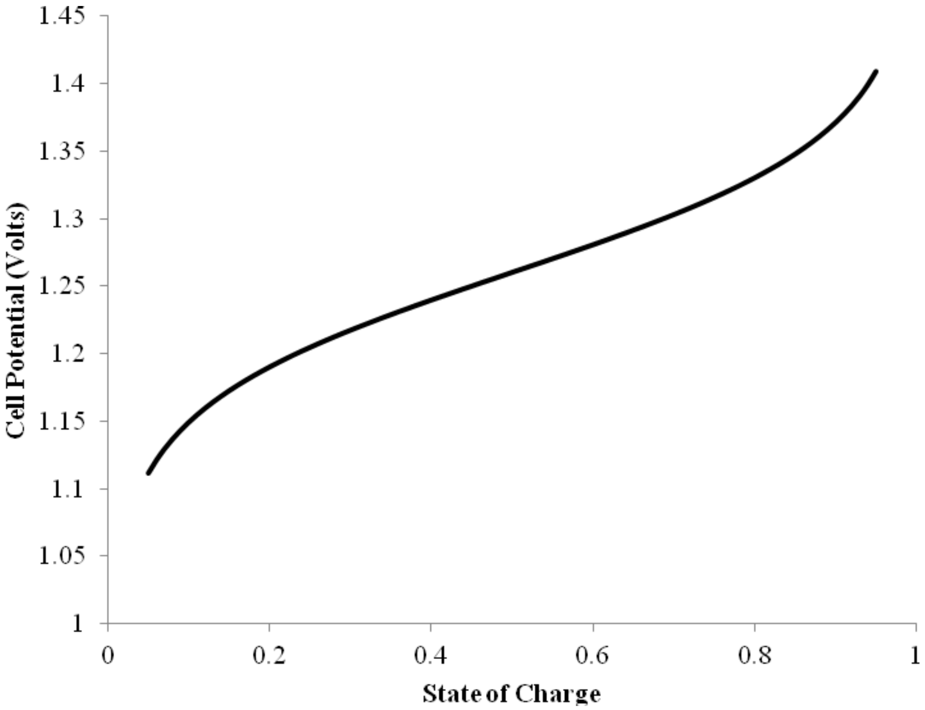

Figure 3. 2 The effect of SOC on cell electrical potential [8].

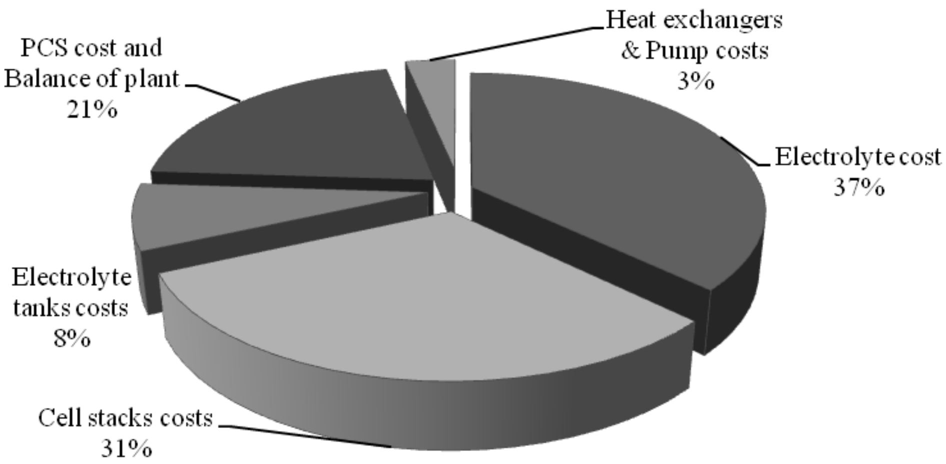

Figure 3. 3 The Capital Costs of the Base Case VRB.

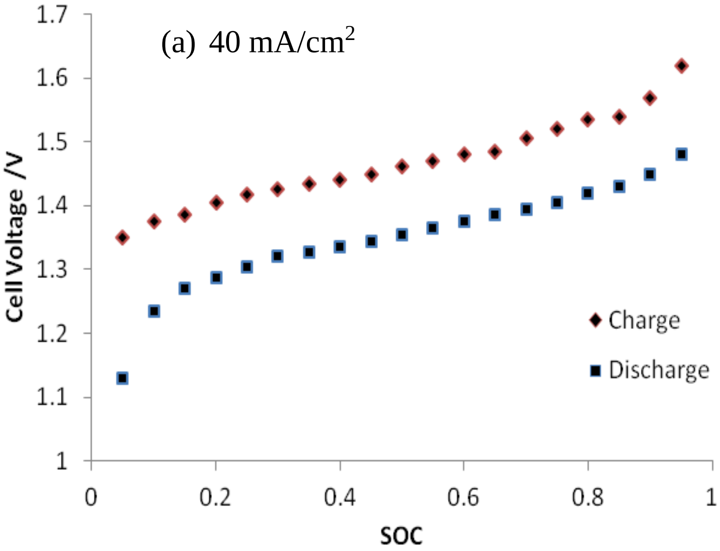

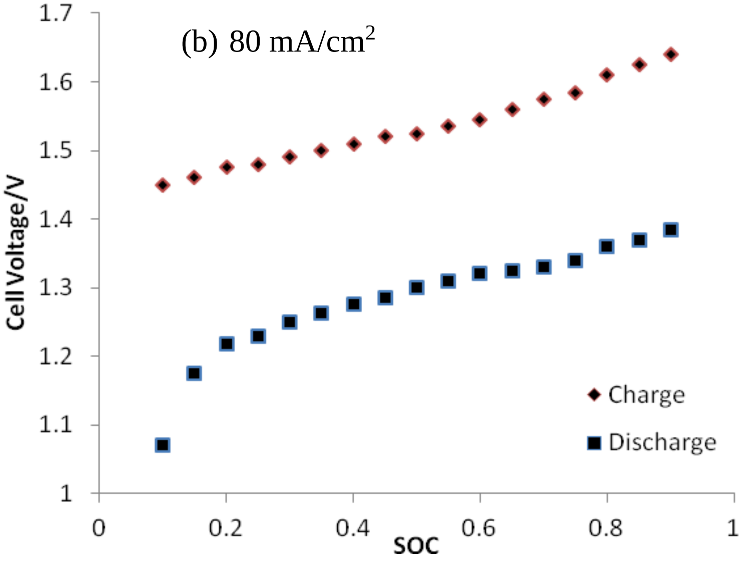

Figure 3. 4 The cell voltage at different SOC for (a) a current density of 40 mA/cm^2 and (b) a current density of 80 mA/cm^2 [6].

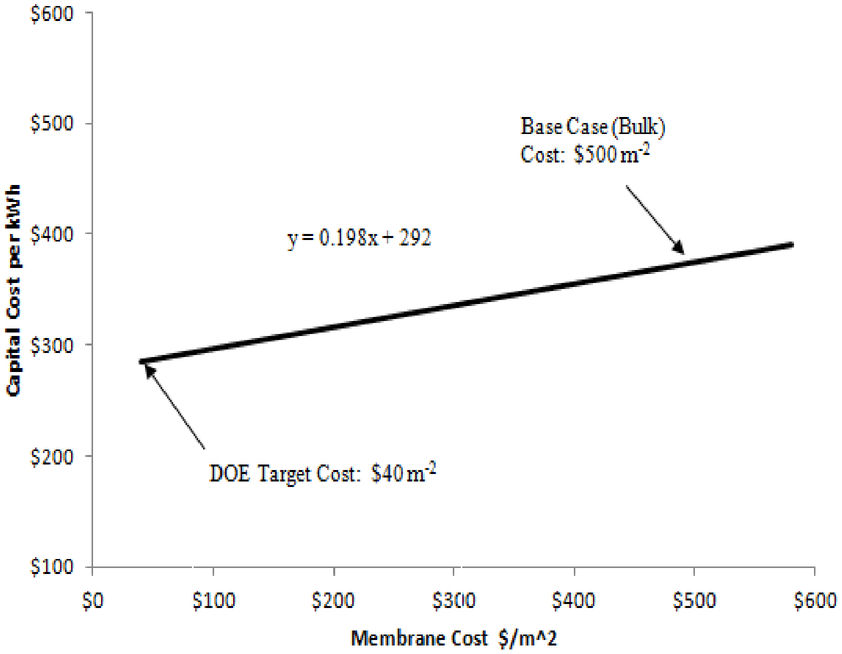

Figure 3. 5 The effect of membrane cost on capital costs.

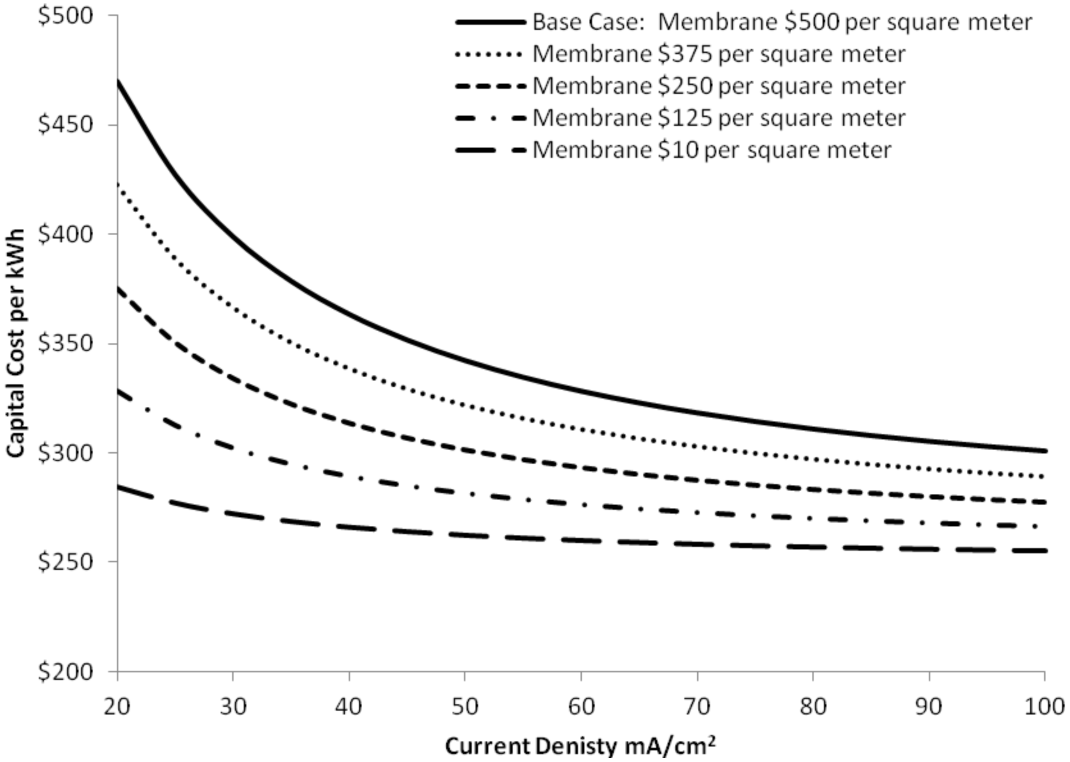

Figure 3. 6 The effect of current density on capital costs.

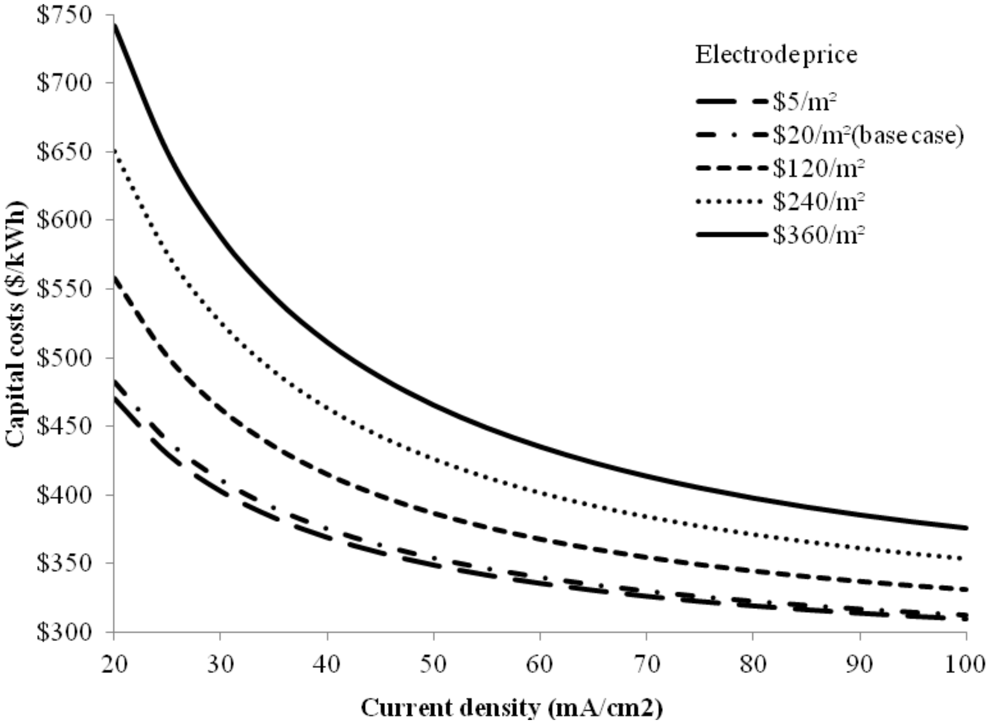

Figure 3. 7 The effect of current density on capital costs for different electrode costs.

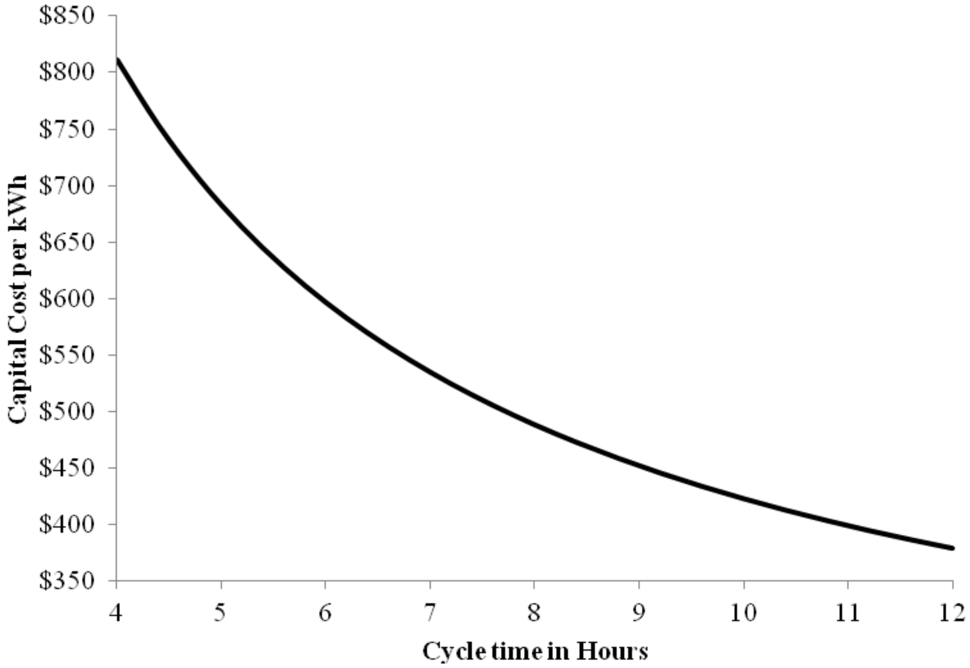

Figure 3. 8 The effect of cycle time on capital cost per kilowatt-hour for a 1 MW VRB.

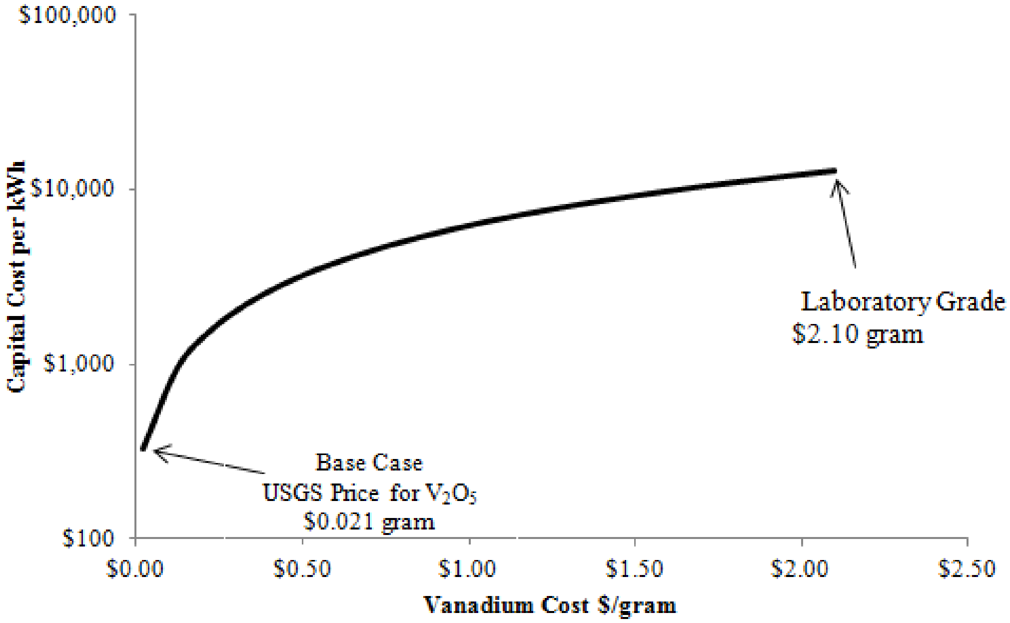

Figure 3. 9 The effect of vanadium electrolyte cost on a VRB.

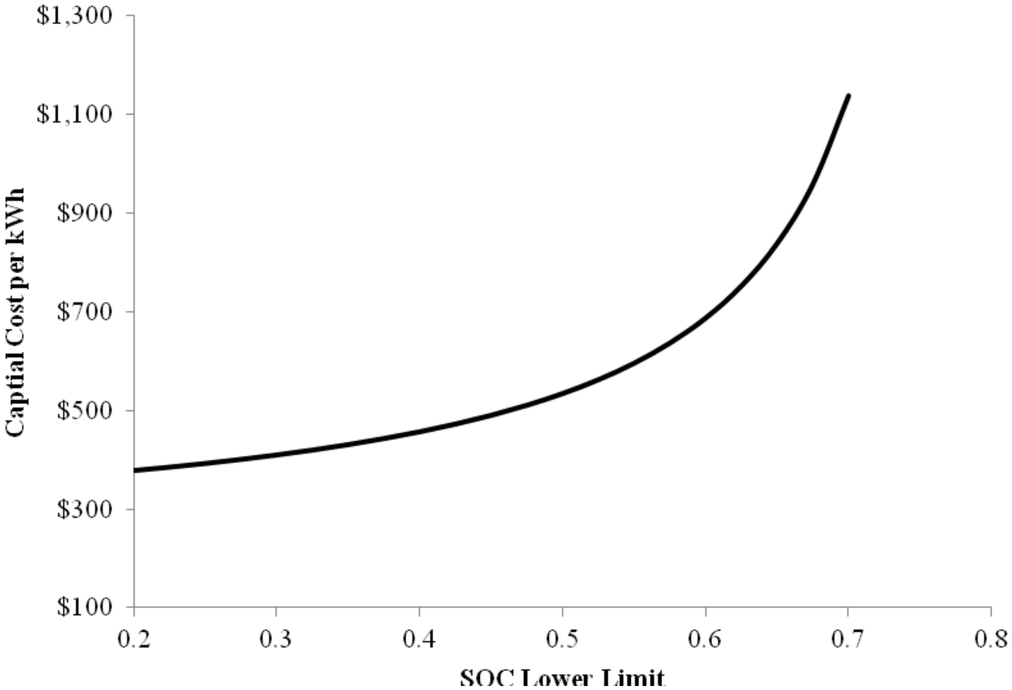

Figure 3. 10 The effect of SOC Limits on capital costs per kilowatt-hour.

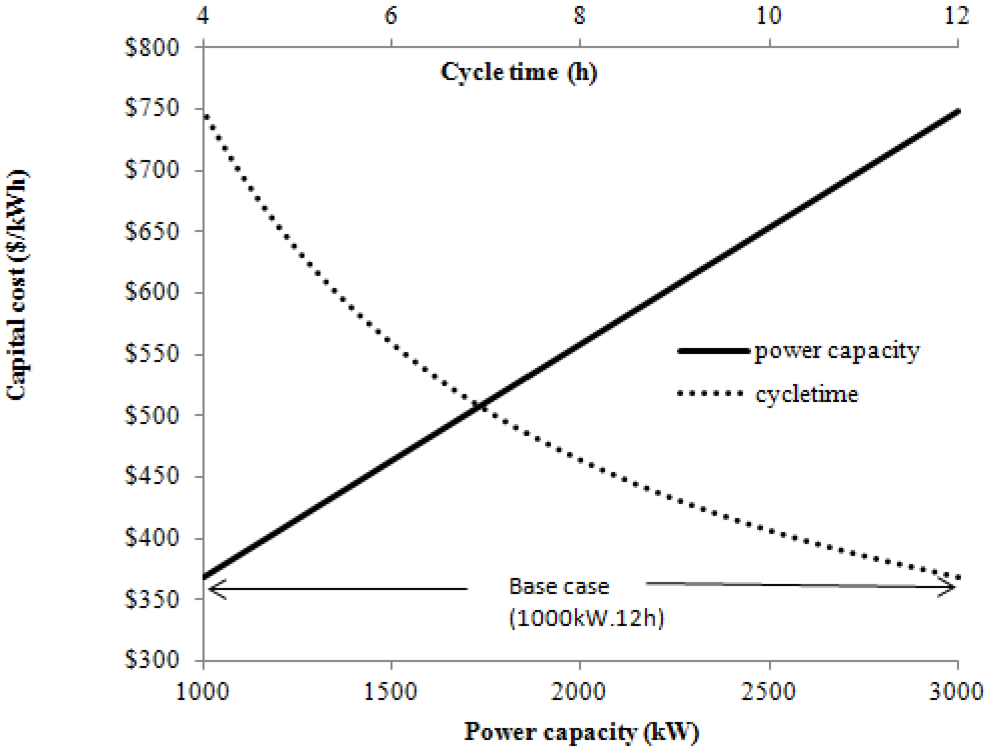

Figure 3. 11 The effect of cycle time and power capacity on capital costs per kilowatt-hour for a 12 MWh VRB.

Table 3. 1 Nomenclature.

Variable	Description	Units
τ_c	Time necessary to fully charge or discharge the VRB.	hr
P	Power capacity of the VRB.	W
C_V	Cost of the vanadium ions.	\$/g
S_{CL}	Lower limit of the SOC.	
η_{OA}	Overall efficiency of the VRB (DC to DC).	
C_M	Cost of the membrane.	\$/m^2
I_D	Current density.	mA/cm^2

Table 3. 2 Summary of relative sensitivity indexes.

		Relative Sensitivity Index
Fixed Power Capacity Variables	Current Density	0.3092
	Cycle Time	0.6101
	Membrane Cost	0.2612
	Electrode Cost	0.021
	Vanadium Cost	0.3337
	Lower SOC Limit	0.1112
Fixed Energy Capacity Variables	Power Capacity	0.4881
	Cycle Time	0.4881

CHAPTER 4

Electrochemistry And Morphology Studies of Aluminum Plating/Stripping in A Chloroaluminate Ionic Liquid on Porous Carbon Materials

4.1 Introduction

Aluminum (Al) is the third most abundant element in the Earth' crust [1] and has three transferable electrons leading to the large theoretical specific capacity (2978Ah/kg) when the aluminum is oxidized and reduced. It has been considered as an excellent candidate for high energy density electrode materials [2]. The Al plating/stripping on/from electrodes at room temperature has been investigated in the mixture of $AlCl_3$ and 1-ethyl-3-methylimidazolium chloride (EMIC) electrolyte [3-9]. The electrochemical reaction on the Al （negative） electrode is written as:

Negative electrode: $4Al_2Cl_7^- + 3e^- \leftrightarrow Al + 7AlCl_4^-$ (1)

Aluminum dendrite formation has, however, been observed, especially at high current density [4,5]; this phenomena can result in a short circuit. To limit dendrite formation, three-dimensional porous carbon materials are being studied for Al plating and stripping. Based on observations of Al plating on porous carbon materials, there are several advantages for plating/stripping Al on porous materials over the solid planar substrates. (1) High surface volume ratio of porous materials provides the possibility of high current densities. (2) By plating/stripping Al inside porous materials, the possibility of the dendrite formation is expected to be limited inside the porous structure. (3) A flow-through electrode could be easily designed for enhancing the plating/stripping performance even further and achieve even higher current densities.

4.2 Experimental

EMIC is synthesized by using the reported procedure [10,11]. $AlCl_3$ (Fluka, >99%) and is further purified by sublimation in a heavy wall glass tube, as described previously[11]. Chloroaluminate melt is prepared by slowly adding EMIC onto solid $AlCl_3$ crystals. The voltammetry cell and the 3 mm diameter disk Glass Carbon (GC) electrode were purchased from Bioanalytical Systems Inc. Carbon paper electrode is prepared by cutting 2050-A carbon paper (Fuel Cell Store) to a 5mm×10mm size and adhering the prepared carbon paper to one end of a copper rod (McMaster-Carr) using a silver conductive epoxy (McMaster-Carr). The electrode surface area of the carbon paper electrode is controlled at c.a. $0.5 cm^2$ (5mm×5mm, double sides) using epoxy to seal the remaining electrode surface. The geometrical electrode area is measured and used to calculate the current density. The reference electrode is a 1 mm diameter Al wire (Alfa Aesar, 99.999%) immersed into the molar ratio 1.5:1 ($AlCl_3$: EMIC) chloroaluminate electrolyte in a glass tube with a porous vycor tip (Bioanalytical Systems Inc.). The counter electrode is a spiral Al wire (Alfa Aesar, 99.999%). Ionic liquids are heated by a hot plate and temperature is measured by a thermometer (Fisher Scientific Inc.). A potentiostat (SP200, BioLogic) is used to measure cyclic voltammetry and chronoamperometry. Hitachi TM-3000 SEM is used to observe the morphology of Al deposits on substrates.

4.3 Results and Discussion

Cyclic voltammetry is conducted on the different substrates, eg. glassy carbon and carbon paper at different scanning rates.

The arrows in Figure 4.1 and 4.2 show the starting direction of scanning voltage. The negative current on the cyclic voltammograms represent the reduction reaction (Al plating process) while the positive current represents the oxidation reaction (Al stripping process). Based on the cyclic voltammograms showed in Figure 4.1 and 4.2, the Al plating/stripping process shows the characteristic of the quasi-reversible reaction because the potential difference (300mV) between reduction reaction and oxidation reaction peaks is over 20mV and this potential difference increases with the scanning rate[12]. This becomes more evident on the cyclic voltammogram of Al plating on carbon paper where the current does not move to a diffusion controlled region at fast scanning rates. In these cyclic voltammograms, especially at 10mV/s scanning rate, Al plating shows only one peak (reduction reaction) but Al stripping shows two peaks (oxidation reaction). The different peaks showed in Al stripping indicates the different electrochemical reaction mechanism on stripping of Al. They could be considered to represent dissolution of bulk Al and Al closed to the carbon surface. The charges of the reduction and oxidation waves at different scanning rates in Figure 4.2 are calculated. The ratio of charges is used to indicate the current efficiency. The current efficiencies are nearly 100% for 100mV/s, 96.5% for 50mV/s and 89.8% for 10mV/s. This indicates that a passivation behavior due to the accumulation of $Al_2Cl_7^-$ at the electrode surface probably occurs at low scanning rate.[4,8]

In Figure 4.3, we show how the electrode materials affect the shape of cyclic volatmmograms for Al plating and stripping. We choose a glassy carbon disk electrode, a graphite disk electrode and a carbon paper electrode for this comparison. The graphite disk electrode is assumed to have similar catalytic kinetics as carbon paper because they are both basically made of graphite. The only difference on these two electrodes is the configuration. One is a solid disk, and the other is a porous paper. For the disk electrodes, graphite shows better catalytic kinetics for Al plating and stripping (the slope of curve is larger than that for glassy carbon disk electrode). Furthermore, Al plating on carbon paper shows even more advantages over glassy carbon disk electrode. Al plating on carbon paper shows more positive potential than that on graphite disk electrode but similar kinetics as the graphite disk electrode. Also, the diffusion limitation of Al plating on carbon paper is less evident than that on the graphite disk electrode. Finally, the peak current density in plating Al on carbon paper leads to twice the peak current density on the graphite disk electrode. This indicates a significant difference in Al plating, especially the diffusion process, occurs on carbon paper because of its porous structure.

To further investigate Al plating in the porous structure, controlled charge chronoamperometry is used to plate Al under different overpotentials. The current transients under different overpotentials are showed in Figure 4.4. These current transients are acquired based on the same amount of electric charge (0.57mA·h). By assuming all the electric charges are utilized in the electrochemical reaction for Al deposition, the total amount of Al deposited on carbon paper should be same for all overpotentials studied.

Figure 4.4 illustrates that the peak currents have different values and positions for Al deposition at different overpotentials. Higher overpotential leads to higher current values earlier in the experiment. The current transients during Al plating on carbon paper are different from those observed during Al plating on disk electrodes after peak currents appear. Steady state current can be observed during Al plating on carbon paper. However, the current transients of Al plating on disk electrodes after the current peaks can follow the Cottrell equation in short times[13]. This difference probably results from the shape and configuration of porous materials. As the carbon paper is composed of graphitized fibers, the ends (tips) of these fibers are on the edge of carbon paper may be active plating areas. When the ends (tips) of graphitized fibers are exposed to the electrolyte, the current at the edge of carbon paper will gradually become an important part of the steady state current. SEM images are also taken to observe the morphology difference for the experiments in Figure 4.5.

In Figure 4.5 these SEM images demonstrate that more Al nuclei can form under higher overpotentials because the higher overpotential results in the increasing number of active cites for Al deposition. All of these SEM images were taken with the same amount of Al deposition by controlling electric charge. So under the lower overpotential, there are fewer nucleation sites for Al deposition, and this results in larger Al deposits on fewer sites. With higher high overpotentials, there are more nucleation sites and smaller Al deposits on each site. Furthermore, the sizes of Al nuclei on the inner fibers of carbon paper are smaller than those on the outer layer of carbon paper. This results from a complex mass transfer issue. When the rate of Al nuclei growth is controlled by diffusion rate of ions to the outer surfaces of the paper, the concentration of $Al_2Cl_7^-$ on the outer layer and inner fibers of carbon paper is close to zero. Then the Al nuclei on the inner fibers of carbon paper will stop growing when the current density is controlled by the diffusion rate. Through the SEM images we also identify that the size of Al nuclei on the inner fibers of carbon paper under lower overpotential is larger than those under higher overpotential. This means that under low overpotential, Al nuclei on the inner fibers of carbon paper can grow continuously for a longer time before the concentration of $Al_2Cl_7^-$ approaches zero. When comparing the morphology of Al nuclei under 350 mV with 400 mV overpotential, no obvious difference of Al nuclei sizes can be identified. This may result because the limiting current is reached, and the current density is only related to the diffusion rate.

The nucleation mechanism is investigated by the widely-used Scharifker and Hills model [3,4]. By plotting the following dimensionless model, the experimental data can be compared with the theoretical prediction in Figure 4.6.

Instantaneous nucleation: $(i/i_m)^2 = 1.9542(t/t_m)^{-1}\{1 - exp[-1.2564(t/t_m)]\}^2$ (2)

Progressive nucleation: $(i/i_m)^2 = 1.2254(t/t_m)^{-1}\{1 - exp[-2.3367(t/t_m)]\}^2$ (3)

where i_m represents the peak current density; t_m means the time when the peak current occur.[13]

The Scharifker and Hills model shows that the current transient consisted of two parts. The current transient first rises to current peak and then decreases following the Cottrell equation [13]. The current peaks are considered as the total contribution from each nuclei and the current drop-off results from the overlapping of diffusion layers of each nuclei. As the plot in Figure 4.6 shows, the dimensionless description of experimental data from current transients do not vary with the overpotential. So the overpotential may not affect the nucleation mechanism. However, the experimental dimensionless data deviates from Scharifker and Hills model prediction, especially after the current peaks because it takes longer for the overlapping of diffusion layers of each Al nuclei on the porous materials. Furthermore, the assumption of Scharifker and Hills model is different from current situation where porous materials are used as substrates. Their model assumed that the deposition takes place on the planar substrate and the diffusion is semi-finite linear diffusion. However, the carbon paper consists of graphitizing fibers (diameter ca.7-8um) and the cylindrical/ spherical diffusion and edge effect in the diffusion process are not taken into consideration in the Scharifker and Hills model.

The molar ratio of $AlCl_3$ and EMIC will affect the concentration of $Al_2Cl_7^-$ and $AlCl_4^-$ in the chloroaluminate melts. $Al_2Cl_7^-$ concentration increases and reach maximum when the molar ratio of $AlCl_3$ and EMIC approches 2. This will leads to fast diffusion mass transfer of $Al_2Cl_7^-$ to the electrode surface. Higher temperature will also result in a fast kinetic process and high diffusivity of $Al_2Cl_7^-$ and $AlCl_4^-$. Increases of these two parameters can lead to higher current densities for Al plating and stripping. The chronoamperometry showed in Figure 4.7 illustrates how molar ratio and temperature can enhance the current density of plating Al.

Al plating involves a nucleation process and Al growth. The Al growth is considered as a diffusion-control process[2-3]. Initially each Al nuclei has a hemi-spherical diffusion zone. But as charge-transfer is fast (large overpotential), these diffusion zones merge together because the concentration of ions near electrode surface is depleted. Finally a semi-finite diffusion layer is formed when the substrate is a planar configuration. To enhance the current density and plate Al on the fibers inside the carbon paper, pulse current deposition is applied. The following SEM images in Figure 4.8 show the difference of Al morphology between controlled constant potential and pulsed currents

Al plating on carbon paper using the pulse current deposition technique allows more Al to be plated on the inner fibers of carbon paper. By applying the current density on the carbon paper at certain frequency, the diffusion layers of each Al nuclei will grow and shrink following the frequency of pulse current and do not have enough time to overlap with each other. So during the relaxation time, ions such as $Al_2Cl_7^-$, will be resupplied to the fiber surfaces not only on the outer carbon paper surfaces, but also inside carbon paper. This indicates that the Al nuclei can continue growing on the fibers inside the carbon paper.

4.4 Conclusion

Al has shown the ability to be plated and stripped on a carbon paper electrode. The porous structure of carbon paper brings the different observations on cyclic voltammorgrams, current transients at controlled potentials and Al morphology. The porous materials can be considered a more promising substrate to enhance the performance of the Al electrode on current density. The overpotential of Al deposition on carbon paper is lower than that on glassy carbon. The current transients of Al deposition on planar substrate and cylindrical substrate are different. So Scharifker and Hills model will not be suitable to express Al nucleation and growth on carbon paper. Edge effect and cylindrical diffusion should be considered to build a new nucleation model for porous substrates. Higher temperatures and higher $AlCl_3$ molar compositions improve the performance of Al plating by raising nucleation rate and diffusion rate of ions. The diffusion of ions to the fibers inside carbon paper should be considered as an important process for Al plating on the carbon paper. This indicates that the enhanced flow-through electrode should be a good option for Al plating on the carbon paper.

Reference

[1] F.W. Clarke, H.S. Washington, *The Composition of the Earth's Crust*, (1924)

[2] Q. Li and N. J. Bjerrum, *Journal of power sources*, **110**, 1–10 (2002).

[3] R. T. Carlin, W. Crawford, and M. Bersch, *Journal of Electrochemical Society*, **139**, 2720–2727 (1992).

[4] T. Jiang, M. J. Chollier Brym, G. Dubé, a. Lasia, and G. M. Brisard, *Surface and Coatings Technology*, **201**, 1–9 (2006).

[5] D. Pradhan, D. Mantha, and R. G. Reddy, *Electrochimica Acta*, **54**, 6661–6667 (2009).

[6] P. Lai and M. Skyllas-Kazacos, *Journal of Electroanalytical Chemistry*, **248**, 431–440 (1988).

[7] S. Schaltin, M. Ganapathi, K. Binnemans, and J. Fransaer, *Journal of The Electrochemical Society*, **158**, D634 (2011).

[8] J. Auborn and Y. Barberio, *Journal of the Electrochemical Society*, **132**, 598 (1985).

[9] F. Endres, M. Bukowski, R. Hempelmann, and H. Natter, *Angewandte Chemie (International ed. in English)*, **42**, 3428–30 (2003).

[10] J. S. Wilkes, J. A. Levisky, R. A. Wilson, and C. L. Hussey, *Inorganic Chemistry*, **21**, 1263–1264 (1982).

[11] P.C. Trulove, *The Chemistry of Proton in Ambient-temperature Chloroaluminate Molten Salts, Thesis,* State of University of New York, Buffalo, 25-44 (1992).

[12] A. J. Bard & L. R. Faulkner, *Electrochemical Methods: Fundamentals and Applications, 2nd ed.*, John Wiley & Sons, Inc, New York, USA, (2001)

[13] B. Scharifker and G. Hills, *Electrochimica Acta*, **28**, 879–889 (1982)

Appendix

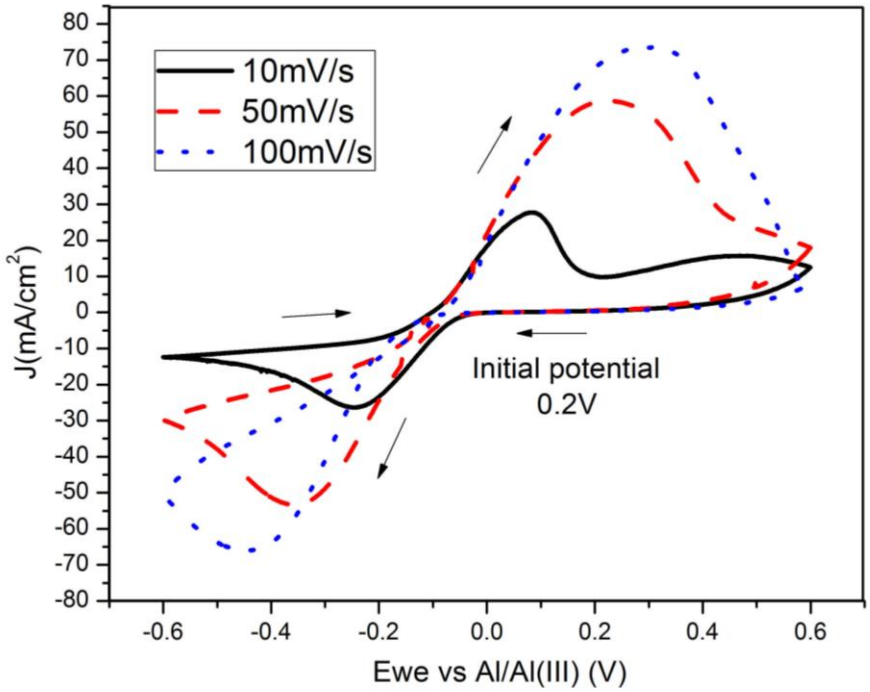

Figure 4. 1 Cyclic voltammetry at different scanning rates on a glassy carbon disk electrode in the ionic liquid with molar ratio $AlCl_3$: EMIC=1.5:1

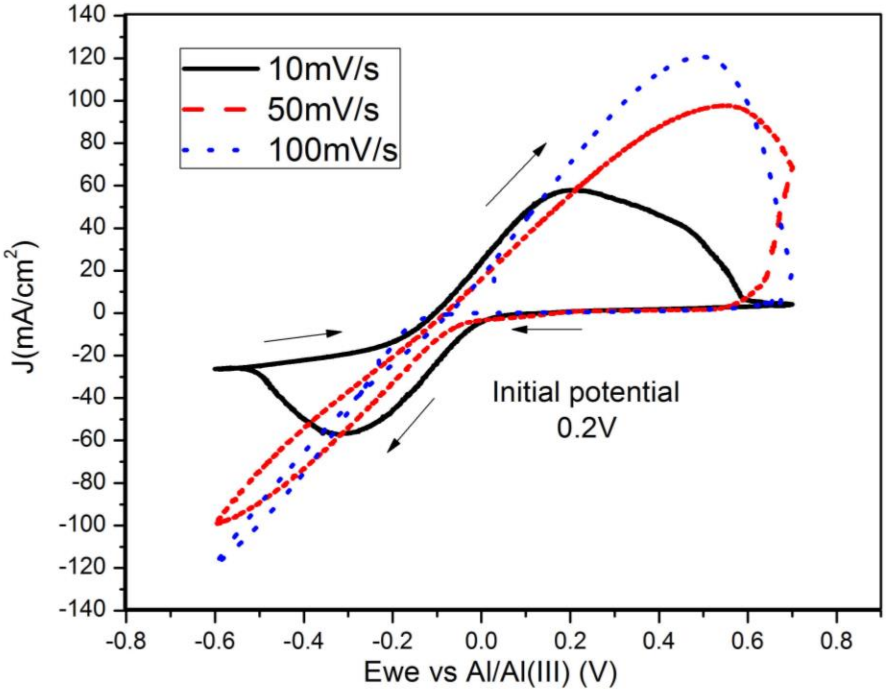

Figure 4. 2 Cyclic voltammetry at different scanning rates on a carbon paper electrode in the ionic liquid with molar ratio $AlCl_3$: EMIC=1.5:1

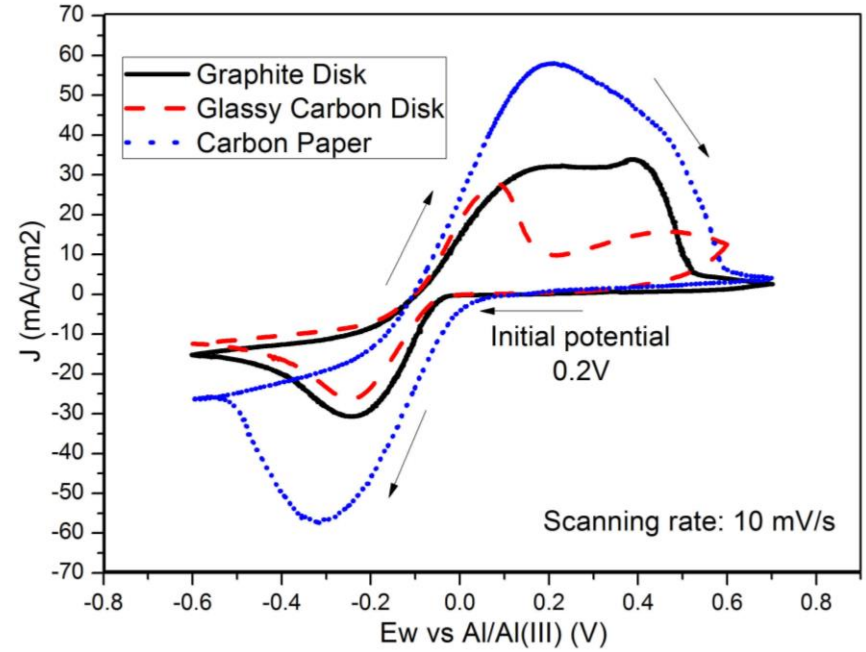

Figure 4. 3 Cyclic voltammetry on three different electrode materials, i.e. graphite, glassy carbon and carbon paper, for Al plating/stripping at 10mV/s

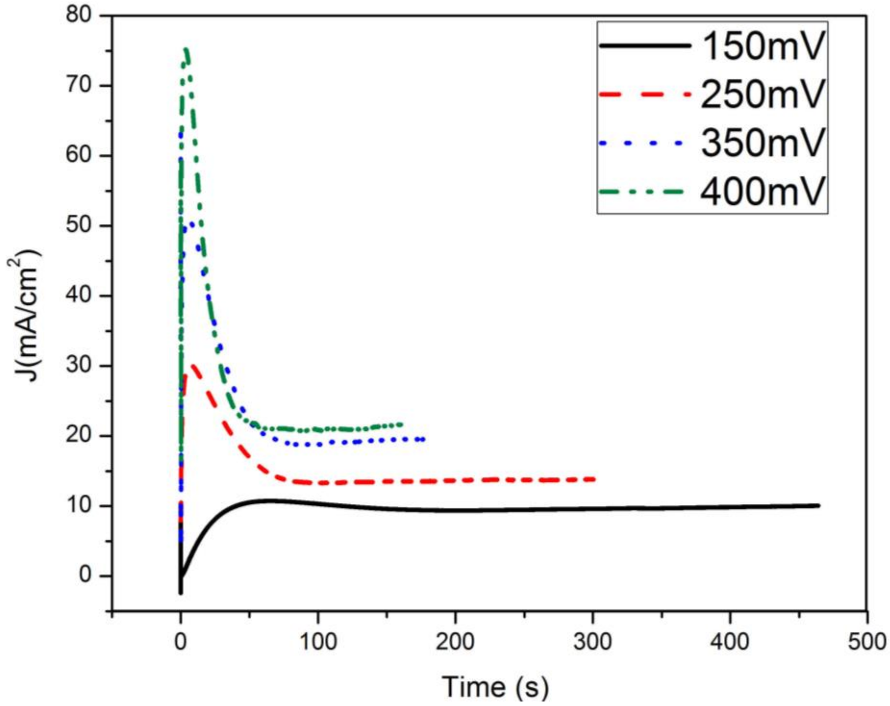

Figure 4. 4 Current transients for Al deposition on carbon paper under different overpotentials at constant electric charge.

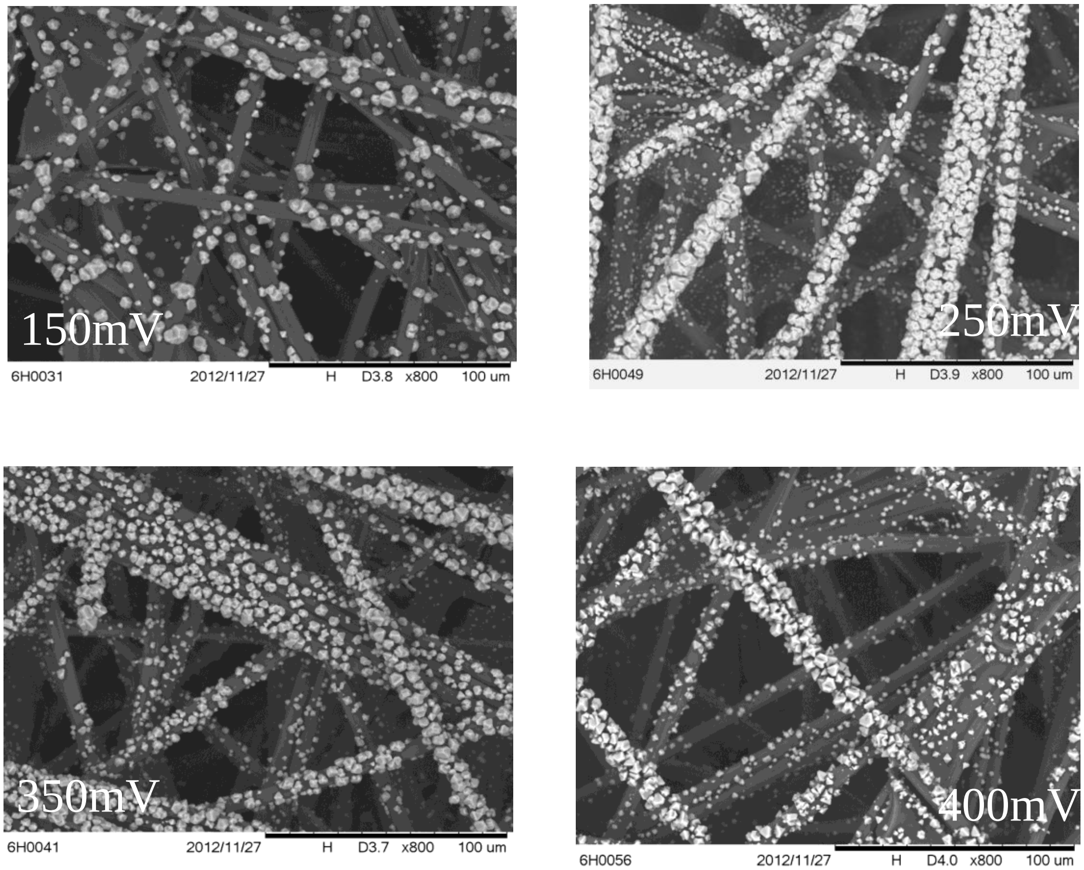

Figure 4. 5 SEM images of Al deposition on carbon papers under different overpotential with constant electric charge.

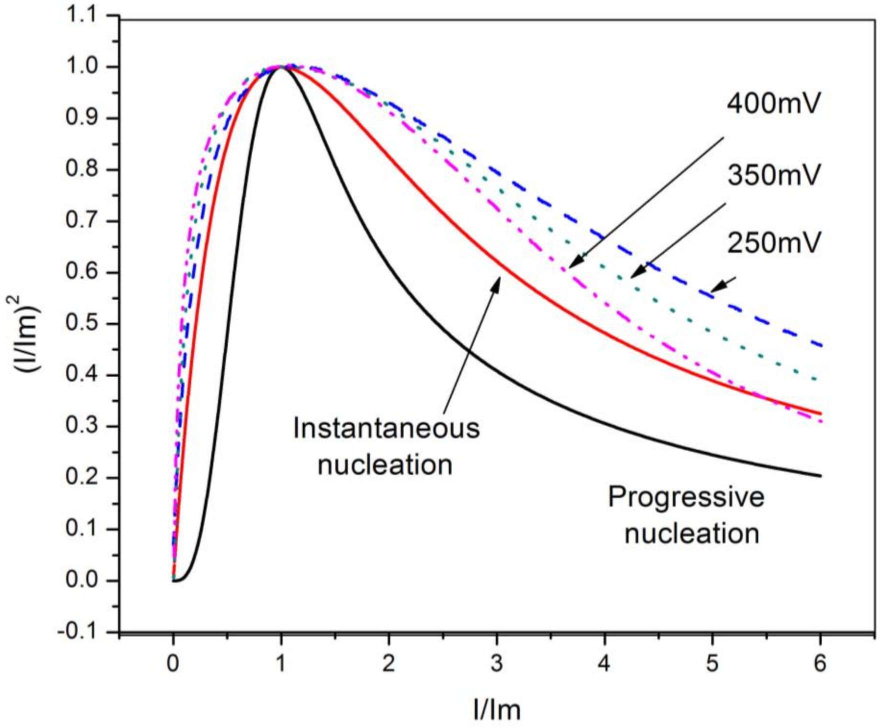

Figure 4. 6 Comparison of dimensionless theoretical nucleation model with experimental data derived from chronoamperometric data.

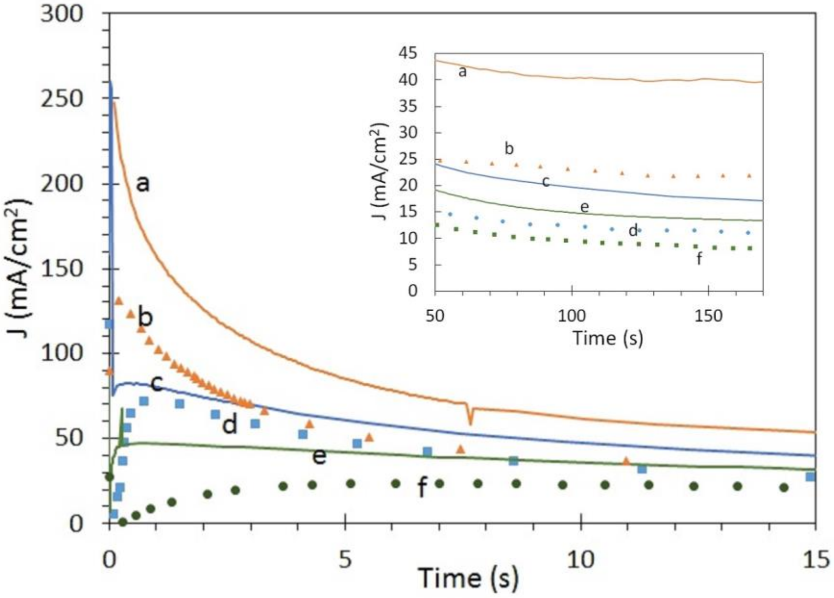

Figure 4. 7 Molar ratio and temperature effect on the chronoamperometry of Al plating on glassy carbon at 300mV overpotential.

(a) 2:1 molar ratio $AlCl_3$/EMIC at 70℃; (b) 1.5:1 molar ratio $AlCl_3$/EMIC at 70℃; (c) 2:1 molar ratio $AlCl_3$/EMIC at 50℃; (d) 1.5:1 molar ratio $AlCl_3$/EMIC at 50℃; (e) 2:1 molar ratio $AlCl_3$/EMIC at 30℃; (f) 1.5:1 molar ratio $AlCl_3$/EMIC at 30℃.

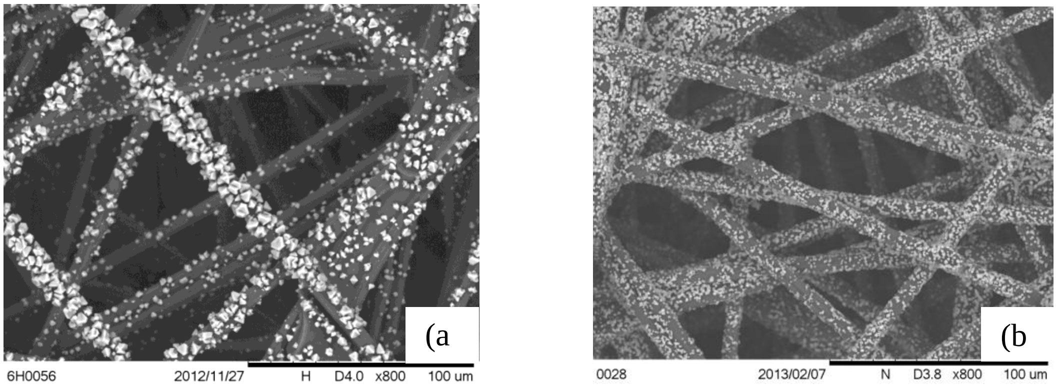

Figure 4. 8 SEM images of Al deposition morphology under different experimental conditions.

(a) controlled potential deposition at 300mV overpotential; (b)pulse current deposition,

apply 80mA/cm^2 for 10ms then relax for 2s.

CHAPTER 5

Melting/ Freezing Points of High Concentrations of $AlCl_3$ in a Saturated Chloroaluminate Ionic Liquid

5.1 Abstract

Melting/ freezing points of $AlCl_3$ in saturated chloroaluminate ionic liquids (Molar ratio 2:1 $AlCl_3$: 1-methyl-3-ethyl imidazolium chloride (EMIC)) are measured by differential scanning calorimetry (DSC). A critical range of temperature data (50-130℃) for $AlCl_3$ dissolution and precipitation from saturated chloroaluminate ionic liquids is obtained. This range of temperature data is of significance to control phase transition of $AlCl_3$ in saturated chloroaluminate ionic liquids. By applying the chloroaluminate ionic liquids to electrolytes for energy storage usage, solid $AlCl_3$ can be partially dissolved and precipitated out during the charging/discharging cycle of energy storage equipment. Therefore, the energy density of the electrolytes is expected to be greatly improved.

5.2 Introduction

It has been widely known that $AlCl_3$ can form eutectic melts at room temperature, i.e. ionic liquids, with different imidazolium chloride compounds.[1-4] The most typical imidazolium chloride compounds is 1-ethyl-3methyl imidazolium chloride (EMIC). This ionic liquid has low viscosity, high conductivity and wide electrochemical window. [2, 4-5] The excellent physical/chemical properties of $AlCl_3$/EMIC ionic liquid indicate that it has potential for energy storage applications.[6-8] The anions composition in $AlCl_3$/EMIC ionic liquid varies with the molar ratio of $AlCl_3$/EMIC (MR). Typically, the chemistry of $AlCl_3$/EMIC ionic liquid can be described in the following chemical reactions.[9]

$MR\ AlCl_3 + EMIC \rightarrow MR\ AlCl_4^{-1} + (1 - MR)\ Cl^{-1} + EMI^{+}$; when MR≤1

$MR\ AlCl_3 + EMIC \rightarrow (MR - 1)\ Al_2Cl_7^{-1} + (2 - MR)\ AlCl_4^{-1} + EMI^{+}$; when MR>1

Therefore, at room temperature the maximum molar ratio of $AlCl_3$: EMIC is 2:1 for the $Al_2Cl_7^-$ to be the main part of total anions in the electrolyte. This characteristic affects the energy density of $AlCl_3$/EMIC ionic liquid for energy storage applications.

Differential Scanning Calorimetry (DSC) is a fundamental technique in the thermal analysis and records the heat flow curve as measured while the temperature varies continuously.[10] In this paper we use DSC to measure melting/freezing point of excess $AlCl_3$ in the saturated $AlCl_3$/EMIC ionic liquid. The melting/freezing point data indicates when the $AlCl_3$ starts to dissolve/precipitate in the saturated $AlCl_3$/EMIC ionic liquid. Additionally, the different shapes of heat flow curves from different mole fractions of $AlCl_3$ in the ionic liquids are discussed based on their phase transition mechanism.

5.3 Experimental

The saturated $AlCl_3$/EMIC ionic liquid was prepared in glovebox using $AlCl_3$ and 1-methyl-3-ethly imidazolium chloride (EMIC) in a 2:1 molar ratio. Molar ratio 1.5:1 and 1:1 ionic liquids were also prepared to test against the data from literature.[5] The transparent $AlCl_3$ crystal was purified from yellowish $AlCl_3$ powder (Fluka, >99% anhydrous) based on the reported method.[1,11] EMIC is synthesized under the help from Dr. Trulove.[11] 1-Methylimidazole is further purified by reflux and distillation before used. EMIC is dissolved and recrystallized in acetonitrile (Sigma-Aldrich, 99.8%) and ethyl acetate (Sigma-Aldrich, 99.8%) for 3 times before it is used to prepare the ionic liquid. Table 5.1 shows the purity and purification methods used for chemicals synthesis and preparation.

Samples for DSC measurements were prepared inside the glovebox using a Tzero press, Tzero standard aluminum pans, and Tzero hermetic lids. The samples were prepared by applying 1, 3, or 5 μL of ionic liquid inside the pans and then adding excess $AlCl_3$. The ratios were determined by subtracting the prerecorded mass of each pan and average mass of at least 3 samples each of 1, 3, and 5 μL ionic liquid from the total sealed sample mass.

Thermal analyses were performed on the samples using differential scanning calorimetry with a TA Instruments DSC Q2000, and data were evaluated using TA Instruments Universal Analysis 2000.

5.4 Results and Discussions

Samples with different mole fractions of $AlCl_3$ are measured by DSC. Generally, during the heating/cooling process the peaks on the heat curve represent the phase transitions, such as melting/freezing, at the certain temperature range. Melting/freezing points of the samples marked by the software’s calculation can be easily obtained. However, to interpret the different shapes of heat curve peaks is difficult. Here, we show two representative heat curves in Figure 5.1 and 5.2 to discuss the reasons of different shapes of peaks.

$AlCl_3$/EMIC ionic liquid is the combination of different anions, i.e. $Al_2Cl_7^-$, $AlCl_4^-$ and Cl^-, and EMI^+ cation. So this ionic liquid belongs to the mixture compound and the melting curves are concave in shape. Their peak maxima are usually considered as the melting point. In Figure 5.1 no obvious endothermic peak is observed during the heating process indicating that the melting phase transition does not occur during this temperature range. However, a wide exothermic peak on the heating curve marked by software indicates that a possible supper-cooling crystallization process occurs after the temperature of ionic liquid decreases below -85℃. This characteristic peak is unique in the sample of the molar ratio 2:1 $AlCl_3$/EMIC ionic liquid. Reference literature reported that the ionic liquid at molar ratio 2:1 undergoes a glassy transition process at the low temperature and no obvious melting/freezing phase transition occurs.

In Figure 5.2 the DSC heat curve shows the heat flow changes in heating/cooling process for the sample of molar ratio 2.7:1 $AlCl_3$/EMIC ionic liquid. At room temperature the maximum molar ratio for the chloroaluminate ionic liquid is only 2:1, as the $AlCl_3$ reacts with EMIC to form the ionic liquid $Al_2Cl_7^-$ and EMI+. The excess $AlCl_3$ will stay as the solid in the ionic liquid at molar ratio 2:1. Although the existence form of $AlCl_3$ in ionic liquid is uncertain, by elevating the temperature to over 50℃, $AlCl_3$ is possible to be further dissolved into the ionic liquid. The heat from the phase transition (or maybe reaction transition) is recorded in Figure 5.2. Both endothermic and exothermic peaks are recorded during the melting and freezing phase transitions of the excess $AlCl_3$ in the saturated ionic liquid. The peaks, especially the endothermic peaks, are wider than the normal peaks obtained from the samples of pure EMIC, pure $AlCl_3$ and ionic liquids with molar ratio less than 2:1. This indicates that the slow diffusion and nucleation process exists during melting and freezing phase transitions of $AlCl_3$ in the saturated $AlCl_3$/EMIC ionic liquid. Similar characteristics occur in both samples with 0.73 and 0.75 mole fractions of $AlCl_3$, while in the samples with higher mole fractions of $AlCl_3$, such as 0.82, 0.85 and 0.89, this characteristic is not obvious and shape of peaks are more similar to those from the pure $AlCl_3$.

The melting/freezing points of $AlCl_3$/EMIC ionic liquids at different mole fractions of $AlCl_3$ are listed in Table 5.2. The freezing point of the sample with mole fraction of $AlCl_3$ 0.6 is not available because the DSC heat curve shows a characteristic of glassy transition during cooling process and no obvious freezing phase transition is obtained. These data together with related data from reference literature are plotted in Figure 5.3 as the complete phase diagram of $AlCl_3$/EMIC ionic liquids.

As seen from the phase diagram of $AlCl_3$/EMIC ionic liquid in Figure 5.3, the melting/freezing curves are steeper between the mole fraction of $AlCl_3$ 0.68 and 0.8. Once the mole fraction of $AlCl_3$ is over 0.8, the melting/freezing point data slowly approaches the value of pure $AlCl_3$. The difference between melting point and freezing point is larger when the mole fraction of $AlCl_3$ is over 0.68. This may result from the slow dissolving and crystallization processes of $AlCl_3$ in the saturated $AlCl_3$/EMIC ionic liquid. From this phase diagram a range of temperature suitable to control $AlCl_3$

dissolving and precipitating from the saturated ionic liquid is established. It is best to adjust temperature in the range from 50℃ to 130℃ to dissolve and precipitate the excess amount of $AlCl_3$.

5.5 Conclusion

DSC heat curves are measured from samples of different $AlCl_3$ mole fractions of $AlCl_3$/EMIC ionic liquids. Melting/freezing points of ionic liquids with different $AlCl_3$ mole factions are obtained from these DSC heat curves. Phase diagram of $AlCl_3$ in ionic liquid, especially the region where excess $AlCl_3$ exists in the saturated ionic liquid, is plotted. A suitable range of temperature (50-130℃) is chosen based on the phase diagram to control the excess amount of $AlCl_3$ dissolving and precipitating from the saturated ionic liquid.

Reference

[1] Wilkes, J. S.; Levisky, J. A.; Wilson, R. A.; Hussey, C. L. Dialkylimidazolium Chloroaluminate Melts-a New Class of Room-Temperature Ionic Liquids for Electrochemistry, Spectroscopy, and Synthesis. *Inorganic Chemistry* **1982**, *21*, 1263–1264.

[2] Wilkes, J. S. A short history of ionic liquids—from molten salts to neoteric solvents. *Green Chemistry*. **2002**, *4*, 73–80.

[3] Dymek, C. J.; Williams, J. L.; Groeger, D. J.; Auborn, J. J. An Aluminum Acid-Base Concentration Cell Using Room-Temperature Chloroaluminate Ionic Liquids. *Journal of the Electrochemical Society*. **1984**, *131*, 2887–2892.

[4] Gifford, P.; Palmisano, J. A substituted imidazolium chloroaluminate molten salt possessing an increased electrochemical window. *Journal of the Electrochemical Society* **1987**, *134,* 610-614.

[5] Fannin, A. A.; Floreani, D. A.; King, L. A.; Landers, J. S.; Piersma, B. J.; Stech, D. J.; Vaughn, R. L.; Wilkes, J. S.; Williams, J. L. Properties of 1,3-Dialkylimidazolium Chloride-Aluminum Chloride Ionic Liquids. 2. Phase Transitions , Densities , Electrical Conductivities , and Viscosities. *Journal of physica Chemistry* **1984**, *88,* 2614–2621.

[6] Dymek, C. J.; Reynolds, G. F.; Wilkes, J. S. A Rechargeable Cadmium-Bromine Battery Using Room Temperature Chloroaluminate Molten Salts. *Journal of Electrochemical Society* **1987**, *134*, 1658–1663.

[7] Carlin, R. T.; Long, H. C. De; Fuller, J.; Trulove, P. C. Dual Intercalating Molten Electrolyte Batteries. *Journal of Electrochemical Society* **1994**, *141,* L73–L76.

[8] Galinski, M.; Lewandowski, a; Stepniak, I. Ionic liquids as electrolytes. *Electrochimica Acta* **2006**, *51*, 5567–5580.

[9] Lipsztajn, M.; Osteryoung, R. A. Electrochemistry in Neutral Ambient-Temperature Ionic Liquids .1.Studies of Iron(Iii), Neodymium(Iii), and Lithium(I). Inorganic Chemistry 1985, 24, 716–719.

[10] Hohne, G. W. H.; Hemminger, W. F.; Flammersheim, H.-J. Differential Scanning Calorimetry, 2nd ed.;Springer-Verlag: Berlin, **2003**.

[11] Trulove, P.C. The Chemistry of Proton in Ambient-temperature Chloroaluminate Molten Salts, Thesis, State of University of New York, Buffalo **1992**, 25-44.

Appendix

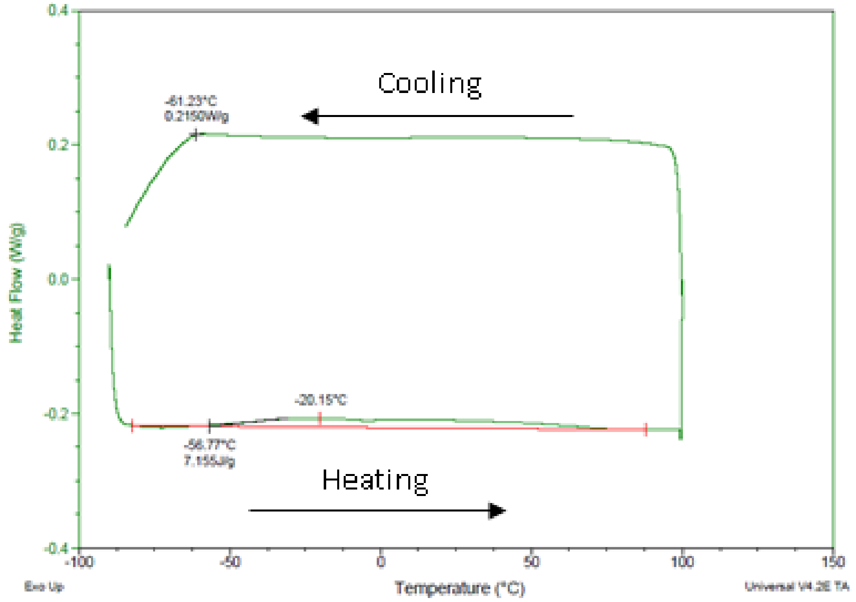

Figure 5. 1 DSC heat curve of molar ratio 2:1 $AlCl_3$: EMIC

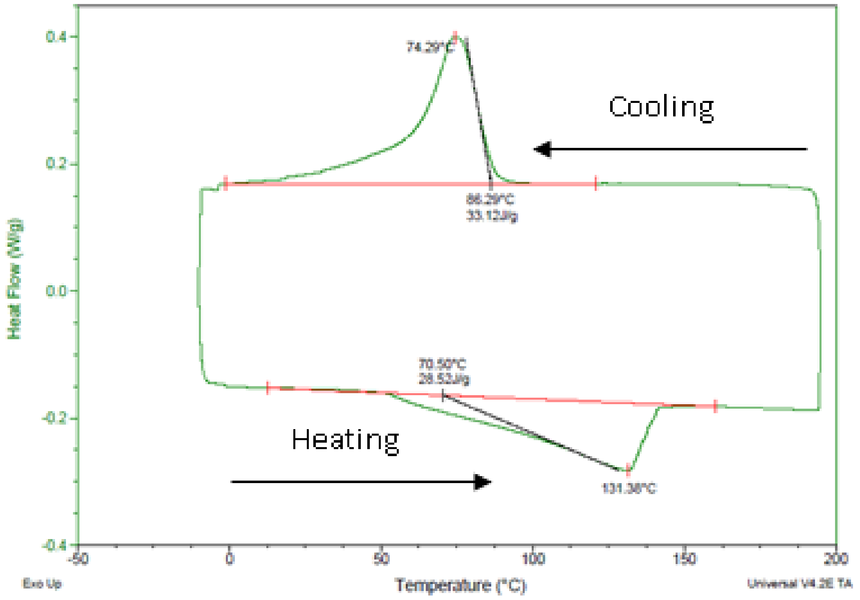

Figure 5. 2 DSC heat curve of molar ratio 2.7:1 $AlCl_3$: EMIC

(Mole fraction of $AlCl_3$ is 0.73)

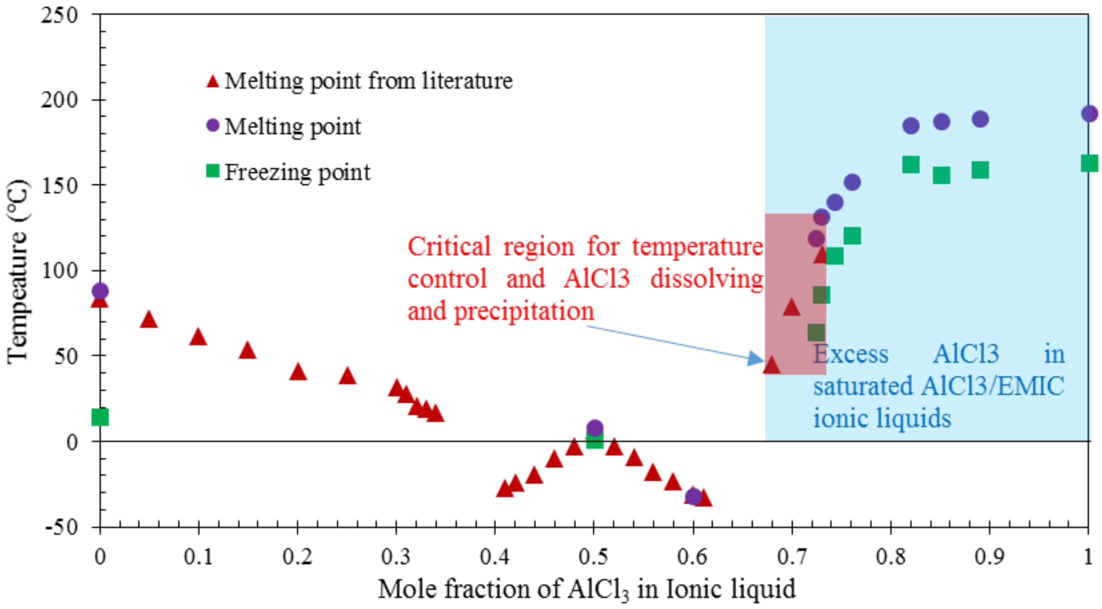

Figure 5. 3 The Phase diagram of $AlCl_3$/EMIC ionic liquids including data from reference literature[5]

Table 5. 1 Purity and Purification of Chemical Compounds Used in Ionic Liquid Preparation

Compound	Source	Purity (mass fraction)	Purification Method
Aluminum Chloride	Fluka	0.99	Sublimation
1-Methylimidazole	Aldrich	0.99	Distillation and reflux
Chloroethane	Aldrich	0.997	-
Acetonitrile	Sigma-Aldrich	0.998	-
Ethyl acetate	Sigma-Aldrich	0.998	-

Table 5. 2 Melting/freezing point of $AlCl_3$/EMIC ionic liquids at different mole fractions of $AlCl_3$

Mole fraction of $AlCl_3$	**Melting Point (℃)**	**Freezing Point (℃)**
0	88.7	14.8
0.5	8.5	1.1
0.6	-31.8	N/A
0.724	119.4	64
0.729	131.4	86.3
0.743	140.2	108.6
0.76	151.8	120.8
0.82	185	162
0.85	187.5	156
0.89	189.1	159
1	192	163

CHAPTER 6

Investigation of Al Deposition on Porous Carbon Materials in a Flow-Through Cell

6.1 Abstract

Development of Al based flow battery arises with issues on storage of Al deposits and high rate growth of Al deposits without dendrite formation. This paper focuses on Al deposition on the carbon paper in a flow-through cell. Fourier transform infrared spectroscopy (FTIR) and scanning electron microscope (SEM) are applied to characterize the Al deposits on the carbon paper. The performances of carbon paper and the solid Al disk as substrates are discussed. In the flow-through cell, the current density of Al deposition on carbon paper is remarkably higher than that on Al disk.. However, dendrites prefer to grow on the Al disk substrate. The electrolyte flow rate and the flow direction also play important roles in determining current densities and dendrite formation for Al deposition on carbon paper.

6.2 Introduction

To decrease pollution and environmental hazards from the use of fossil energy, the utilization of sustainable energy such as wind, solar has become a recent focus of energy research.[1-6] However, the electricity converted from wind and solar energy should be utilized immediately or stored. Energy storage is necessary for utilization of these energy sources that are available only during part of a day or at irregular times.[1, 4-7] The recent applications of all-vanadium redox flow battery (VRFB) in wind or solar farms gradually get success on electrical grid management.[6, 8-12] But the VRFB naturally comes with a disadvantage on low volumetric energy density (ca.25-40Wh/L) because of low solubility of the vanadium salts and the low electrochemical window of the aqueous electrolyte.[6] In addition, the low reserve of vanadium in the Earth’s Crust also limits the costs of

VRFB and its large-scale application. Thus, it is of high priority to develop new electrochemical energy storage systems (ESS) with higher energy density and low capital cost.[6, 12-16]

Aluminum (Al) is the third most abundant element in the Earth's Crust and maintain the low cost compared with vanadium.[17] As the Al has three transferable electrons, the theoretical specific capacity is 2978Ah/kg which is much higher than that of the vanadium. Therefore, Al based batteries may potentially become an excellent candidate in ESS. Historically, Al based batteries are divided to two categories: primary batteries and rechargeable batteries. Al/MnO2, Al/NiOOH and Al/air electrochemical systems belong to the primary batteries category because Al cannot be electrodeposited in an aqueous electrolyte system.[18-21] However, in a non-aqueous electrolyte system, such as alkali chloroaluminate molten salts ($AlCl_3$-NaCl system, $AlCl_3$-NaCl-KCl system)[22-25] and room temperature ionic liquids[26-33], Al can be reversibly plated and stripped on the conductive substrates. For example using $AlCl_3$/1,2-dimethyl-3-propylimidazolium chloride (DMPIC) ionic liquid as the electrolyte, a Al/Cl_2 rechargeable battery was investigated.[34] As the charging process of the Al/Cl_2 rechargeable battery equals to the consumption of the active materials ($AlCl_3$) in the ionic liquid and the acidic chloroaluminates may contain 66.7% mole fraction of $AlCl_3$ at maximum, the energy density of this Al/Cl_2 rechargeable battery should exceed 450Wh/L which is more than 10 times higher than that of VRFB. In order to store large amount of Al reduced from

$Al_2Cl_7^-$ in the ionic liquid without triggering short-circuit of the battery, the dendrite formation and growth which should be suppressed during the charging process.

Even though Al electrodeposition can occur on most conductive substrates such as steel, glassy carbon, copper, tungsten, gold and platinum,[28-33] a multi-step electrode reaction mechanism for Al deposition still exists.[35] It has been found that Al electrodeposition occurs under an important nucleation process for the $Al_2Cl_7^-$ reduction reaction controlled by a diffusion process.[26-27,30] The issue of dendrite formation during Al plating process still inhibits the development of the Al based rechargeable battery. The possible method to limit the dendrite formation may require one to maintain the ion diffusion process on the same level at different regions of an electrode surface. The developments of Zinc/air and soluble lead flow battery also provide valuable experience on limit metal dendrite growth.[13, 36] It has been reported that the flowing electrolyte, pulse charge mode and horizontal cell configuration can effectively limit Zn dendrite formation and growth. The experimental results on soluble lead flow battery indicate that lead (Pb) and lead oxide (PbO_2) can be plated on the reticulated vitreous carbon (RVC). However, both dendrites of Pb and PbO_2 can result in the battery failure if the cell configuration, electrolyte flow distribution and operating conditions are not optimized.[13, 37] Therefore, the dendrite formation and growth during Al deposition may also be suppressed by flowing electrolyte through a porous carbon substrate.[27]

Our recent study of Al deposition on porous carbon materials in the mixture of $AlCl_3$ and 1-ethyl-3-methylimidazolium chloride (EMIC) electrolyte has indicated that dendrite formation can be limited by plating Al on the non-planar electrode such as carbon paper or RVC.[27] In this paper, we further design a Teflon-structure three-electrode flow-through test cell to investigate the morphology and electrochemical performance of Al deposition on porous carbon materials.

6.3 Experimental

EMIC is synthesized by using the following procedure.[38] A pressure bottle is used as the reactor for synthesis of EMIC. 1-methylimidazole (Sigma Aldrich, 99%), chloroethane (Sigma Aldrich, 99.7%), and acetonitrile (Sigma Aldrich, 99%), are purified and water-removed before filled the pressure bottle for the synthesis reaction. The reaction takes about 2 weeks at room temperature with a rapidly-stirring magnetic stirrer. When the EMIC is fully precipitated from the reaction solvent, the reaction is close to complete. The purification of EMIC is required to remove the excess chloroethane, unreacted 1-methyimidazole and organic solvents. Acetonitrile is first added to the flask containing the reaction products, and EMIC should be dissolved in the excess of acetonitrile. Then the solution is slowly dropped into the flask containing ethyl acetate. EMIC should then crystalize in the ethyl acetate before the precipitate is vacuum filtered. After carefully repeated the same purification process 3 times, the final precipitates is removed from acetonitrile under vacuum for one week. Then the purified EMIC is acquired. $AlCl_3$ (Fluka, >99%) and is further purified by sublimation in a heavy wall glass tube.

The detailed purification process for $AlCl_3$ is described as follow. The main target of $AlCl_3$ purification process is to remove $FeCl_3$ leading to a yellowish color of $AlCl_3$. The tube for $AlCl_3$ sublimation is made of heavy-wall Pyrex glass which aims to prevent the explosion under $AlCl_3$ vapor pressure. A certain amount of NaCl and a 4cm length Al (Sigma Aldrich, 99.999%) wires are added to the heavy-wall glass tube to remove the $FeCl_3$ and Al_2O_3 before $AlCl_3$ powder is filled into the tube. All these assembly processes are operated under an Ar atmosphere in a glovebox. The glass tube containing $AlCl_3$, NaCl and Al wire is heated to 90℃ overnight under vacuum. Then a torch is used to seal the glass tube under vacuum. The sealed glass tube is further heated to 250℃ in the furnace for 4 hours before it is slowly pulled from the furnace. The cold air outside the furnace can let $AlCl_3$ vapor form a solid. Finally, purified $AlCl_3$ crystals are fully prepared. Chloroaluminate melt is prepared by slowly adding EMIC onto solid $AlCl_3$ crystals before the EMIC and $AlCl_3$ are weighted accurately. Figure 6.1 shows the schematic design of the three-electrode flow-through cell. The cell is built of Teflon to avoid corrosion and side chemical reactions with ionic liquids.

The carbon paper electrode is fixed between the electrolyte chamber and the right stopper cap. When the stopper cap is tighten, the flow-through cell is sealed without electrolyte leaking. The distance between the working electrode and counter electrode are minimized to 20mm in order to decrease the impact from the electrolyte resistance and provide enough space for a reference electrode designed to be close to the working electrode. The electrolyte is transferred to the flow-through cell by a syringe pump while the outlet of the cell close to the counter electrode leads the electrolyte to a beaker. The designed surface area of counter electrode is 4 times larger than that of the working electrode. This aims to prevent side reactions (expect Al dissolution) occurring on the counter electrode (CE).

Working electrodes are prepared by pouching 2050-A carbon paper (Fuel Cell Store) to a Φ11.11mm disk (the effective diameter is 10mm). The current density is calculated based on the geometrical surface area instead of the real surface area. The reference electrode is a 1 mm diameter Al wire (Alfa Aesar, 99.999%) immersed into the molar ratio 1.5:1 ($AlCl_3$: EMIC) chloroaluminate electrolyte in a glass tube with a porous vycor tip (Bioanalytical Systems Inc.). The counter electrode is a Φ20mm Al disk (purity 99.99%). A potentiostat (SP200, BioLogic) is used for controlled potential/current electrodeposition. A Bruker Vertex 70 Fourier transform Infrared (FTIR) Spectrometer is used to characterize the change of functional groups before and after the Al deposition on carbon paper. Hitachi TM-3000 SEM is used to observe the morphology of Al deposits on substrates.

6.4 Results and Discussions

6.4.1 FTIR characterization of Al deposition on carbon paper

FTIR is a useful tool to analyze the functional groups of chemical compounds and carbon materials.[39] The position of band usually helps to determine the type of functional groups and analyze the molecular structure. In Figure 6.2 the FTIR technique is applied to characterize carbon paper before and after Al deposition. The band at 3655cm^{-1} may be related to Al----O-H. Minor oxidation of Al forming Al_2O_3 may contribute to the band at 1384cm^{-1}. There are several bands such as 970 cm^{-1} and 760 cm^{-1} which disappear after carbon paper is plated with Al. Other bands at 2500cm^{-1} -2300cm^{-1} and 2900cm^{-1} may offset regular positions because Al particles are adsorbed on the surface of carbon paper.

6.4.2 Al deposition on carbon paper by the flow-through method

In our recent study of Al deposition on carbon paper, Al growth is shown to br a diffusion-controlled process. The insufficient diffusion of $Al_2Cl_7^-$ ion to the graphitized fibers of carbon paper can lead to no Al growth on the inner fibers of carbon paper which occurs especially at high overpotential. As we expect to store more Al deposits inside of carbon paper, the forced flow of electrolyte through th eelectrode (carbon paper) may help to achieve the goal. Therefore, we investigated plating of Al on carbon paper in a flow-through cell. The electrolyte has a molar ratio of 1.5 $AlCl_3$: EMIC ionic liquid and is transferred at selected flow rates by a syringe pump. So during Al plating process the fresh ionic liquid is continually transferred to the surface of porous materials. In Figure 6.3, the morphology of Al deposition on carbon paper under flow-through condition is shown. The morphology of Al depositsunder no-flow condition is illustrated in the embedded figure on top left.. For the flow-through condition, it is clearly shown that Al deposits have continually grown on the inner fibers of carbon paper as both inner and outer fibers are covered by Al deposits.

If the flow through the carbon paper electrolyte is not applied, Al growth on inner fibers may gradually decrease or even stops when the hemispherical diffusion layer of each Al nucleus merge to the semi-finite diffusion layer. Figure 6.4 shows the cross-section view of Al deposit morphology on carbon paper under the flow-through condition. The cross-section view indicates that some of Al deposits can grow on the inner fibers. However, the Al deposits are not averagely distributed throughout the carbon paper. Al deposits actually prefer to grow on one side of carbon paper facing to the counter electrode. The opposite side, however, has much less Aluminum growth. This suggests that the current distribution also varies largely at different region of carbon paper, even though the electrolyte is thoroughly transferred through the carbon paper.

In addition, when the overpotential further increases to 600mV as shown in Figure 6.5, the density of nucleation sites increases where it brings the smaller size of Al nuclei. The more nuclei form on the substrate, the higher transient current density become. Thus, the expansion of diffusion controlled zones of nuclei becomes fast. Even by improving the electrolyte flow rate to 5 ml/min, the diffusion-controlled effect cannot be attenuated thus only Al nuclei on outer layer of carbon paper can accept the ionic diffusion flux leading to the thickness of Al deposits on outer fibers thicker than those on inner fibers. Even the Al deposition process only last 1 minute, the difference on the thickness of Al deposits on various layers (see Figure 6.5) of carbon paper become obvious as listed in Table 6.1. Compared with 1st layer of carbon paper, the thickness of Al deposits on the 3rd layer decreases 74% Al deposits.

6.4.3 Performance tests for Al deposition on the carbon paper and Al disk substrate

Nevertheless, porous carbon materials, such as carbon paper, may still be a good choice for Al deposition/ dissolution in the design of the flow battery. In order to test the real performance of porous carbon materials on Al deposition, we compare the difference of plating Al on carbon paper and Al disk for 10 hours under the current-controlled method. To avoid the run out of electrolyte, as the syringe can only hold 50ml electrolyte at maximum, the flow rate of electrolyte for Al deposition on carbon paper is adjusted to 0.05 ml/min. The morphology of Al deposits on carbon paper shown in Figure 6.6 indicates that Al morphology varies at different locations. On the upper side (see the illustration in Figure 6.6) of carbon paper, a layer of Al deposits covers the fibers of carbon paper, and the size of Al crystals is small. However, on bottom side of carbon paper, the boulder-like Al deposits grow on the Al coated carbon paper. This result might derive from the the fact that the outlet for electrolyte is designed on top of the flow-through cell's chamber. As viscous ionic liquid is transferred at the low rate, the electrolyte on top ofthe flow-through cell's chamber may leave more easily than the electrolyte on the bottom. So after long time, the electrolyte at the bottom should have much less acidity than that in the upper layer. The decrease of acidity in the electrolyte may induce the appearance of boulder-like Al deposits. In cross-section view of carbon paper with Al deposits, the Al deposits are still dispersed differently on two sides of the carbon paper. Al prefers to be plated on the side facing to the counter electrode. The effect of electrical field may play an important role on Al deposition process.

Compared to the performance of Al deposition on carbon paper under flow-through condition, Al disk brings more dendrite formation and finally short-circuit. As the Al disk is a planar substrate, the Al deposition process is operated in the static electrolyte. Figure 6.7 shows dendrite forms on the Al wire current collector which directly contacts with the Al disk. The dendrite continually grow towards to the counter electrode and result in the decrease of overpotential from 0.9V to 0.1V. Finally the dendrite touches the counter electrode and the cell fails after Al deposition is operated for 7hr and 59min. The granular Al deposits also have a poor attachment to the Al disk surface and can be easily washed off by water.

Furthermore, we investigated the steady-state polarization curves of Al deposition on the carbon paper and Al disk. The polarization curve for the Al disk is measured in the static electrolyte, however, the flow rate effects on polarization curve for carbon paper were investigated. In general, to achieve the same level of current density, carbon paper should be a better choice for Al deposition than a flat solid Al disk substrate. Significant electrolyte resistances are observed in this series of polarization curves for both carbon paper and Al disk electrode because the large distance (20mm) between working and counter electrode. The different types of substrates, porous and planar, lead to the difference on the electrolyte resistance. As the flow rate has the positive effect on ionic diffusion to the surface of carbon paper, especially the inner fibers, the current density of Al deposition under the same level of overpotential can be improved by the increasing flow rate.

6.4.4 Flow direction effect on Al deposition on carbon paper.

The unique aspect of Al deposition in the chloroaluminate ionic liquids is the reduction of anion $Al_2Cl_7^-$ (a negatively charged ion) on the negative electrode. This characteristic may magnify the effect of electric field. As the anions have to overcome the resistance from the electric field to reach the negative electrode, the diffusion process should be strong enough to promote the reduction reaction. This might be the reason why Al deposits rarely grow on the inner fibers of carbon paper. Here, we investigate how Al forms the deposition when the flow direction follows the electric field direction in Figure 6.9. The common flow direction is defined as the electrolyte first flows through the working electrode and then counter electrode. The opposite flow direction is just the opposite of the common flow direction. During Al deposition, the opposite flow direction follows the electric field direction. The Al morphology is found to be boulder-like but without any dendrite formation for 10 hours Al deposition. The mass of Al deposits divided by the theoretic Al deposits mass calculated from total coulombs determines the current efficiency. The current efficiency reaches 91.2%, twice higher than that under the common flow direction. This indicates that most Al deposits are firmly attached to the carbon paper, while the dendrite formation and poor attachment of Al deposits leads to the low current efficiency (45.4%) under the common flow direction. This result may derive from the increasing acidity by the dissolution of Al on the counter electrode. So it may be better to maintain the acidity at the high level to limit the dendrite formation and growth.

6.5 Conclusions

In order to explore the potential porous carbon substrates for the application in the Aluminum based flow battery, Aluminum deposition on the carbon paper in the acidic $AlCl_3$/EMIC chloroaluminate ionic liquid is investigated by a three-electrode flow-through cell. The disappearance and offset of some band positions in the FTIR characterization of the Al coated carbon paper indicate the adsorption between Al particles and the functional groups of carbon paper. At low overpotential (350mV) Al can be plated on the inner fibers of carbon paper by the flow-through method. However, at high overpotential (600mV) even with the help of the enhanced flow-through process, the growth of Al deposits still maintain different rates on different layers of carbon paper. The growth of Al deposits prefers on the outer surface of the carbon paper. In the comparison of the performances of Al deposition in the flow-through cell, the growth of Al deposits on carbon paper has less issue on dendrite formation and faster rate shown in the polarization curves. The flow rate has the positive effect on the ionic diffusion and thus could improve current density of Al deposition. By adjusting the flow direction following the electric field direction, Al deposits on carbon paper can continually grow without dendrite formation. Therefore, the carbon paper has the huge potential in the application of the Al based flow battery.

Reference

[1] Nema, P., Nema, R. K., & Rangnekar, S. (2009). A current and future state of art development of hybrid energy system using wind and PV-solar: A review. *Renewable & Sustainable Energy Reviews*, *13*(8), 2096–2103. doi:10.1016/j.rser.2008.10.006

[2] Kang, B., & Ceder, G. (2009). Battery materials for ultrafast charging and discharging. *Nature*, *458*(7235), 190–193. doi:Doi 10.1038/Nature07853

[3] Divya, K. C., & Ostergaard, J. (2009). Battery energy storage technology for power systems-An overview. *Electric Power Systems Research*, *79*(4), 511–520. doi:DOI 10.1016/j.epsr.2008.09.017

[4] Yang, Z. G., Zhang, J. L., Kintner-Meyer, M. C. W., Lu, X. C., Choi, D. W., Lemmon, J. P., & Liu, J. (2011). Electrochemical Energy Storage for Green Grid. *Chemical Reviews*, *111*(5), 3577–3613. doi:Doi 10.1021/Cr100290v

[5] Wills, R. G., Collins, J., Stratton-Campbell, D., Low, C. T. J., Pletcher, D., & Walsh, F. C. (2009). Developments in the soluble lead-acid flow battery. *Journal of Applied Electrochemistry*, *40*(5), 955–965. doi:10.1007/s10800-009-9815-4

[6] Li, L., Kim, S., Wang, W., Vijayakumar, M., Nie, Z., Chen, B, Yang, Z. (2011). A stable vanadium redox-flow battery with high energy density for large-scale energy storage. *Advanced Energy Materials*, *1*(3), 394–400. doi:10.1002/aenm.201100008

[7] Barton, J. P., & Infield, D. G. (2004). Energy storage and its use with intermittent renewable energy. *Ieee Transactions on Energy Conversion*, *19*(2), 441–448. doi:Doi 10.1109/Tec.2003.822305

[8] Skyllas-Kazacos, M. (1986). New All-Vanadium Redox Flow Cell. *Journal of The Electrochemical Society*. doi:10.1149/1.2108706

[9] Rychcik, M., & Skyllas-Kazacos, M. (1988). Characteristics of A New All-Vanadium Redox Flow Battery. *Journal of Power Sources*, *22*(1), 59–67.

[10] Zhang, M., Moore, M., Watson, J. S., Zawodzinski, T. A., & Counce, R. M. (2012). Capital Cost Sensitivity Analysis of an All-Vanadium Redox-Flow Battery. *Journal of the Electrochemical Society*, *159*(8), A1183–A1188. doi:10.1149/2.041208jes

[11] Moore, M., Watson, J. S., Zawodzinski, T. A., Zhang, M., & Counce, R. M. (2012). Capital Cost Sensitivity Analysis of an All-Vanadium Redox-Flow Battery. *ECS Transactions*. doi:10.1149/1.3684787

[12] Weber, A. Z., Mench, M. M., Meyers, J. P., Ross, P. N., Gostick, J. T., & Liu, Q. (2011). Redox flow batteries: a review. *Journal of Applied Electrochemistry*, *41*(10), 1137–1164. doi:10.1007/s10800-011-0348-2

[13] Pletcher, D., & Wills, R. (2004). A novel flow battery—A lead-acid battery based on an electrolyte with soluble lead(II)I. flow cell studies. *Physical Chemistry Chemical Physics*, *6*, 1779–1785.

[14] Wills, R. G. a., Collins, J., Stratton-Campbell, D., Low, C. T. J., Pletcher, D., & Walsh, F. C. (2009). Developments in the soluble lead-acid flow battery. *Journal of Applied Electrochemistry*, *40*(5), 955–965. doi:10.1007/s10800-009-9815-4

[15] Suppes, G. J., Sawyer, B. D., & Gordon, M. J. (2011). High-Energy Density Flow Battery Validation. *AIChE Journal*, *57*(7), 1961–1967. doi:10.1002/aic

[16] De Leon, C. P., Frias-Ferrer, A., Gonzalez-Garcia, J., Szanto, D. A., & Walsh, F. C. (2006). Redox flow cells for energy conversion. *Journal of Power Sources*, *160*(1), 716–732. doi:DOI 10.1016/j.jpowsour.2006.02.095

[17] F.W. Clarke, H.S. Washington, *The Composition of the Earth's Crust*, (1924)

[18] D.S. Keir, M.J. Pryor, P.R. Speery, *Journal of Electrochemical Society*. 116 (1969) 319.

[19] D. Linden (Ed.), *Handbook of Batteries and Fuel Cells*, McGrow- Hill, New York, 1984.

[20] Licht, S. (1995). A High Energy and Power Novel Aluminum/Nickel Battery. *Journal of The Electrochemical Society*, *142*(10), L179. doi:10.1149/1.2050036

[21] Li, Q., & Bjerrum, N. J. (2002). Aluminum as anode for energy storage and conversion : a review, *110*(October 2001), 1–10.

[22] Lantelme, F., Alexopoulos, H., Devilliers, D., Chemla, M., Electrochimie, L., Pierre, U., & Cedex, F. P. (1991). A Gas Electrode : Behavior of the Chlorine Injection Electrode in Fused Alkali Chlorides. *Journal of Electrochemical Society*, *138*(6), 1665–1671.

[23] Lantelme, F., & Alexopoulos, H. (1989). Role of gas bubbles adsorbed on a carbon electrode: electroreduction of chlorine gas in fused salts. *Journal of Applied Electrochemistry*, *19*, 649–656.

[24] Knutz, B. C., Hjuler, H. A., Berg, R. W., & Bjerrum, N. J. (1993). Mechanism of Reaction in NaAlCl4 Molten Salt Batteries with Nickel Felt Cathodes and

Aluminum Anodes I . Modeling of the Battery Properties at Thermodynamic Equilibrium. *Journal of Electrochemical Society*, *140*(12), 3374–3379.

[25] Li, Q., Hjuler, H. A., Berg, R. W., & Bjerrum, N. J. (1990). Electrochemical Deposition of Aluminum from NaCl-AlCl3 Melts. *Journal of The Electrochemical Society*, *137*(2), 593–598. doi:10.1149/1.2086512

[26] Carlin, R. T., Crawford, W., & Bersch, M. (1992). Nucleation and Morphology Studies of Aluminum Deposited from an Ambient-Temperature Chloroaluminate Molten Salt. *Journal of Electrochemical Society*, *139*(10), 2720–2727.

[27] Zhang, M., Watson, J. S., Counce, R. M., Trulove, P. C., & Zawodzinski, T. a. (2014). Electrochemistry and Morphology Studies of Aluminum Plating/Stripping in a Chloroaluminate Ionic Liquid on Porous Carbon Materials. *Journal of the Electrochemical Society*, *161*(4), D163–D167. doi:10.1149/2.048404jes

[28] Takahashi, S., Akimoto, K., & Saeki, I. (1989). Aluminum Plating From the Room Temperature Molten Salt Electrolyte. *Hyomen Gijutsu*, *40*(1), 134–135.

[29] Auborn, J., & Barberio, Y. (1985). An Ambient Temperature Secondary Aluminum Electrode : Its Cycling Rates and Its Cycling Efficiencies. *Journal of Electrochemical Society*, *132*(3), 598–601.

[30] Robinson, J. I., & Osteryoung, R. A. (1980). The Electrochemical Behavior of Aluminum in the Low Temperature Molten Salt System n Butyl Pyridinium Chloride : Aluminum Chloride and Mixtures of This Molten Salt with Benzene. *Journal of Electrochemical Society*, *1166*(January), 122–128.

[31] Jiang, T., Chollier Brym, M. J., Dubé, G., Lasia, a., & Brisard, G. M. (2006). Electrodeposition of aluminium from ionic liquids: Part I—electrodeposition and surface morphology of aluminium from aluminium chloride (AlCl3)–1-ethyl-3-methylimidazolium chloride (EMIC) ionic liquids. *Surface and Coatings Technology*, *201*(1-2), 1–9. doi:10.1016/j.surfcoat.2005.10.046

[32] Jiang, T., Brym, M. J. C., Dube, G., Lasia, A., & Brisard, G. M. (2006). Electrodeposition of aluminium from ionic liquids: Part II - studies on the electrodeposition of aluminum from aluminum chloride ($AlCl_3$) - trimethylphenylammonium chloride (TMPAC) ionic liquids. *Surface & Coatings Technology*, *201*(1-2), 10–18. doi:DOI 10.1016/j.surfcoat.2005.12.024

[33] Endres, F. (2002). Ionic liquids: Solvents for the electrodeposition of metals and semiconductors. *ChemPhysChem*, *3*(2), 144–145. Retrieved from <Go to ISI>://000174036200002

[34] Gifford, P., & Palmisano, J. (1988). An aluminum/chlorine rechargeable cell employing a room temperature molten salt electrolyte. *Journal of the Electrochemical Society*, *135*(13), 650–654. Retrieved from http://link.aip.org/link/?JESOAN/135/650/1

[35] Ahn, S. J., Jeong, K., & Lee, J. J. (2009). Mechanism of Electrochemical Al Deposition from Room-Temperature Chloroaluminate Ionic Liquids. *Bull. Korean Chem. Soc*, *30*(1), 233.

[36] Pei, P., Wang, K., & Ma, Z. (2014). Technologies for extending zinc-air battery's cyclelife: A review. *Applied Energy*, *128*, 315–324. doi:10.1016/j.apenergy.2014.04.095

[37] Wills, R. G. a., Collins, J., Stratton-Campbell, D., Low, C. T. J., Pletcher, D., & Walsh, F. C. (2009). Developments in the soluble lead-acid flow battery. *Journal of Applied Electrochemistry*, *40*(5), 955–965. doi:10.1007/s10800-009-9815-4

[38] Trulove, P.C. The Chemistry of Proton in Ambient-temperature Chloroaluminate Molten Salts, Thesis, State of University of New York, Buffalo **1992**, 25-44.

[39] Saikia, B. J., & Parthasarathy, G. (2010). Fourier Transform Infrared Spectroscopic Characterization of Kaolinite from Assam and Meghalaya, Northeastern India. *Journal of Modern Physics*, *01*(October), 206–210. doi:10.4236/jmp.2010.14031

Appendix

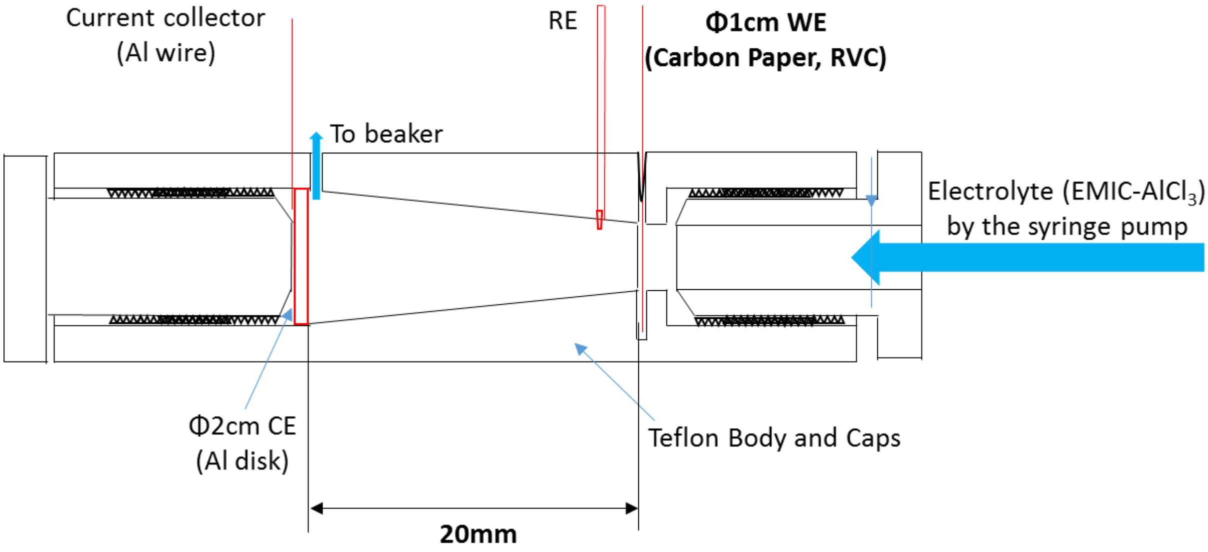

Figure 6. 1 Schematic illustration of the three-electrode flow-through cell for the Al deposition investigation

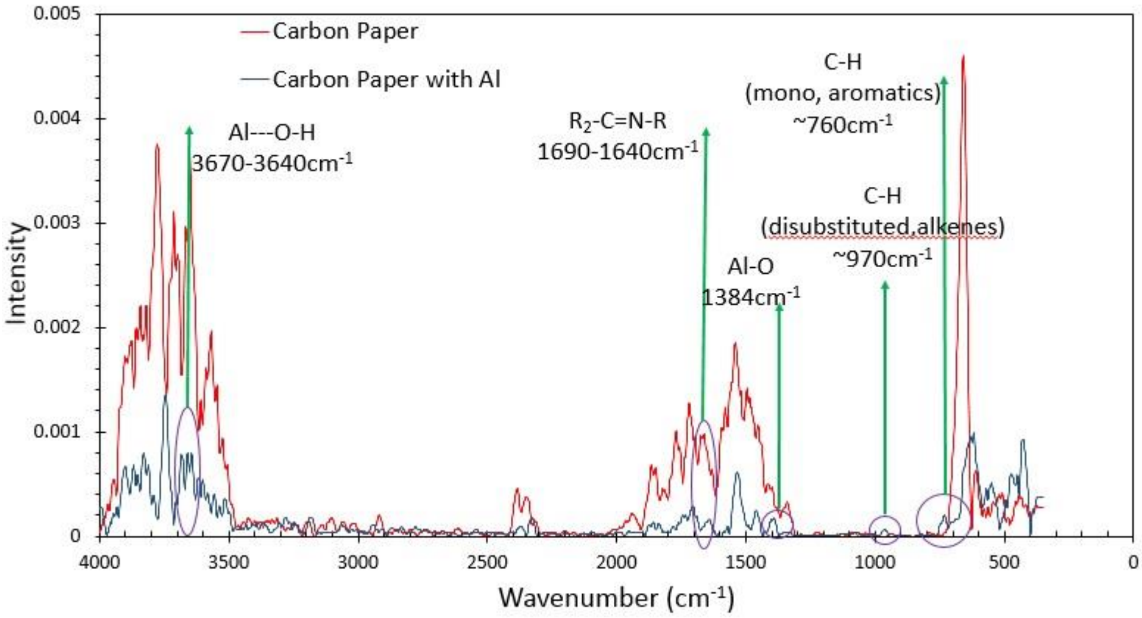

Figure 6. 2 FTIR characterization of carbon paper before and after Al deposition

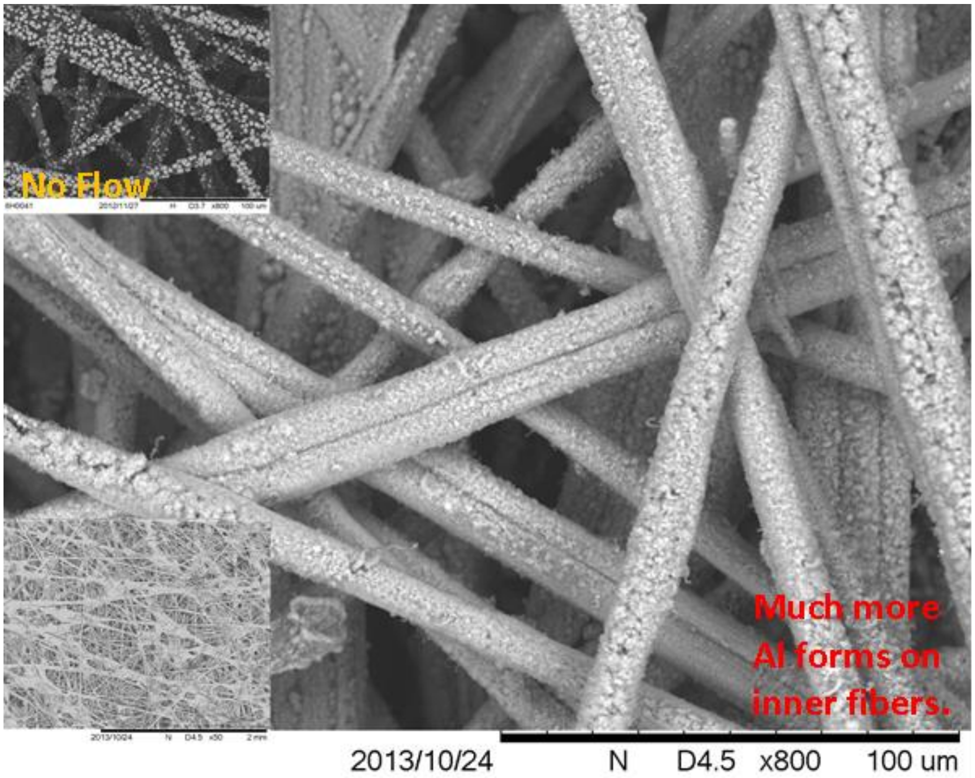

Figure 6. 3 . Comparison of morphology of Al electrodeposition on carbon paper.

Al is electrodeposited at controlled potential (350mV vs Al/Al(III)) in 1.5$AlCl_3$:EMIC ILs for 10mins with 1ml/min flow rate. The top left image shows the morphology of Al deposition by controlled potential (350mV vs Al/Al(III)) in 1.5$AlCl_3$:EMIC ILs for 3mins without flowing electrolyte. The bottom left image shows the global morphology view of the same sample under the flow-through condition.

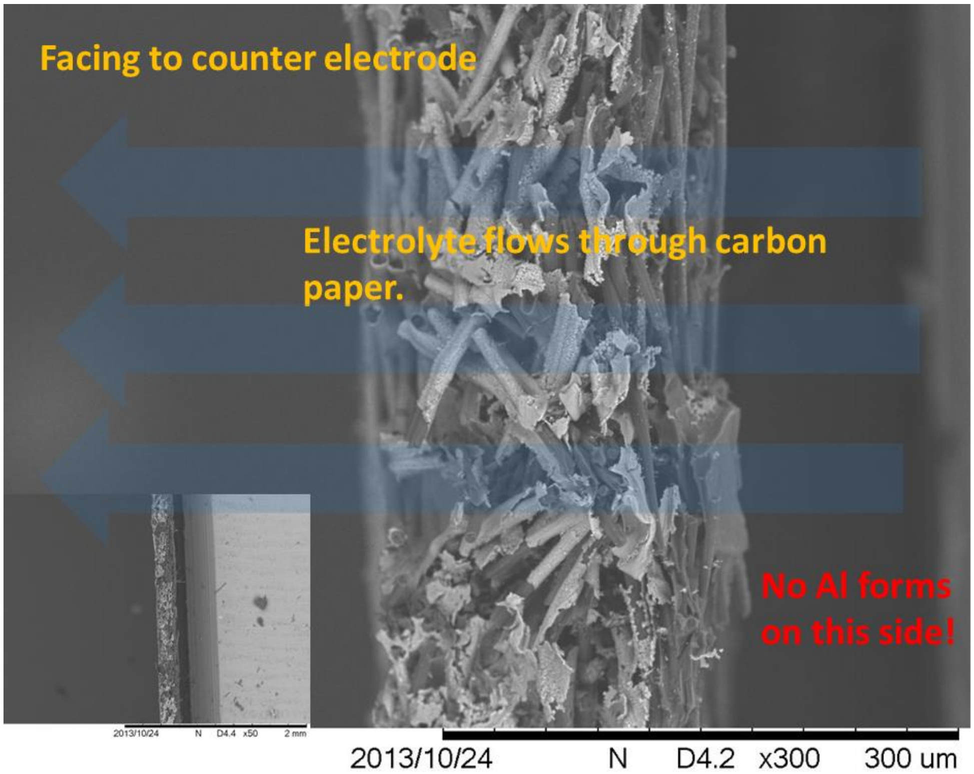

Figure 6. 4 Cross-section view of Al deposit morphology on carbon paper.

Al is electrodeposited at controlled potential (350mV vs Al/Al(III), average current density 16.4 mA/cm^2) in 1.5AlCl$_3$:EMIC ILs for 10mins with flow rate at 1ml/min.

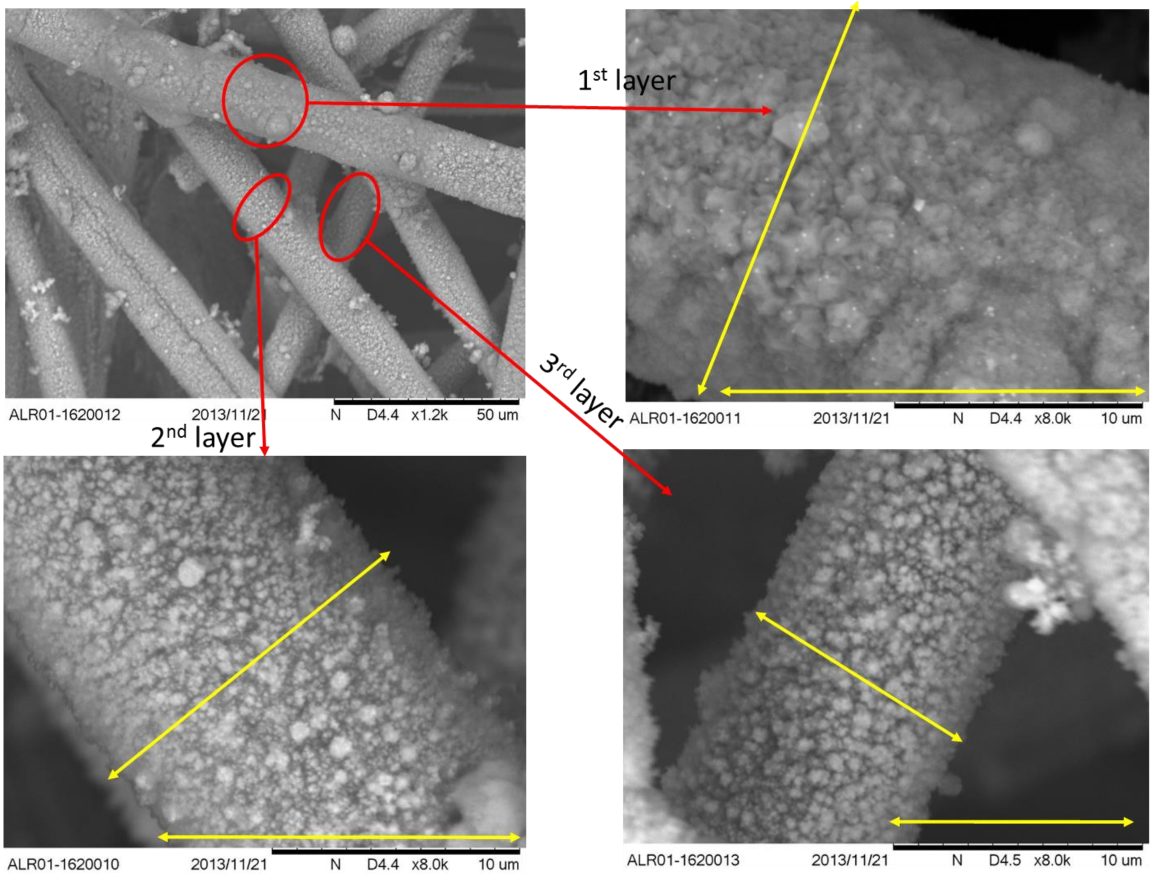

Figure 6. 5 Comparison of the thickness of Al deposits on different layers of carbon paper Al is electrodeposited at controlled potential (600mV vs Al/Al(III), average current density 39.1 mA/cm^2) in 1.5AlCl$_3$:EMIC ILs for 1 min with flow rate at 5 ml/min.

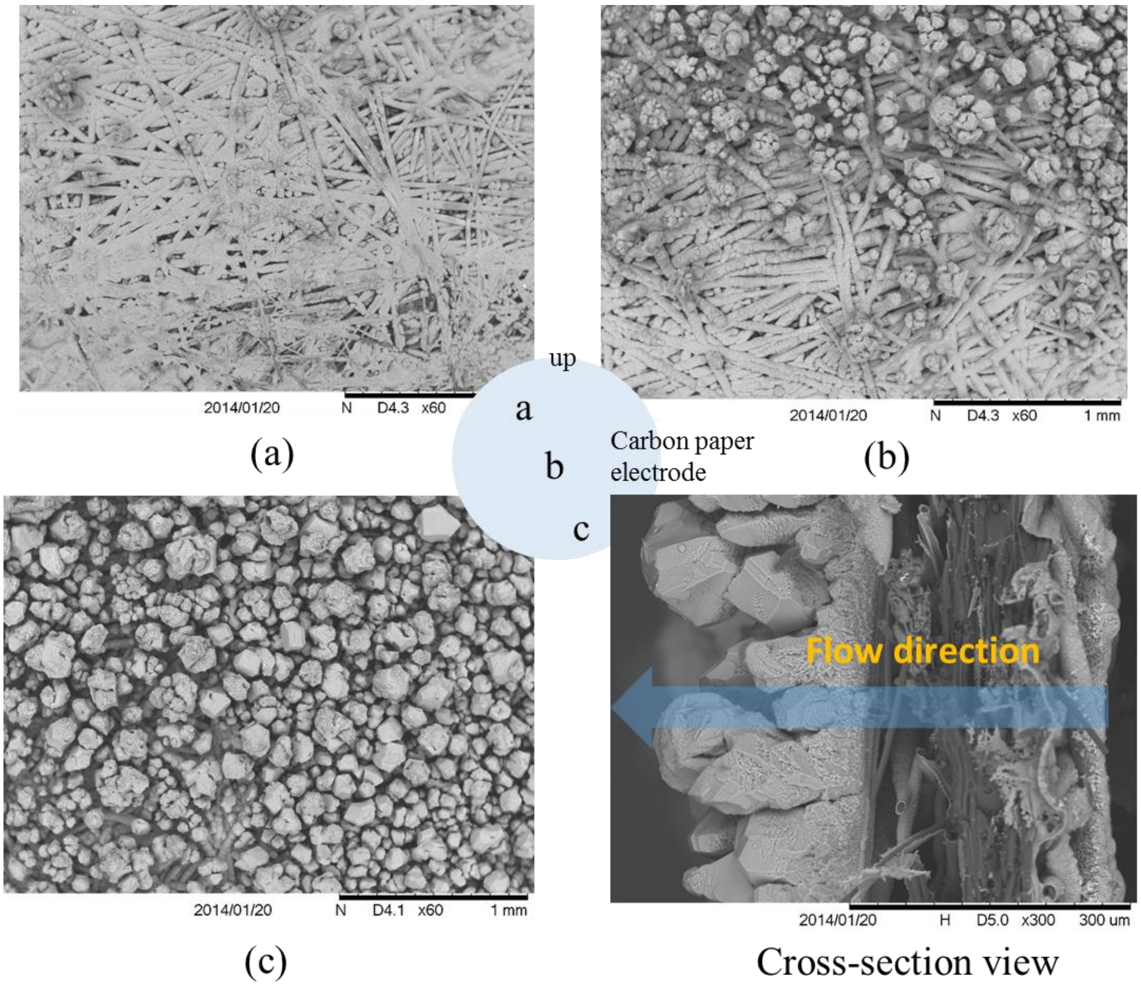

Figure 6. 6 Morphology of Al deposits on carbon paper in the 10 hours Al plating test

The figures (a), (b) and (c) correspond to Al morphology of different regions of carbon paper marked in the middle of the figure. Al is electrodeposited with controlled current method (the nominal current density 26.6 mA/cm^2, overpotential varies 400-500mV) in 1.5AlCl$_3$: EMIC ILs for 10 hours with flow rate at 0.05 ml/min.

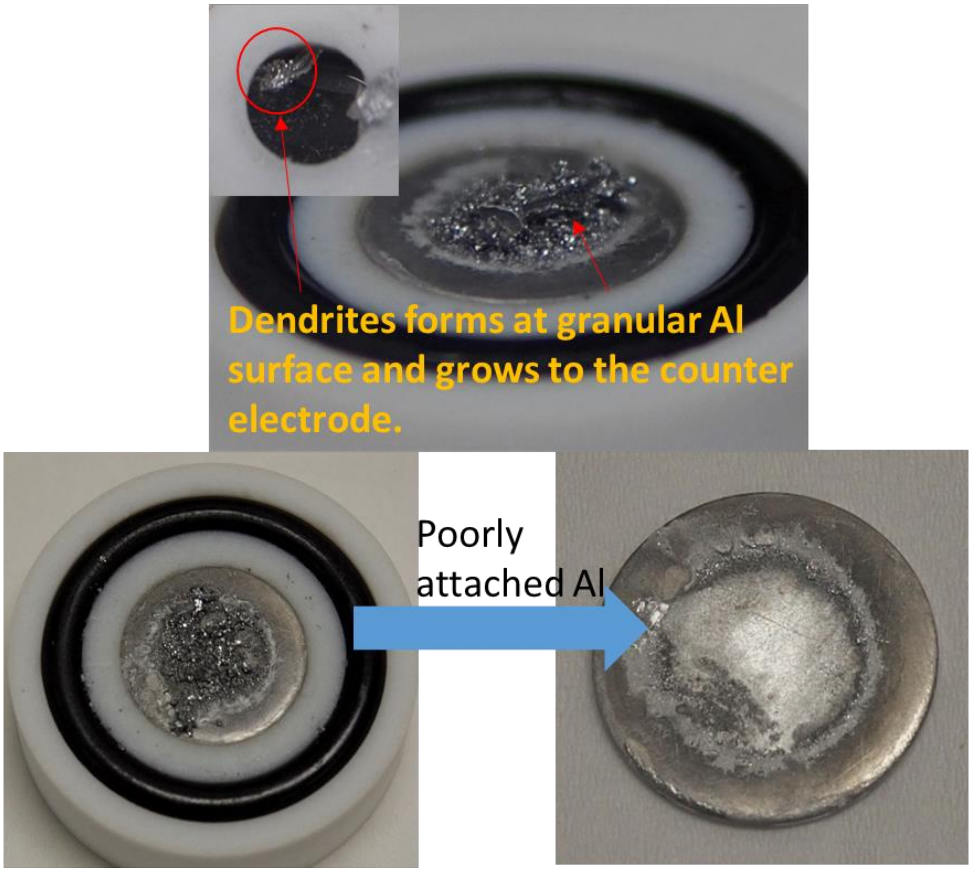

Figure 6. 7 Morphology of Al deposits on Al disk substrate in the 10 hours Al plating test

Al is electrodeposited with controlled current method (the nominal current density 25.6 mA/cm^2, overpotential varies 1000-100mV) in $1.5AlCl_3$: EMIC ILs for 10 hours.

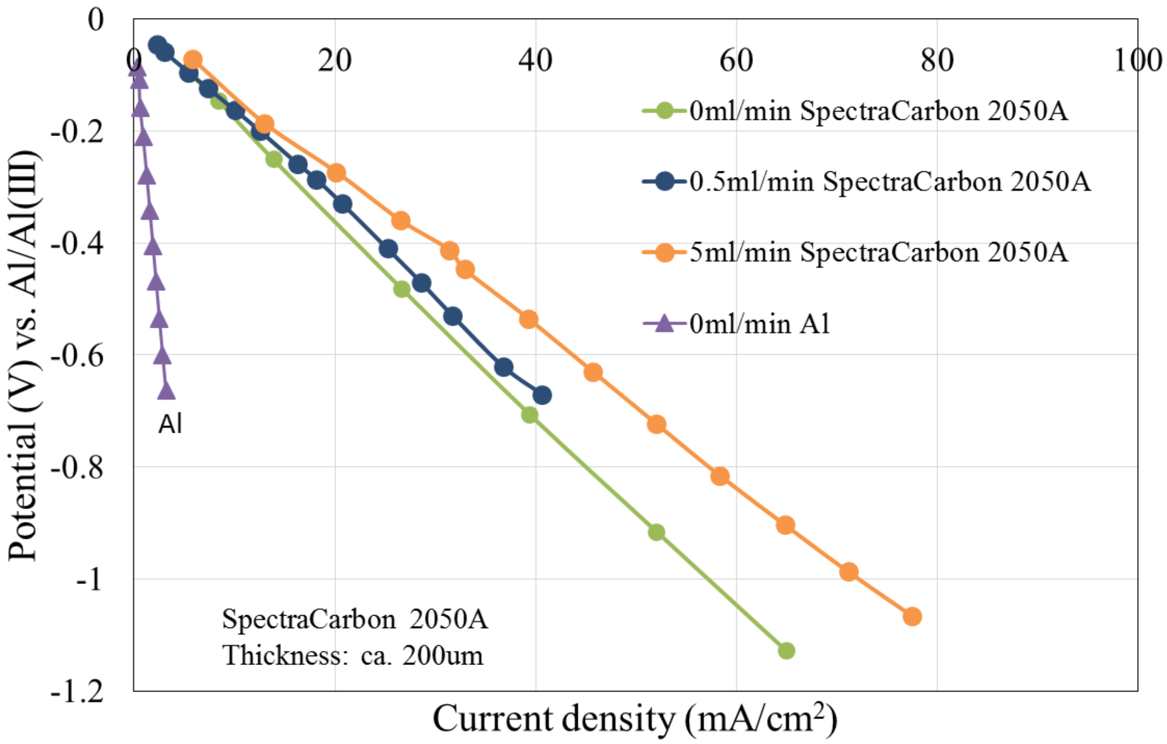

Figure 6. 8 Steady-state polarization curves of Al deposition on Al disk and carbon paper at different flow rates.

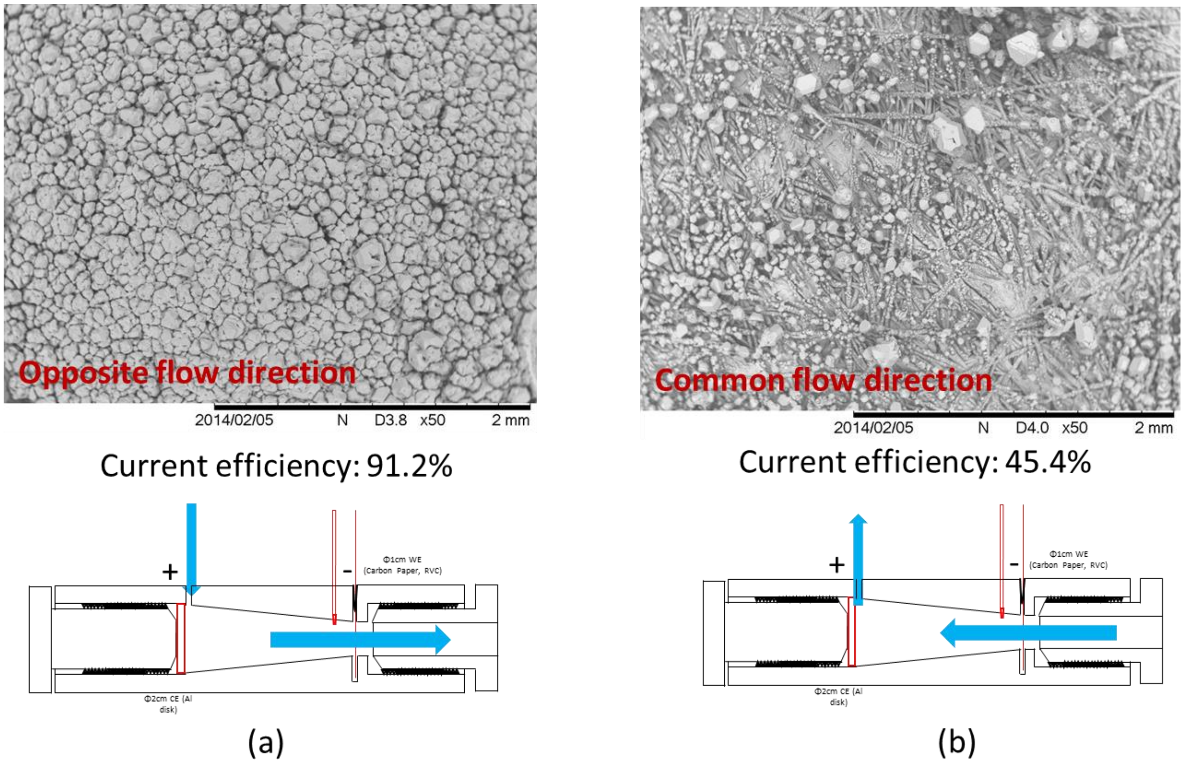

Figure 6. 9 Comparison of Al deposits on carbon paper under different flow directions

Al is electrodeposited with controlled current method (the nominal current density 26.6 mA/cm^2, overpotential varies 400-500mV) in 1.5$AlCl_3$: EMIC ILs for 10 hours with flow rate at 0.05 ml/min.

Table 6. 1 Estimated thickness of Al deposits on different layers of carbon paper.

Layer number	**Thickness of Al deposits (um)**	**Percentage of the decreased thickness**
1	5	0
2	3.8	24%
3	1.3	74%

CHAPTER 7

An Aluminum Based Hybrid Supercapacitor with The Acidic $AlCl_3$/1-Ethyl-3-Methylimidazolium Chloride Ionic Liquid

7.1 Abstract

In this paper we successfully demonstrate an Al based hybrid supercapacitor using high surface area carbon materials in 1.5 $AlCl_3$: EMIC chloroaluminate ionic liquid. The graphene and activated carbon are tested for the material and electrochemical characterizations. The graphene may not be compatible with the chloroaluminate ionic liquid because of the high catalytic ability for Cl_2 evolution at lower potential. However, the activated carbon with an amorphous structure is less likely to have catalytic properties and can be applied for the Al based hybrid supercapacitor. The mismatch between the small pore size of activated carbon and the large ionic-diameter of complex ions results in the high charge-transfer resistance. Based on the electrochemical impedance measurements the contact resistance maintains at 1.25ohm however the charge-transfer resistances decrease with overpotentials. Furthermore, the wettability effect is investigated on the choice between Polytetrafluoroethylene (PTFE) and the aqueous base modified styrene butadiene rubber (SBR). The hydrophilic property of SBR may promote the entrance of ions to the micropores of activated carbon. The activated carbon electrode using $3\%_{mass}$ SBR leads to an improved specific capacitance (70F/g) and energy density (34Wh/kg) competitively with the recent reports on the metal based hybrid supercapacitor.

7.2 Introduction

Recently the increasing demand on carbon dioxide emission reduction and the emerging market of electric vehicles (EVs) promote related researches on electrochemical energy storage devices.[2-8] The research and development (R&D) of Lithium (Li)-ion battery

(LIB) become predominant because the low molecular weight of Li leads to high energy densities.[9-11] However, there are several disadvantages of LIB limiting its application in the markets of EVs and large-scale electric energy storage (EES).[12-15] First, the Li reserve is not abundant in the Earth's crust which will limit the expansion of LIB market. Secondly, the organic solvents widely applied to the electrolytes for LIB raises the safety issues for the use of LIB in EVs should be seriously considered. Thirdly, the LIB relies on slow kinetics and sluggish Li^+ diffusion in anode/cathode materials.[16-17] The rate of charging LIB become a barrier to its application in EVs.

Electric double-layer capacitors (EDLC), also known as supercapacitors or ultracapacitors, are an electric energy storage devices that reversibly adsorb/desorbs ions by the electrostatic force on the electrode/electrolyte interfaces. The mechanism of EDLC result in a high power density, high energy efficiency and excellent cycle ability.[18-19] The EDLC usually has a symmetric structure with high surface area carbon materials on both electrodes. The capacitance of electrode materials which is proportional to the surface area and the electrochemical window of electrolytes determine the maximum energy density, while the low equivalent inner resistance leads to the power density of EDLC one order magnitude higher than that of LIB.[18-20] However, for example, the EDLC using aqueous electrolyte usually has energy density less than 5Wh/kg. Thus, more and more research has focused on the ionic liquid electrolytes whose electrochemical windows can be over 4V.[20, 21]

Therefore, the emerging development and expansion of EVs requires a new energy storage device that merges advantages from both LIB and EDLC. The hybrid battery/ EDLC has gradually attracted more scientific attention. Generally, the hybrid battery/ EDLC has an asymmetric structure with a battery electrode where the Faradaic reaction occurs and an EDLC electrode which provides the interface to form electric double-layer. Typically, the lithium rich compound, such as $Li_4Ti_5O_{12}$, $LiMn_2O_4$, Li_2FeSiO_4 and $LiCoPO_4$, are chosen as the battery electrode materials.[22-27] However, the slow kinetics and low columbic efficiency of Li de/intercalation do not match the fast reversible de/adsorption of ions on the electrode/electrolyte interface. Among these battery electrode candidates, only nano-size $Li_4Ti_5O_{12}$ growing on the carbon nanofiber shows its compatibility with the EDLC electrode and can be charged/discharged at high rate with the excellent cycle life.[27]

However, we may underestimate the potential application of metal electrodeposition/dissolution in the field of the hybrid battery/EDLC. The reversibly electrodeposition/dissolution of multivalent metals, such as Magnesium (Mg) and Aluminum (Al) at room temperature has become feasible in specially prepared non-aqueous electrolytes. The electrolyte contains phenyl-magnesium-chloride (PhMgCl)/THF has been applied for Mg deposition at room temperature without dendrite formation.[28] Al deposition/dissolution can also occur in the various pyridinium/imidazolium based chloroaluminate ionic liquids.[29-34] The current density of Al deposition can reach over $20mA/cm^2$ with only a small sacrifice of overpotential and can maintain the columbic efficiency of Al deposition/dissolution closed to 100%.[32,35] These characteristics indicate that Al electrode has potential to be the part of the hybrid battery/EDLC. Here we propose an Al based hybrid supercapacitor using the acidic $AlCl_3$/1-ethyl-3-methylimidazolium chloride (EMIC) ionic liquid. The ionic liquid become acidic when the molar ratio of $AlCl_3$: EMIC is over 1. EMI^+, $AlCl_4^-$ and $Al_2Cl_7^-$ are the major ions in this acidic chloroaluminate ionic liquid. The possible electrode reactions for this Al based hybrid supercapacitor is shown as below.

Positive side (EDLC): $AlCl_4^- + nC \leftrightarrow AlCl_4^- \cdot C_n^+ + e^-$ (1)

Negative side (Battery): $4Al_2Cl_7^- + 3e^- \leftrightarrow 7AlCl_4^- + Al$ (2)

7.3 Experimental

7.3.1 Electrolyte preparations

The acidic $AlCl_3$/EMIC ionic liquid is prepared by slowly adding purified EMIC onto solid $AlCl_3$ crystals. EMIC is synthesized by using the procedure described below.[36] A pressure bottle is used as the reactor for synthesis of EMIC. 1-methylimidazole (Sigma Aldrich, 99%), chloroethane (Sigma Aldrich, 99.7%), and acetonitrile (Sigma Aldrich, 99%), are purified and water is removed before being transferred into the pressure bottle for the synthesis reaction. The reaction takes about 2 weeks at room temperature with a rapidly-stirring magnetic stirrer. When the EMIC is fully precipitated from the reaction solvent, the reaction is closed to completion. The purification of EMIC requires removal of the excess chloroethane, unreacted 1-methyimidazole and organic solvents. Acetonitrile is first added to the flask containing the reaction products and EMIC should be dissolved in the excess of acetonitrile. Then the solution is slowly dropped into the flask containing ethyl acetate. EMIC should then crystalize in the ethyl acetate before the precipitate is vacuum filtered. After carefully repeated the same purification process 3 times, the final precipitates is removed from acetonitrile under vacuum for one week. Then the purified EMIC is acquired. $AlCl_3$ (Fluka, >99%) and is further purified by sublimation in a heavy wall glass tube. The detailed purification process of $AlCl_3$ is described as follow. The main target of $AlCl_3$ purification process is to remove $FeCl_3$ leading to a yellowish color of $AlCl_3$. The tube for $AlCl_3$ sublimation is made of heavy-wall Pyrex glass which aims to prevent the explosion under $AlCl_3$ vapor pressure. Selected amount of NaCl and 4cm length Al (Sigma Aldrich, 99.999%) wires are added to the heavy-wall glass tube to remove the $FeCl_3$ and Al_2O_3 before the $AlCl_3$ powder is filled into the tube. All these assembly processes are operated under an Ar atmosphere in a glovebox. The glass tube containing $AlCl_3$, NaCl and Al wire is heated to 90℃ overnight under vacuum. Then a torch is used to seal the glass tube under vacuum. The sealed glass tube is further heated to 250℃ in the furnace for 4 hours before it is slowly pulled from the furnace. The cold air outside the furnace can let $AlCl_3$ vapor form a solid on the tube wall. Then, the $AlCl_3$ crystals are fully purified.

7.3.2 Electrode preparations

The high surface area carbon materials come from different sources: C-grade graphene nanoplatelets (GnP, XG Science), acid-washed and steam treated activated carbon (stAC, DarcoG-60), Supra 30 activated carbon (Norit). Polytetrafluoroethylene (PTFE) powder (Sigma Aldrich) and aqueous base modified styrene butadiene rubber (SBR) (Targary

Inc.) are used as the polymer binder. The slurry of carbon materials for EDLC is prepared by mixing high surface area carbon, carbon black (Sigma Aldrich), and polymer binder with the mass ratio 90:7:3 with specified amount of DI water. The slurry is stirred by a magnetic stirrer under vacuum for 1 hour to remove any possible gas from carbon materials. The prepared slurry is pasted on the carbon coated Al foil (Z-flo® 2651, Coveris Advanced Coatings) before a blade is carefully used to remove the excess slurry. The electrode is then placed into an oven at 70℃ for overnight. The prepared electrode is finally cut to the 2x2cm size for further experiments. This procedure ensure the loadings of carbon materials will be maintained at around 1-2mg/cm^2.

7.3.3 Cell assembly

A simple sandwich cell using microscope slides and clips is used for electrochemical characterization of the Al based hybrid supercapacitor. Figure 7.1 illustrates the assembly of the sandwich test cell. The sandwich cell contains a 2x2cm EDLC electrode, two pieces of 2x6cm carbon coated Al foil current collectors, one piece of 2.5x2.5cm separator (Celgard 3501), two pieces of microscope slides and several clips are used to ensure the assembly firmly contacted. The size of the separator is larger than the electrode area to avoid any short-circuit between the positive and negative electrodes. One of the carbon coated Al foil is regarded as the substrate for Al deposition/dissolution. The celgard separator and EDLC electrode materials should be fully wetted by adding the drops of electrolyte to their surfaces before the parts of cell are carefully assembled. During the assembling process, the electrode materials should firmly contact the current collector and separator without leaving gas bulbs in the cell assembly. Finally, the excess electrolyte should be added between two microscope slides to avoid a decrease of $AlCl_3$ content in the electrolyte.

7.3.4 Materials and electrochemical characterization

The BET surface areas of carbon materials are measured by N_2 physical adsorption using Quantachrom instrument. The morphology of graphene and activated carbon materials is observed by Hitachi TM 3000. The two-electrode sandwich cell is applied to cyclic voltammetry, charging/discharging experiments and impedance experiments. The negative electrode where the Al deposition/dissolution occurs is regarded as the both counter electrode and reference electrode. Among all electrochemical characterization experiments, the molar ratio of 1.5 $AlCl_3$: EMIC ionic liquid is used. Electrochemical related characterizations and cell tests are made using a Biologic SP 200 potentiostat.

7.4 Results and Discussions

7.4.1 BET and morphologic characterization of carbon materials

In order to investigate the performance of EDLC electrode in the acidic $AlCl_3$/EMIC ionic liquid, three commercialized high surface area carbon materials, i.e. GnP, stAC and Supra 30, are chosen. In Table 7.1 BET N_2 de/adsorption characterization shows that Supra 30 has the largest specific surface area close to $1230 m^2/g$. The specific surface area of GnP and stAC is approximately the same

.

From Figure 7.2 the high surface area of Supra30 may derive from the larger number of micropores (pore diameter < 2nm) and the smaller pore volume. These factors also lead to the density of Supra 30 obviously lower than that of GnP and stAC.

Compared with the particle size of GnP (ca. 500nm with less than 10nm thick), the particle size of activated carbon is larger (on the order of micrometer) and the morphology of activated carbon varies in the amorphous formation as shown in Figure 7.3 (c) and (d). Typically, the smaller size of particles lead to the higher surface area. Though the size of stAC particles shown in the Figure 7.3 (c) is smaller than that of Supra 30 particles, Supra 30 has more surface area. This may be due to the large number of micropores on Supra 30 contributing to the N_2 ad/desorption. In addition, the larger size of the amorphous carbon particles may lead to low catalytic activity on electrochemical reactions

7.4.2 Electrochemical characterizations

In order to simulate the real working condition of the Al based hybrid supercapacitor, two-electrode cyclic voltammetry methods are adopted while the negative electrode is regarded as the reference and counter electrode. Ideally, the shapes of the cyclic voltammograms for high surface area materials in the supercapacitor should be close to a rectangle whose shapes and sizes does not depend on the scan rate. However, in Figure 7.4, the shapes and sizes of cyclic voltammograms for the GnP electrode change with the different scan rate. In addition, at slow scan rate such as 1mV/s, oxidation and reduction peaks obviously appear at 1.8V and 0.2V vs Al/Al (III) and indicate the Faradaic reactions start to occur. At the fast scan rate, the oxidation and reduction peaks are not obvious because of the overpotential existence. It has been widely understood that graphite can be used as the cathode material for $AlCl_4^-$ de/interclation and Cl_2 evolution in the chloroaluminate ionic liquids but the reactions typically take place at 2V vs Al/Al(III). The result that Cl_2 evolution shifts to a lower a potential (1.8V vs Al/Al(III)) may result from the high catalytic activity of nano-size of GnP. In addition, as GnP consists of multi-layer graphene (less than 20 layers), the reduction current from Cl_2 deinterclation is not obvious in the cyclic voltammograms. Therefore, the high catalytic activity of GnP in the acidic chloroaluminate ionic liquid adversely affect its application in the Al based hybrid supercapacitor. It might not be suitable to choose carbon materials with single graphite or graphene structures in the chloroaluminate ionic liquids after considering $AlCl_4^-$ intercaltion and Cl_2 evolution. The first criteria for a compatible carbon material with the chloroaluminate becomes the high specific surface area but low catalytic activity for Cl_2 evolution to enlarge the electrochemical window.

The stAC has the similar specific surface area ($787m^2/g$) to GnP but with an amphorous structure. It may be more compatible with the chloroaluminate ionic liquid. The cyclic voltammograms of stAC electrode ($3\%_{mass}$ PTFE) at different cycles (scan rate: 100mV/s) are shown in the Figure 7.5. The potential on the stAC electrode varies from 0.1V to 1.95V vs Al/Al (III). The initial capacitance (ca. 14F/g) from the electric double-layer formation is obvious at the 1st cycle. However, the capacitance continues to decrease as the voltage cycling. In the end of the 3rd cycle the capacitance from desorption of ions is less than 10F/g. At the lower region (0.1V to 0.4V vs Al/Al(III)) of the potential range, the capacitance from ion adsorption even drops to zero. This indicates that during the continuous cyclic voltammetry experiments ions first enter the pores of stAC to form the electric double-layer but collapse the pore structure of stAC leading to ions failing to reversibly leave pores. Additionally, the expansion of pore structure of stAC after the entrance of ions may result in the loss of stAC electrically contacting with the current collector.

Therefore, the poor of cyclability performance may limit the application of the stAC electrode in the Al based hybrid supercapacitor. Furthermore, we investigate the carbon material (Supra 30) specially produced for the symmetric supercapacitor with the aqueous electrolyte. The cyclic voltammograms of Supra 30 electrode ($3\%_{mass}$ PTFE) in the 1.5 $AlCl_3$:1 EMIC ionic liquid at different cycles (scan rate: 100mV/s) are shown in Figure 7.6. Unlike the stAC electrode, the Supra 30 electrode has the capacitance (20F/g) due to the higher specific surface area and provides better cyclability. However, the pore size of Supra 30 may not be compatible with size of ions (EMI^+, $Al_2Cl_7^-$ and $AlCl_4^-$) in the chloroaluminate ionic liquid. As indicated in the cyclic voltammograms in Figure 7.6, in the potential region (0.4V to 0.8V vs Al/Al(III)) almost no capacitance is observed. Especially, at the 1st cycle the non-Faradaic current from the electric double-layer formation starts to appear after 0.8V vs Al/Al(III). Compared to the 1st cycle of cyclic voltammograms in Figure 7.6, the onset potential for the electric double-layer formation decreases to 0.65V vs Al/Al (III). This may result from the expansion of pore size of Supra 30 after ions enter the pore of Supra 30 in the 1st cycle and also indicates that some remaining ions which support the pore expansion still stay in the pores after the cycle is finished. Therefore, it is of high priority to develop the high surface area carbon materials with the large pore size compatible with the ion sizes in the chloroaluminate ionic liquids. In Figure 7.7 the result that the capacitance of Supra 30 changes with the scan rates is shown in cyclic voltammetry experiments of Supra 30 electrode ($3\%_{mass}$ PTFE) in the 1.5$AlCl_3$:1 EMIC ionic liquid at scan rates. Theoretically the shapes and sizes of the cyclic voltammograms do not vary with the scan rates if the kinetics of ion ad/desorption to the pores of carbon materials is sufficiently fast. However, in practical cases, factors such as slow kinetics or high contact resistances may contribute to the shapes and sizes of cyclic voltammorgrams for the supercapacitor tests. In our case at slow scan rate (10mV/s) the capacitance of Supra 30 increases to almost 40F/g. This result can predict that the charging/discharging performance of the Supra 30 electrode in the Al based hybrid supercapacitor will be better at lower charging/discharging specific current. In addition, at lower scan rate, more capacitance appears at higher potential during discharging. For example, at scan rate 10mV/s, the capacitance for ionic desorption appears at 1.8V vs Al/Al(III). However, at scan rate 100mV/s the capacitance shows at 1.6V. This difference may result from the slow kinetics for ionic ad/desorption and relative high contact resistance in the Supra 30 EDLC electrode.

Furthermore, we test the charging/discharging performance of the Al based hybrid supercapacitor using different sources of carbon materials as EDLC electrodes. Figure 7.8 shows a series of charging/discharging curves for carbon materials at different specific current (0.5A/g, 1A/g and 2A/g). The charging/discharging test is operated by constant current methods. The test cells are first charged from open circuit voltage (OCV) and then discharged at the same constant currents after the cell voltages reach the cut-off voltage (2.15V). However, the cut-off voltage for the cell with GnP electrode is set at 1.5V to avoid Cl_2 evolution that chemically reacts with the cation (EMI^+) in the ionic liquid electrolyte. The values of the areas under discharging curves multiplied by the specific current give the estimated specific energy of each cell made with different carbon materials. Limited by the cut-off voltage, the cell with the GnP electrode has the specific energy only 1/4 that of the cell with the Supra 30 electrode. In addition, the voltage of the cell with the GnP electrode drops (from 1.5V to 1.1V) more quickly than the cell with activated carbon. This indicates that the kinetic resistance of GnP electrode is large. Among the charging/discharging curves for three carbon materials at specific current 1A/g, the cell with Supra 30 electrode perform best in terms of specific energy. This result could be also shown from cyclic voltammorgrams of Supra 30 electrode based higher capacitance, reversibility and stability. Additionally, when comparing the charging/discharging results among three carbon materials at specific current 0.5A/g, the cell with Supra 30 (the charging/discharging curve is not shown completely to show the other curves more clearly) outperforms and the discharging time reaches 200s which is 2 times higher than that of the cell with the stAC electrode. This may result from the less side reaction and reversibility for ion ad/desorption in Supra 30 improved by the slow specific current. Therefore, Supra 30 may become a starting point for future investigations of suitable carbon materials in the Al based hybrid supercapacitor. Methods to increase pore size of Supra 30 without changing the functional groups composition on activated carbon surface should be included in future studies of ways to modify carbon materials.

7.3 Polymer binder effect

The PTFE powder is chosen for most of the electrochemical characterization experiments. The reason for choosing this material is its inert chemical property in the chloroaluminate ionic liquids. However, SBR binder also has become popular in the application of Li-ion battery. It may have the potential application in the Al based hybrid supercapacitor as well, but its chemical stability in contact with the chloroaluminate ionic liquids is unclear. Additionally, the difference between PTFE and SBR properties relevant to the chloroaluminate ionic liquids is hydrophobicity/ hydrophilicity. While PTFE is known for its hydrophobic properties, SBR binder is hydrophilic. Therefore, when these polymer binders are added to the carbon slurry for the EDLC electrode preparation, the wettability of EDLC electrodes can be different. Due to the hygroscopic ionic liquid, we do not observe the wettability (size and shape of the ionic liquid droplet) changes on the EDLC electrodes based on different polymer binders. We do notice that the droplet of the ionic liquid is much easier to disperse on the EDLC electrode using the SBR binder. Furthermore, we measure the cyclic voltammogram of the Supra30 electrode

($3\%_{mass}$ SBR) in the 1.5AlCl$_3$:1 EMIC ionic liquid at scan rate 100mV/s shown in Figure 7.10. The specific capacitance improved to 70F/g which almost 3 times higher than that of the electrode with PTFE binder.

However, the loss of capacitance is in the potential region (from 0.25V to 0.75V vs Al/Al(III)) indicates that the pore size of Supra 30 activated carbon still does not match the ionic diameter in the ionic liquid. The mix of contact and kinetic resistances is high from 2V to 1.75V vs Al/Al(III) during the discharging cycle. Thus the improvement in the electric conductivity of activated carbon and modified preparation process for EDLC electrode could be beneficial to improve the energy efficiency of the cell. The reason SBR binder is more compatible with the chloroaluminate ionic liquid that PTFE binder might be the improvement of wettability on a macroscale. From a micro point of view, the hydrophilic SBR around micropores of activated may promote the entrance of ions to the micropores of activated carbon while PTFE may take an opposite effect. This also indicates that modification of the activated carbon surface with improvements of the amount of hydrophilic functional groups, such as the hydroxyl group, carbonyl group, carboxyl group may increase of specific capacitance.

In addition, the charging/discharging performance of the cell using SBR binder is tested. The result, shown in Figure 7.10, matches the high specific capacitance observed on the cyclic voltammogram. It takes over 120s to discharg the cell at 1A/g from 2.15V. The energy density of the Supra 30 electrode with the SBR binder is calculated based on the area under the discharging curve multiplied by the constant specific current (1A/g) is 37Wh/kg comparable to the energy density (34Wh/kg) of activated carbon electrode reported for Magnesium (Mg) based hybrid supercapacitor.[28] The electrolyte used for Mg based hybrid supercapacitor have LiCl as the additive to attenuate the pore size effect from the mismatch between pore size of activated carbon cloth and ionic diameter. In our case, it would also be possible to add LiCl to the electrolyte. The result on the energy density is expected to be a further improvement.

7.4.4 Impedance measurements

In addition, we measure the change of impedances dependent on the overpotential relative to OCV from 0V to 1200mV. This aims to investigate how the contact resistance and charge-transfer (kinetic) resistance of the Supra 30 EDLC electrode change with overpotential. Here the overpotential is specially defined as the part of potential that is higher than the OCV. In our case for impedance measurement, OCV is around 47mV vs Al/Al(III). As we know the contact resistance is the value where the impedance curve first intercepts with X-axis in the Nyquist plot. The contact resistance that we measure for the Al based hybrid capacitor is 1.25ohm which is significantly higher than that in symmetric supercapacitors. This might result from the structure of the particular cell assembly used for the initial demonstration. The notable decreasing trend of charge-transfer resistances with the increasing overpotential indicates that a slow kinetic process leads to the energy deficiency. This slow kinetic process may result from a mismatch between the small pore size of activated carbon and the large ion sizes of complex ions such as $AlCl_4^-$, $Al_2Cl_7^-$ and EMI^+.

7.5 Conclusions

We successfully demonstrates an Al based hybrid supercapacitor using high surface area carbon materials as EDLC electrodes in 1.5 $AlCl_3$: EMIC chloroaluminate ionic liquid. The graphene may not be compatible with the chloroaluminate ionic liquid because of the high catalytic ability for Cl_2 evolution leading to side chemical reactions and a narrow electrochemical window. However, the activated carbon (Supra 30) with the amorphous structure instead of graphitic layer structure can be applied as the electrode materials for the Al based hybrid supercapacitor. The mismatch between the small pore size of activated carbon and the large ionic-diameter of complex ions such as $AlCl_4^-$, $Al_2Cl_7^-$ and EMI^+ results in a low specific capacitance (24F/g) especially the loss of capacitance observed in potential region (from 0.25V to 0.75V vs Al/Al(III)). Comparison of the charging/discharging curves at different specific current shows that more discharged electric energy can be acquired at low specific current indicating that there is significant contact resistance and charge-transfer resistance in the cell. These resistances are also measured by the electrochemical impedance method at different overpotentials. The contact resistance remains at 1.25ohm however the charge-transfer resistances decrease with overpotentials. Furthermore, the polymer binder effect is investigated on the choice between PTFE and SBR. The hydrophilic property of SBR may promote the entrance of ions to the micropores of activated carbon. The EDLC electrode using SBR leads to an improved specific capacitance (70F/g) and energy density (34Wh/kg) competitively with the recent reports on the metal based hybrid supercapacitor. Further investigation on the modification of activated carbon with high specific surface area should emphasize large pore size and high percentages of hydrophilic function groups of the EDLC electrode.

Reference

[1] Frankignoulle, M., Abril, G., Borges, A., et al. (1998). Carbon dioxide emission from European estuaries. *Science*, *282*(5388), 434-436.

[2] Divya, K. C., & Ostergaard, J. (2009). Battery energy storage technology for power systems-An overview. *Electric Power Systems Research*, *79*(4), 511–520. doi:DOI 10.1016/j.epsr.2008.09.017

[3] Kang, B., & Ceder, G. (2009). Battery materials for ultrafast charging and discharging. *Nature*, *458*(7235), 190–193. doi:Doi 10.1038/Nature07853

[4] Balducci, A., Jeong, S. S., Kim, G. T., Passerini, S., Winter, M., Schmuck, M., Tran, N. (2011). Development of safe, green and high performance ionic liquids-based batteries (ILLIBATT project). *Journal of Power Sources*, *196*(22), 9719–9730. doi:10.1016/j.jpowsour.2011.07.058

[5] Vlad, a, Singh, N., Rolland, J., Melinte, S., Ajayan, P. M., & Gohy, J.-F. (2014). Hybrid supercapacitor-battery materials for fast electrochemical charge storage. *Scientific Reports*, *4*, 4315. doi:10.1038/srep04315

[6] Wang, G., Zhang, L., & Zhang, J. (2012). A review of electrode materials for electrochemical supercapacitors. *Chemical Society Reviews*, *41*, 797. doi:10.1039/c1cs15060j

[7] Skyllas-Kazacos, M., Chakrabarti, M. H., Hajimolana, S. A., Mjalli, F. S., & Saleem, M. (2011). Progress in Flow Battery Research and Development. *Journal of The Electrochemical Society*, *158*(8), R55. doi:10.1149/1.3599565

[8] Nema, P., Nema, R. K., & Rangnekar, S. (2009). A current and future state of art development of hybrid energy system using wind and PV-solar: A review. *Renewable & Sustainable Energy Reviews*, *13*(8), 2096–2103. doi:10.1016/j.rser.2008.10.006

[9] Aifantis, K. E., Hackney, S. A., & Kumar, R. V. (Eds.). (2010). *High energy density lithium batteries: materials, engineering, applications*. John Wiley & Sons.

[10] Wang, Y., & Cao, G. (2008). Developments in nanostructured cathode materials for high-performance lithium-ion batteries. *Advanced Materials*, *20*, 2251–2269. doi:10.1002/adma.200702242

[11] Wang, H., Cui, L., Yang, Y., & Casalongue, H. S. (2010). Mn_3O_4-Graphene Hybrid as a High-Capacity Anode Material for Lithium Ion, 13978–13980.

[12] Zhang, S. S. (2006). A review on electrolyte additives for lithium-ion batteries. *Journal of Power Sources*, *162*(July), 1379–1394. doi:10.1016/j.jpowsour.2006.07.074

[13] Lu, L., Han, X., Li, J., Hua, J., & Ouyang, M. (2013). A review on the key issues for lithium-ion battery management in electric vehicles. *Journal of Power Sources*, *226*, 272–288. doi:10.1016/j.jpowsour.2012.10.060

[14] Tarascon, J. M., & Armand, M. (2001). Issues and challenges facing rechargeable lithium batteries. *Nature*, *414*(November), 359–367. doi:10.1038/35104644

[15] Kiani, M. a., Mousavi, M. F., & Rahmanifar, M. S. (2011). Synthesis of nano-and micro-particles of $LiMn_2O_4$: Electrochemical investigation and assessment as a cathode in li battery. *International Journal of Electrochemical Science*, *6*, 2581–2595. doi:10.1039/c1ee01598b

[16] Dunn, B., Kamath, H., & Tarascon, J. (2011). Electrical Energy Storage for the Grid : A Battery of Choices. *Science*, *334*(6058), 928–935.

[17] Larcher, D., & Tarascon, J. (2014). Towards greener and more sustainable batteries for electrical energy storage. *Nature Publishing Group*, *7*(January). doi:10.1038/nchem.2085

[18] Zhai, Y., Dou, Y., Zhao, D., Fulvio, P. F., Mayes, R. T., & Dai, S. (2011). Carbon materials for chemical capacitive energy storage. *Advanced Materials*, *23*(42), 4828–50. doi:10.1002/adma.201100984

[19] Yang, Z. G., Zhang, J. L., Kintner-Meyer, M. C. W., Lu, X. C., Choi, D. W., Lemmon, J. P., & Liu, J. (2011). Electrochemical Energy Storage for Green Grid. *Chemical Reviews*, *111*(5), 3577–3613. doi:Doi 10.1021/Cr100290v

[20] Zhu, Y., Murali, S., Stoller, M. D., Ganesh, K. J., Cai, W., Ferreira, P., Ruoff, R. S. (2011). Carbon-based supercapacitors produced by activation of graphene. *Science (New York, N.Y.), 332*(6037), 1537–41. doi:10.1126/science.1200770

[21] Lu, W., Qu, L., Henry, K., & Dai, L. (2009). High performance electrochemical capacitors from aligned carbon nanotube electrodes and ionic liquid electrolytes. *Journal of Power Sources*, *189*, 1270–1277. doi:10.1016/j.jpowsour.2009.01.009

[22] Karthikeyan, K., Aravindan, V., Lee, S. B., Jang, I. C., Lim, H. H., Park, G. J., Lee, Y. S. (2010). A novel asymmetric hybrid supercapacitor based on Li2FeSiO 4 and activated carbon electrodes. *Journal of Alloys and Compounds*, *504*(1), 224–227. doi:10.1016/j.jallcom.2010.05.097

[23] Wang, R., Lang, J., Zhang, P., Lin, Z., & Yan, X. (2015). Fast and Large Lithium Storage in 3D Porous VN Nanowires-Graphene Composite as a Superior Anode Toward High-Performance Hybrid Supercapacitors. *Advanced Functional Materials*, n/a–n/a. doi:10.1002/adfm.201404472

[24] Vlad, A., Singh, N., Rolland, J., Melinte, S., Ajayan, P. M., & Gohy, J.F. (2014). Hybrid supercapacitor-battery materials for fast electrochemical charge storage. *Scientific Reports*, *4*, 4315. doi:10.1038/srep04315

[25] Kim, H., Park, K. Y., Cho, M. Y., Kim, M. H., Hong, J., Jung, S. K. & Kang, K. (2014). High-Performance Hybrid Supercapacitor Based on Graphene-Wrapped $Li_4Ti_5O_{12}$ and Activated Carbon. *ChemElectroChem*,(1), 125-130.

[26] Vasanthi, R., Kalpana, D., & Renganathan, N. G. (2008). Olivine-type nanoparticle for hybrid supercapacitors. *Journal of Solid State Electrochemistry*, *12*, 961–969. doi:10.1007/s10008-007-0438-6

[27] Naoi, K., Ishimoto, S., Isobe, Y., & Aoyagi, S. (2010). High-rate nano-crystalline Li4Ti5O12 attached on carbon nano-fibers for hybrid supercapacitors. *Journal of Power Sources*, *195*(18), 6250–6254. doi:10.1016/j.jpowsour.2009.12.104

[28] Yoo, H. D., Shterenberg, I., Gofer, Y., Doe, R. E., Fischer, C. C., Ceder, G., & Aurbach, D. (2014). A Magnesium-Activated Carbon Hybrid Capacitor. *Journal of the Electrochemical Society*, *161*(3), A410–A415. doi:10.1149/2.082403jes

[29] Hudak, N. S. (2014). Chloroaluminate-doped conducting polymers as positive electrodes in rechargeable aluminum batteries. *Journal of Physical Chemistry C, 118*, 5203–5215. doi:10.1021/jp500593d

[30] Tsuda, T., Kokubo, I., Kawabata, M., Yamagata, M., Ishikawa, M., Kusumoto, S.,Kuwabata, S. (2014). Electrochemical Energy Storage Device with a Lewis Acidic AlBr3-1-Ethyl-3-methylimidazolioum Bromide Room-Temperature Ionic Liquid. *Journal of the Electrochemical Society*, *161*(6), A908–A914. doi:10.1149/2.029406jes

[31] Carlin, R. T., Crawford, W., & Bersch, M. (1992). Nucleation and Morphology Studies of Aluminum Deposited from an Ambient-Temperature Chloroaluminate Molten Salt. *Journal of Electrochemical Society*, *139*(10), 2720–2727.

[32] Zhang, M., Watson, J. S., Counce, R. M., Trulove, P. C., & Zawodzinski, T. a. (2014). Electrochemistry and Morphology Studies of Aluminum Plating/Stripping in a Chloroaluminate Ionic Liquid on Porous Carbon Materials. *Journal of the Electrochemical Society*, *161*(4), D163–D167. doi:10.1149/2.048404jes

[33] Takahashi, S., Akimoto, K., & Saeki, I. (1989). Aluminum Plating From the Room Temperature Molten Salt Electrolyte. *Hyomen Gijutsu*, *40*(1), 134–135.

[34] Auborn, J., & Barberio, Y. (1985). An Ambient Temperature Secondary Aluminum Electrode : Its Cycling Rates and Its Cycling Efficiencies. *Journal of Electrochemical Society*, *132*(3), 598–601.

[35] Jiang, T., Chollier Brym, M. J., Dubé, G., Lasia, a., & Brisard, G. M. (2006). Electrodeposition of aluminium from ionic liquids: Part I—electrodeposition and surface morphology of aluminium from aluminium chloride (AlCl3)–1-ethyl-3-methylimidazolium chloride (EMIC) ionic liquids. *Surface and Coatings Technology, 201*(1-2), 1–9. doi:10.1016/j.surfcoat.2005.10.046

[36] Trulove, P.C. The Chemistry of Proton in Ambient-temperature Chloroaluminate Molten Salts, Thesis, State of University of New York, Buffalo (1992), 25-44.

Appendix

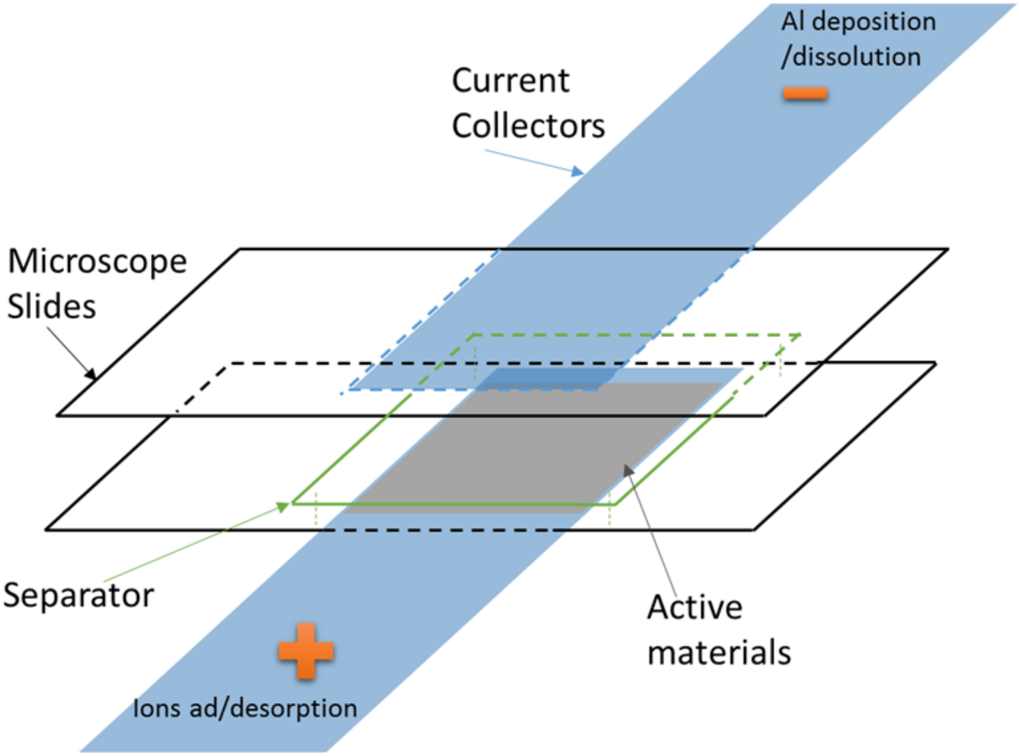

Figure 7. 1 Schematic illustration of a sandwich cell assembly

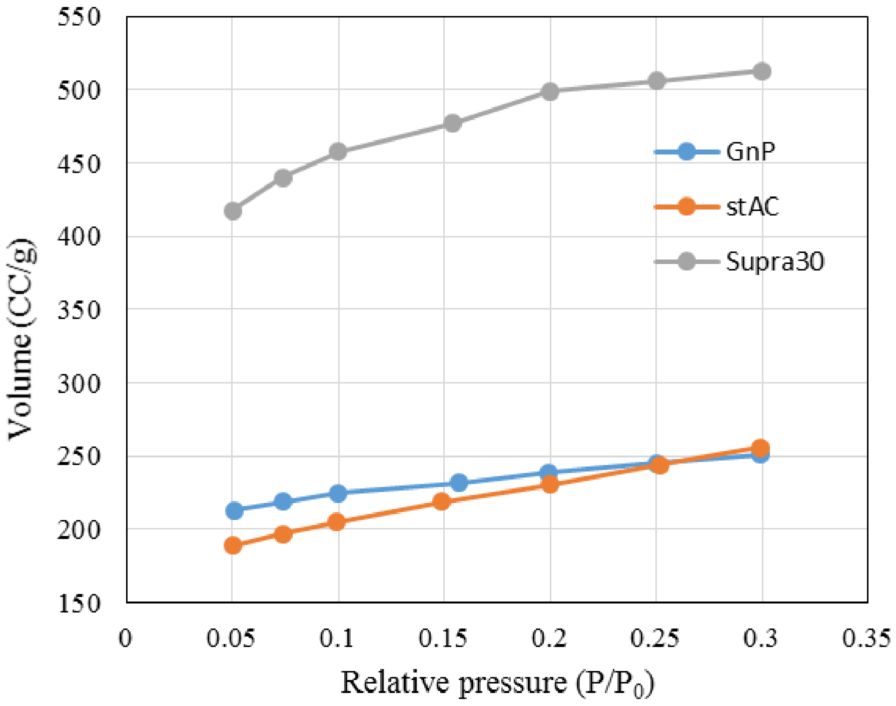

Figure 7. 2 The relationship between volume and relative pressure of different carbon materials.

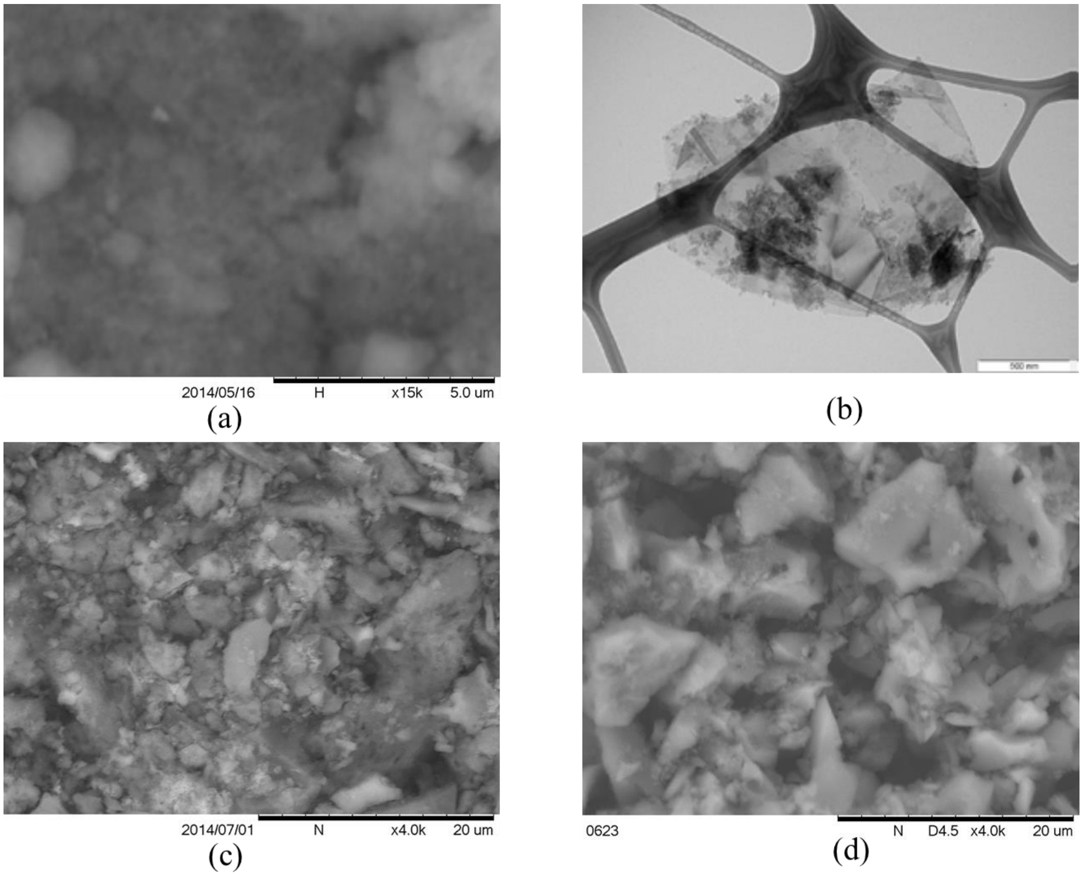

Figure 7. 3 Morphology of GnP, stAC and Supra 30 by SEM.

(a) the sample of GnP is prepared by the drop-casting of GnP ink ($80\%_{mass}$ DI water) on the Al foil. (b) SEM image cited from the website of XG sciences. (c) stAC EDLC electrode ($3\%_{mass}$ PTFE) (d) Supra 30 EDLC electrode ($3\%_{mass}$ SBR).

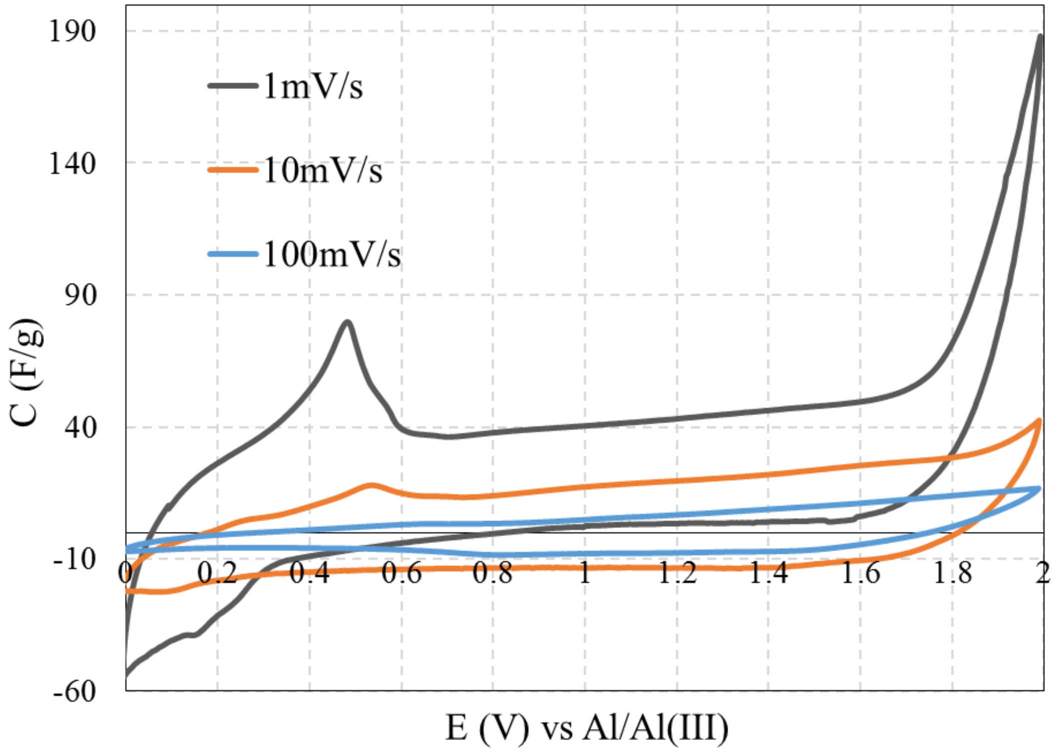

Figure 7. 4 Cyclic voltammograms of GnP electrode (3%$_{\text{mass}}$ PTFE) in the 1.5$AlCl_3$:1 EMIC ionic liquid at different scan rate.

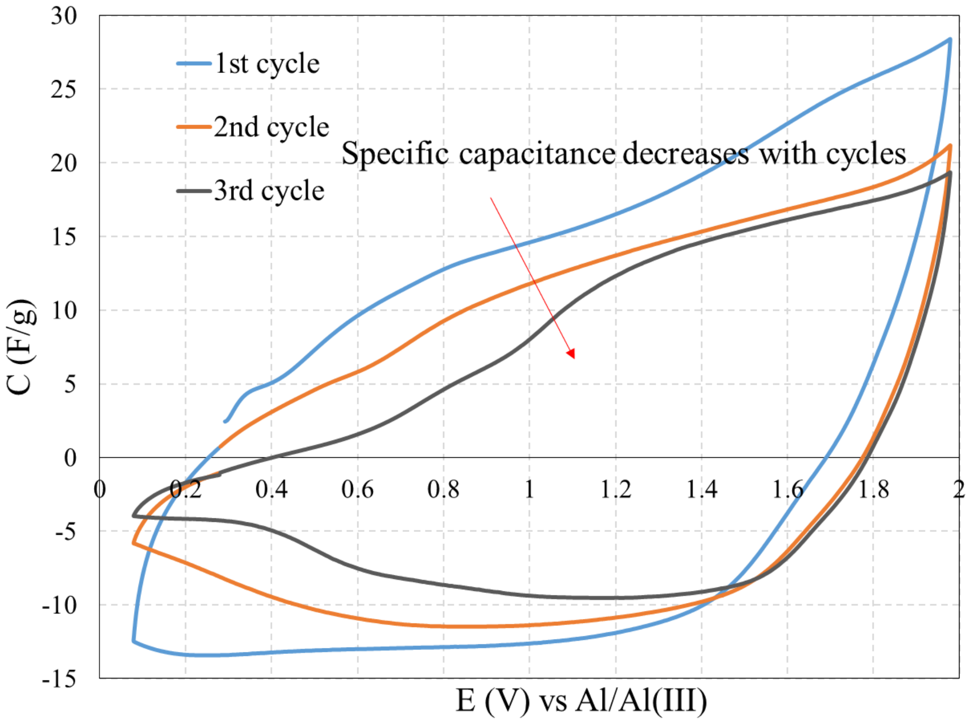

Figure 7. 5 Cyclic voltammograms of stAC electrode (3%$_{\text{mass}}$ PTFE) in the 1.5AlCl$_3$:1EMIC ionic liquid at different cycles (scan rate: 100mV/s).

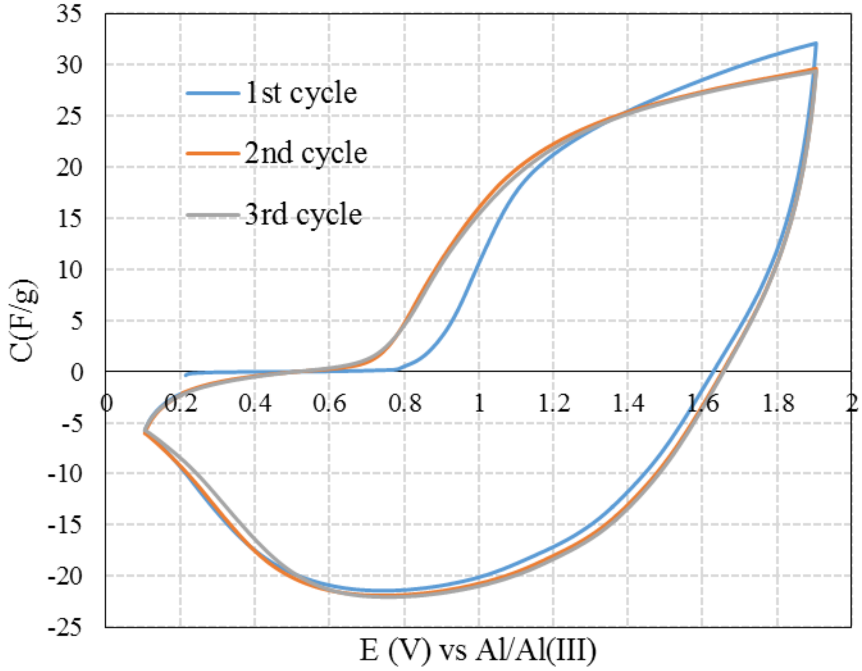

Figure 7. 6 Cyclic voltammograms of Supra 30 electrode (3%$_{mass}$ PTFE) in the 1.5$AlCl_3$:1 EMIC ionic liquid at different cycles.

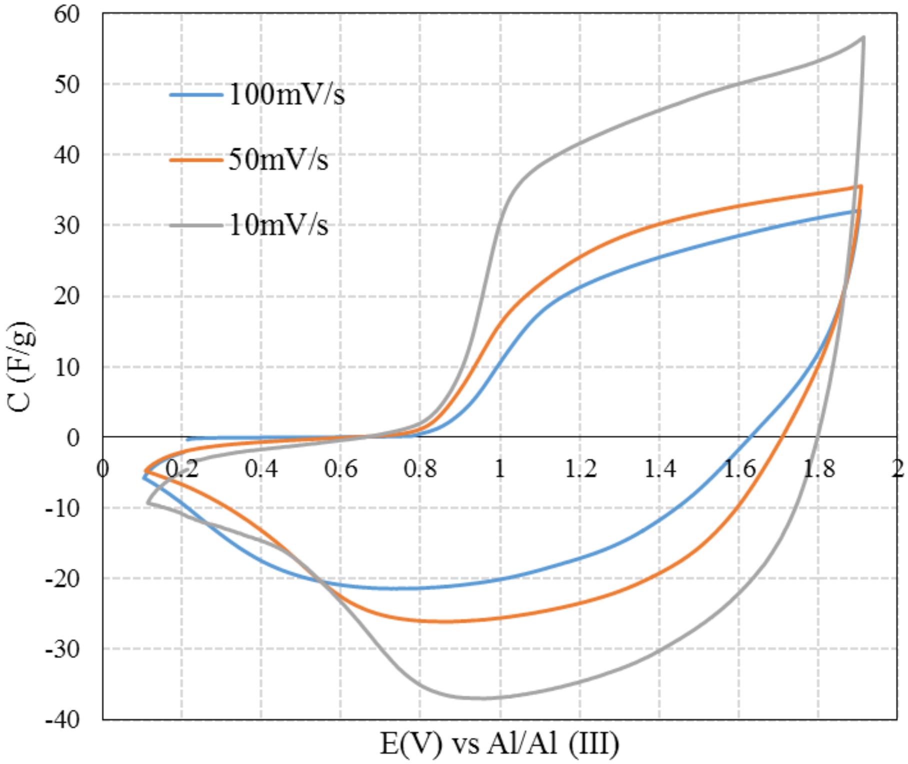

Figure 7. 7 Cyclic voltammograms of Supra 30 electrode (3%$_{mass}$ PTFE) in the 1.5AlCl$_3$:1 EMIC ionic liquid at scan rates.

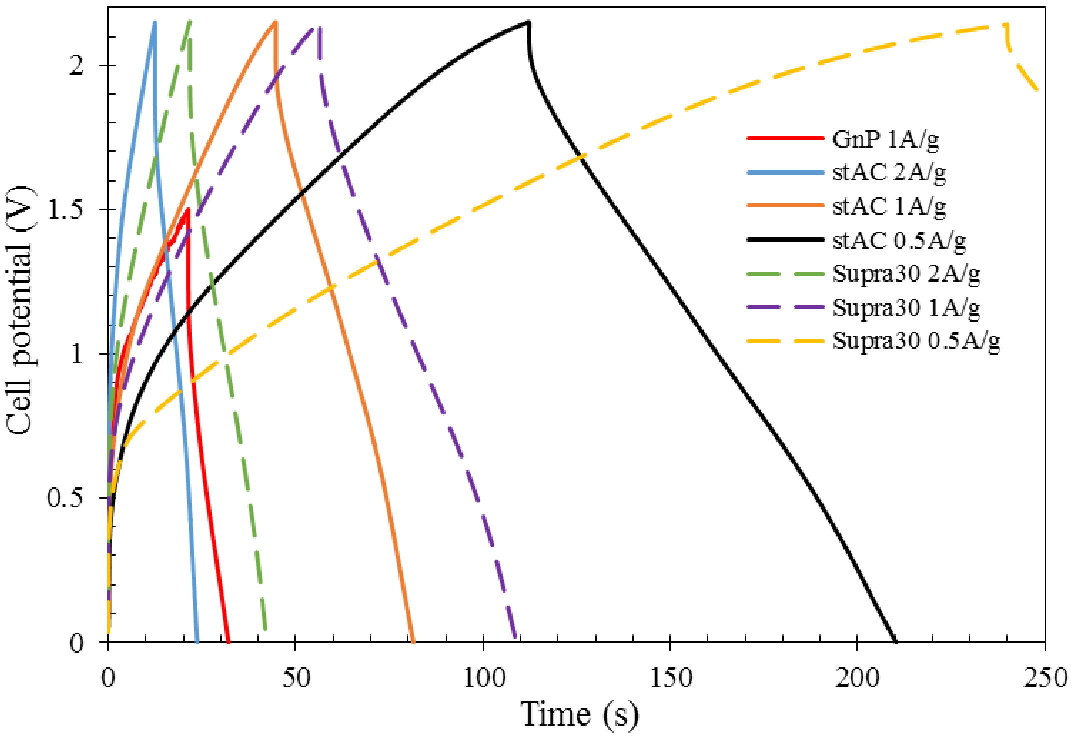

Figure 7. 8 Charging and discharging curves for Al based hybrid supercapacitors with various carbon materials at different charging/discharging rates.

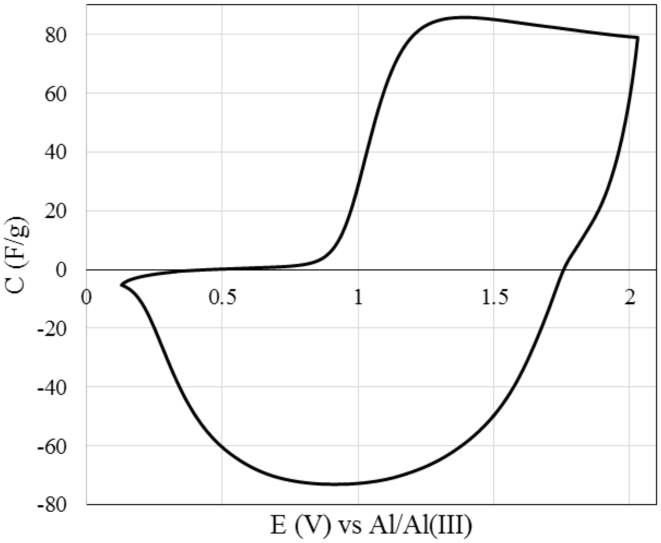

Figure 7. 9 Cyclic voltammogram of Supra30 electrode (3%$_{mass}$ SBR) in the 1.5AlCl$_3$:1 EMIC ionic liquid at the scan rate 100mV (3rd cycle).

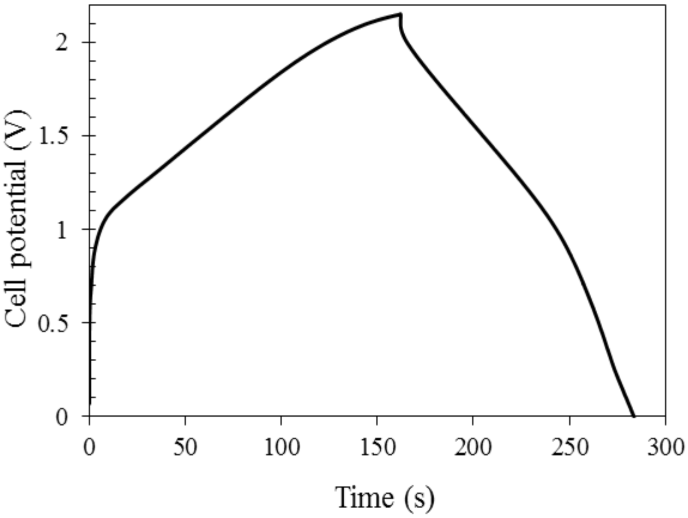

Figure 7. 10 The charging and discharging curve for Al based hybrid supercapacitors with Supra 30 EDLC electrode (3%$_{mass}$ SBR) at 1A/g charging/discharging rate.

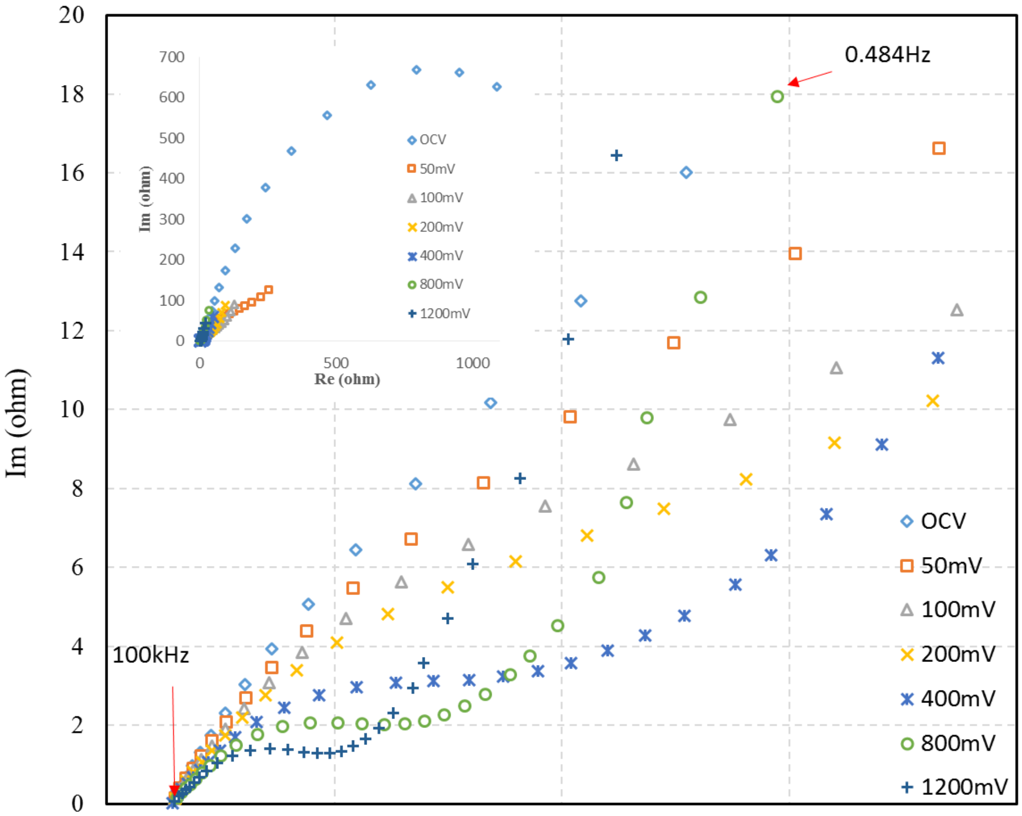

Figure 7. 11 Impedance measurements of Supra 30 electrode in the sandwich cell from 100 kHz to 0.484 Hz.

The Nyquist plots are measured for the Supra 30 electrode (3%$_{\text{mass}}$ PTFE) at different overpotential vs Al/Al(III) where OCV is 47mV. The embedded figure on the top left represents the all recorded impedances from 100 kHz to 0.01 Hz.

Table 7. 1 BET surface area characterization of carbon materials

	GnP	**stAC**	**Supra 30**
BET surface area (m^2/g)	762	787	1227

CHAPTER 8

Summary

In this dissertation, porous carbon materials as the substrates for Al deposition/dissolution in an Al based ionic liquid flow battery (ILFB) are developed and an Al based hybrid supercapacitor is demonstrated. The Aluminum chloride/ 1-ethyl-3-methylimidazolium chloride ($AlCl_3$/EMIC) chloroaluminate ionic liquid is utilized as the electrolyte for both of these Al based energy storage devices. The capital cost of all-vanadium redox flow battery (VRFB) is first calculated based on a step-by-step method and the sensitivity analysis indicated the importance of the cost of vanadium electrolyte to the total capital cost. Thus, the ILFB should have less capital cost than the all-vanadium redox flow battery (VRFB) because of the inexpensive $AlCl_3$. A critical range of temperature data (50-130℃) for $AlCl_3$ dissolution and precipitation from saturated chloroaluminate ionic liquids is measured by differential scanning calorimetry (DSC). The process of Al deposition on porous carbon materials is investigated in the static electrolyte and a flow-through cell aiming to improve the current density, the amount of Al deposits stored in substrates and limit the dendrite growth. Fourier transform infrared spectroscopy (FTIR) and scanning electron microscope (SEM) are applied to characterize the Al deposits on the porous carbon materials. By the flow-through method providing enhanced diffusion to porous carbon materials, the current density of Al deposition on carbon paper is remarkably higher than that on Al disk. However, dendrites prefer to grow on the Al disk substrate. The electrolyte flow rate and the flow direction also play important roles in determining current densities and dendrite formation for Al deposition on porous carbon materials. In addition, we successfully demonstrate an Al based hybrid supercapacitor using high surface area carbon materials such as graphene and activated carbon. The activated carbon is preferred because of less catalytic ability to evolve Cl_2. The mismatch between the small pore size of activated carbon and the large ion size of complex ions results in the high charge-transfer resistance measured by the electrochemical impedance measurements. The wettability of electrodes determined by different polymer binders, Polytetrafluoroethylene (PTFE) and the aqueous base modified styrene butadiene rubber (SBR), has a significant effect on specific capacitance of activated carbon. The hydrophilic property of SBR may promote the entrance of ions to the micropores of activated carbon.

In Chapter 3, the relative sensitivity index for a fixed power capacity shows the importance of the costs of the vanadium to the overall capital costs. In addition, the capital costs per kilowatt-hour showed the greatest range when the vanadium costs were varied from the cost of industrial grade vanadium to the costs of laboratory grade vanadium. It is clear that using vanadium costs near that of the lowest grade vanadium will be necessary to keep the capital costs of the VRFB down. When the energy capacity is held constant and the power capacity and cycle time are manipulated, the increased costs of the components related to the power capacity far outweigh the savings in the cost for the vanadium electrolyte and the tanks due to the lowered cycle time. This shows that there is a greater economic feasibility for VRFB designs with a lower power capacity and longer cycle time for a set energy capacity.

In Chapter 4, the porous substrates such as carbon paper are investigated for Al deposition in the chloroaluminate ionic liquid. Al has shown the ability to be plated and stripped on a carbon paper electrode. The porous structure of carbon paper brings the different observations on cyclic voltammorgrams, current transients at controlled potentials and Al morphology. The porous materials can be considered a more promising substrate to enhance the performance of the Al electrode on current density. The overpotential of Al deposition on carbon paper is lower than that on glassy carbon. The current transients of Al deposition on planar substrate and cylindrical substrate are different. So Scharifker-Hills model will not be suitable to express Al nucleation and growth on carbon paper. Edge effect and cylindrical diffusion should be considered to build a new nucleation model for porous substrates. Higher temperatures and higher $AlCl_3$ molar compositions improve the performance of Al plating by raising nucleation rate and diffusion rate of ions. The diffusion of ions to the fibers inside carbon paper should be considered as an important process for Al plating on the carbon paper. This indicates that the enhanced flow-through electrode should be a good option for Al plating on the carbon paper.

In Chapter 5, differential scanning calorimetry (DSC) heat curves are measured from samples of different $AlCl_3$ mole fractions of $AlCl_3$/EMIC ionic liquids. Melting/freezing points of ionic liquids with different $AlCl_3$ mole factions are obtained from these DSC heat curves. Phase diagram of $AlCl_3$ in ionic liquid, especially the region where excess $AlCl_3$ exists in the saturated ionic liquid, is plotted. A suitable range of temperature (50-130°C) is chosen based on the phase diagram to control the excess amount of $AlCl_3$ dissolving and precipitating from the saturated ionic liquid.

In Chapter 6, Al deposition on the carbon paper in the acidic $AlCl_3$/EMIC chloroaluminate ionic liquid is investigated by a three-electrode flow-through cell. The disappearance and offset of some band positions in the FTIR characterization of the Al coated carbon paper indicate the adsorption between Al particles and the functional groups of carbon paper. At low overpotential (350mV) Al can be plated on the inner fibers of carbon paper by the flow-through method. However, at high overpotential (600mV) even with the help of the enhanced flow-through process, the growth of Al deposits still maintain different rates on different layers of carbon paper. The growth of Al deposits prefers on the outer surface of the carbon paper. In the comparison of the performances of Al deposition in the flow-through cell, the growth of Al deposits on carbon paper has less issue on dendrite formation and faster rate shown in the polarization curves. The flow rate has the positive effect on the ionic diffusion and thus could improve current density of Al deposition. By adjusting the flow direction following the electric field direction, Al deposits on carbon paper can continually grow without dendrite formation. Therefore, the carbon paper has the huge potential in the application of the Al based flow battery.

In Chapter 7, an Al based hybrid supercapacitor is demonstrated. This hybrid supercapacitor is equipped with high surface area carbon materials as EDLC electrodes in 1.5 $AlCl_3$: EMIC chloroaluminate ionic liquid. The graphene may not be compatible with the chloroaluminate ionic liquid because of the high catalytic ability for Cl_2 evolution leading to side chemical reactions and a narrow electrochemical window. However, the activated carbon (Supra 30) with the amorphous structure instead of graphitic layer structure can be applied as the electrode materials for the Al based hybrid supercapacitor. The mismatch between the small pore size of activated carbon and the large ionic-diameter of complex ions such as $AlCl_4^-$, $Al_2Cl_7^-$ and EMI^+ results in a low specific capacitance (24F/g) especially the loss of capacitance observed in potential region (from 0.25V to 0.75V vs Al/Al(III)). Comparison of the charging/discharging curves at different specific current shows that more discharged electric energy can be acquired at low specific current indicating that there is significant contact resistance and charge-transfer resistance in the cell. These resistances are also measured by the electrochemical impedance method at different overpotentials. The contact resistance remains at 1.25ohm however the charge-transfer resistances decrease with overpotentials. Furthermore, the polymer binder effect is investigated on the choice between PTFE and SBR. The hydrophilic property of SBR may promote the entrance of ions to the micropores of activated carbon. The EDLC electrode using SBR leads to an improved specific capacitance (70F/g) and energy density (34Wh/kg) competitively with the recent reports on the metal based hybrid supercapacitor. Further investigation on the modification of activated carbon with high specific surface area should emphasize large pore size and high percentages of hydrophilic function groups of the EDLC electrode.

VITA

Mengqi Zhang was born in a city famous for the steel industry, Panzhihua, Sichua, China. He moved to another steel city, Ma’anshan, Anhui with his parents when he was 4 years old. He left his home town to enter the Nanjing University of Technology for the undergraduate study in 2006. During the last 2 years of his undergraduate life, he took part in a research project on cellulosic ethanol led by Prof. He Huang and Prof. Hongman Zhang. Mengqi earned his bachelor’s degree in Biological Engineering in 2010. Then he left China to pursue the Ph.D in Chemical Engineering in the University of Tennessee, Knoxville. He joined the research group of Governor’s Chair Professor Dr. Thomas Zawodzinski in Department of Chemical and Biomolecular Engineering. He was under the instruction of Dr. Zawodzinski and Dr. Counce. He worked on the research projects, such as capital cost analysis for all-vanadium redox flow battery, Aluminum deposition on porous materials for an ionic liquid flow battery and Aluminum based hybrid supercapacitor.